


FINAL REPORT  
AUTOMATICALLY SCANNED ANTENNA SYSTEMS


Prepared by  
ANTENNA RESEARCH LABORATORY  
E. R. GRAF, PROJECT LEADER  
January 20, 1966

CONTRACT NAS8-11251  
GEORGE C. MARSHALL SPACE FLIGHT CENTER  
NATIONAL AERONAUTICS AND SPACE ADMINISTRATION  
HUNTSVILLE, ALABAMA

APPROVED BY

  
C. H. Holmes  
Head Professor  
Electrical Engineering

SUBMITTED BY

  
H. M. Summer  
Professor of  
Electrical Engineering

## FOREWORD

Auburn Research Foundation submitted a proposal which resulted in Contract NAS8-11251 on May 1, 1964. The contract was awarded by the George C. Marshall Space Flight Center, National Aeronautics and Space Administration, Huntsville, Alabama, and was active until November 30, 1965.

This report is a summary of the work accomplished by the Electrical Engineering Department, Auburn University, in the performance of the contract.

TABLE OF CONTENTS

LIST OF TABLES.....	iv
LIST OF FIGURES.....	v
I. INTRODUCTION.....	1
II. THEORETICAL DISCUSSION.....	3
A. Direction Finding System	
B. Digital Switching System	
C. Electronic Phase Shifter	
D. Electronically Scanned Antenna Arrays	
III. RESULTS.....	124
IV. CONCLUSIONS AND RECOMMENDATIONS.....	125
REFERENCES.....	128

LIST OF TABLES

1.	Insertion Loss and Voltage Standing Wave Ratio Measurements for Various Phase Shifts.....	54
----	--	----

## LIST OF FIGURES

1.	Block Diagram of the AROD Antenna System.....	5
2.	The Coordinate System.....	6
3.	A Four Element Array of Isotropic Antennas.....	8
4-a	The Direction Finding Antenna and Its Image.....	17
4-b	A Photograph of the VHF Direction Finder Prototype.....	18
5. - 8.	Directional Characteristics of Received Signal.....	19 - 22
9.	Half-Wave Dipole Pattern Factor.....	23
10.	Horizontal and Vertical Image Array Factors, $h = \lambda/4$ ...	25
11.	Null Angles as a Function of Antenna Height.....	26
12.	The VHF Direction Finding System.....	29
13.	The Digital Switching System.....	32
14.	System Clock.....	33
15.	An Output Hold Circuit.....	33
16-a	Three-bit Switched Line Phase Shifter.....	38
16-b	Periodically Loaded Transmission Line Phase Shifter....	38
17.	A Schematic of the Hybrid Ring.....	41
18.	A PIN-Diode Equivalent Circuit.....	46
19a,b	Phase and Loss Characteristics of (a) $180^\circ$ , (b) $90^\circ$ Phase Bits.....	51
20a,b	Phase and Loss Characteristics of (a) $45^\circ$ , (b) $22.5^\circ$ Phase Bits.....	52
21.	A Photograph of a Four Bit, Hybrid Phase Shifter.....	53

22a,b	Diode in (a) Forward State, (b) Reverse State.....	57
23.	Basic Circuit of Transistor Switch.....	60
24.	Circuit Diagram of Driver for One Bit of Phase Shifter.	63
25.	Circuit Diagram for Two Volt Bias Supply.....	64
26.	A Photograph of the Driver and Phase Shifter.....	68
27.	Waveform and Driver Input of Two Typical Phase Shifts..	68
28.	A Block Diagram of the Circuit Employed for Testing the Driver as a Phase Shifter.....	69
29.	Rise Time Waveforms.....	70
30.	Fall Time Waveforms.....	71
31.	A Photograph of the 36 Element, Crossed Slot Receiving Array.....	73
32.	6 x 6 Array Dimensions.....	74
33.	Array Geometry.....	75
34.	A Simplified Array Consisting of Parallel Slots.....	80
35.	A Hemisphere Showing a Plot of Beam Pointings.....	83
36. - 42.	The Azimuth Pattern of the $E_{\phi}$ Component for the 36 Element Array for Various Values of L and M...86 - 92	
43.	Single Slot Geometry.....	96
44.	The Geometry for Two Parallel Slots that are $\lambda/2$ in Length.....	100
45.	Crossed Slot Geometry.....	103
46.	Variation of the $E_{\theta}$ Component in the $\phi = 0^{\circ}$ Plane .....	109
47.	Variation of the $E_{\phi}$ Component in the $\phi = 0^{\circ}$ Plane .....	110
48.	Measured Resonant Frequency Versus the Frequency .....	111
	of Occurrence	
49.	Resonant Frequency Shift Versus Depth of Tuning Screw..	112

50.	The Average Value of $E_{\phi}$ .....	115
51.	A Photograph of a Single Crossed-Slot Antenna.....	116
52.	A Photograph of a Four Element Crossed Slot Array.....	116
53.	A Combined Polarization Pattern of Two Linear Polarized Sources (Equal Amplitudes).....	117
54.	A Combined Polarization Pattern of Two Linear Polarized Sources (3 db Amplitude Mismatch).....	118
55.	Polarization Pattern of the 36 Elements Receiving Array for the $L = 0, M = 0$ Beam Pointing.....	119
56.	A 36-way power Divider Employing Seven 6-way Power Dividers.....	121
57.	Hybrid Ring Configuration for 6-way Power Divider.....	122
58.	Photograph of the 6-way Power Divider.....	122

## SUMMARY

The scope of work for Contract NAS8-11251 included the development of requirements, design, and fabrication and testing of an antenna system suitable for use with AROD transponder stations.

A suitable design was determined to consist of a direction finding device coupled with the required logic to electronically scan an antenna array.

Initial work began with the evaluation of a commercial circularly polarized antenna for use as a tracking element. Development then began on an elliptically polarized antenna to be used as an element in a direction finding array. More recent work has ended in the development of a direction finding array employing crossed dipoles as the array elements.

The tracking array requires the use of logic circuitry in order to employ the direction finder information. This circuitry allows the various antenna elements of the scanning array to be fed with a signal of the proper phase. The beam of the tracking antenna is scanned by changing the phase of the input signal to the individual elements which make up the array.

A prototype of a phase shifting device and a solid-state driver to activate this device were developed and constructed



A program was devised to compute the antenna pattern of the scanning array for various scan angles using an IBM 7040 digital computer. This program includes the effects of mutual coupling between the antenna elements. This study is the subject of Technical Report Number 4.

Five technical reports were completed under contract NAS8-11251.

## I. INTRODUCTION

E.R. Graf, C.C. Carroll, H.P. Neff, Jr., R.J. Coleman  
J.W. Rogers, J.L. Hilburn, P. Johnson, Jr., and W.F. Hayes

Contract NAS8-11251 was the result of a technical proposal submitted to the George C. Marshall Space Flight Center. The Electrical Engineering Department of Auburn University, under the auspices of the Auburn Research Foundation, proposed to conduct studies pertaining to a prototype antenna system to be used with AROD transponder stations.

Due to the complexity of the entire system the following discussion is presented in component parts. The system is as follows:

(A) Direction Finding System - The system consists of a direction finder antenna and the associated electronics necessary to measure the phase of an incoming signal. The antenna ideally should be omni-directional and able to respond to a signal of any polarization. A prototype model consisting of four crossed-dipole elements located at an optimum position above a ground plane approaches the desired characteristics.

(B) Switching System or Logic - A logic network is required to convert the output of the direction finding system to a form which is usable by the electronic scanning array. The information from the direction finder is digitized through an analog to digital converter. This provides eight digital inputs, represented in an appropriate binary code, to a basic combinational switching network. The switching

network provides 140 digital outputs that switch the electronically scanned antenna phasing devices.

(C) Phase Shifter - The phase of each subradiator in the scanning array will be controlled by a phase shifter. The phase shifter is digital and produces a total phase shift of  $360^{\circ}$  in  $22.5^{\circ}$  increments. A prototype model employs transmission line segments terminated in diodes. A phase reference is determined by a single state of the diode. A phase differential is obtained by changing the state of the diode. This changes the reflection coefficient and produces a discrete phase shift. The prototype employs PIN type diodes in a printed strip line configuration.

A solid-state driver is employed to provide the necessary bias to change the state of the diode.

(D) Electronically Scanned Antenna Arrays - The tracking antenna will actually consist of two antennas; a receiving array operating at a center frequency of 2.214 GHz with a 30MHz bandwidth and a transmitting array with 1.80 GHz as the center frequency with a 30 MHz bandwidth. A digital computer has been used to study the beam shape for various pointings. The prototype antenna consists of thirty six elements. Each element is a crossed-slot, cavity backed antenna phased to give circular polarization when the array is in the in-phase condition. The single element or subradiator of the array achieves elliptical polarization with only one input to the cavity by the use of a parasitic feed coupled to the input.

## II. THEORETICAL DISCUSSION

The theoretical discussion is submitted in the following parts:

- A. Direction Finding System
- B. Digital Switching System
- C. Electronic Phase Shifter
- D. Electronically Scanned Antenna Arrays

## A. Direction Finding System

### 1. The System in General

The purpose of the direction finding system under development is to measure the direction of arrival of an incoming signal. This is to be accomplished by electronic means.

The direction finding antenna is an array of dipole elements. The direction of the incoming signal is determined by measuring the phase difference of the received signal at selected elements in the array. It is necessary to examine the antenna pattern to establish the receiving properties of the array. The array consists of four elements. These elements are composed of two crossed dipole antennas. The crossed elements are necessary for the array to respond to a signal of any polarization. The array may be thought of as composed of two parts; a vertical array of dipoles, and a horizontal array of similar antennas. A matrix system of phase lines allows the desired signal to be extracted from the antenna array. The signals obtained are voltages with associated phase angles. These are proportional to the direction cosines of the signal arriving at the array.

### 2. Theory

An ideal direction finding antenna for the system under development would possess a hemispherical radiation pattern and respond equally well to both  $\theta$  and  $\phi$  polarization. This is necessary since

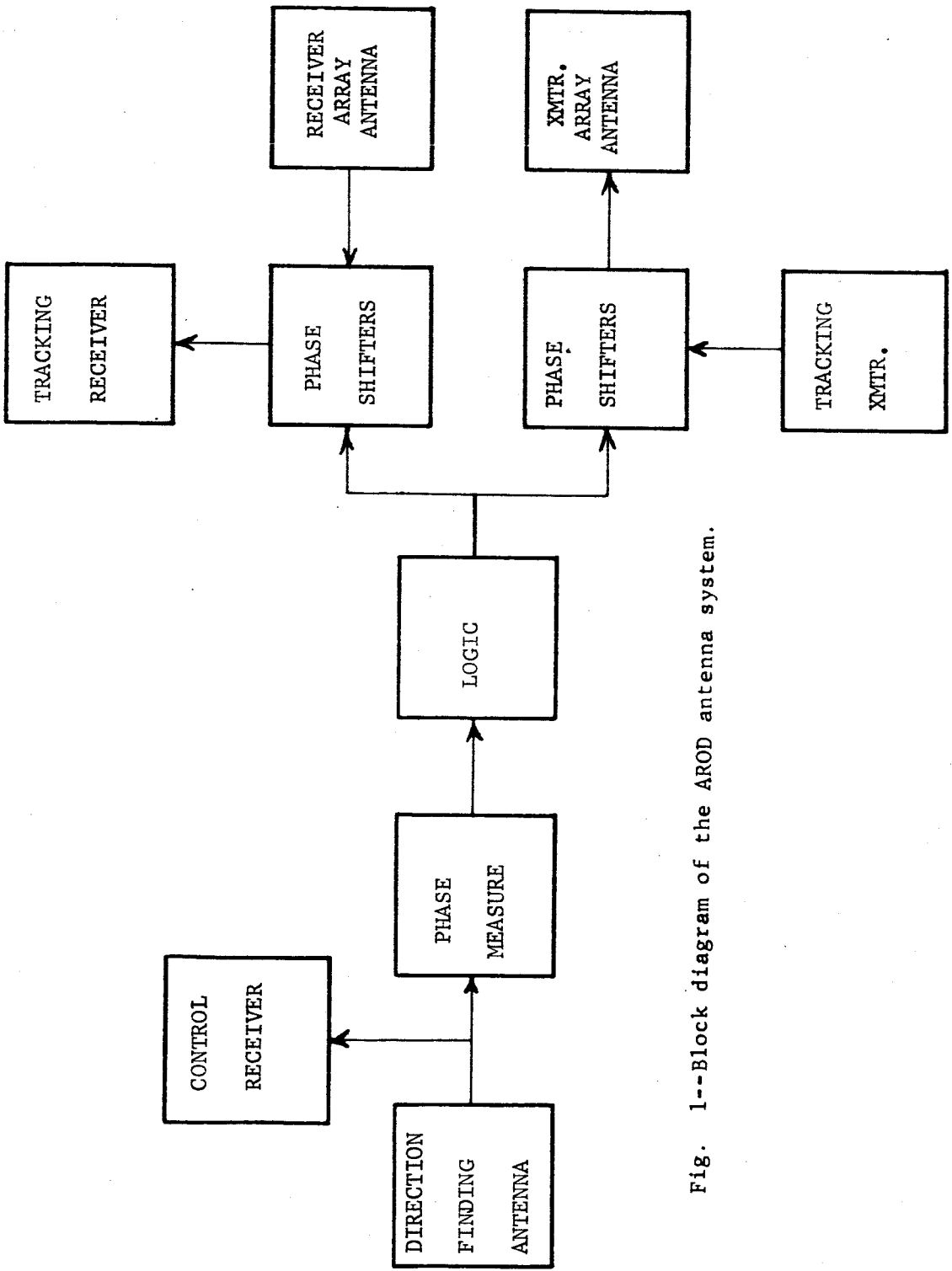


Fig. 1--Block diagram of the AROD antenna system.

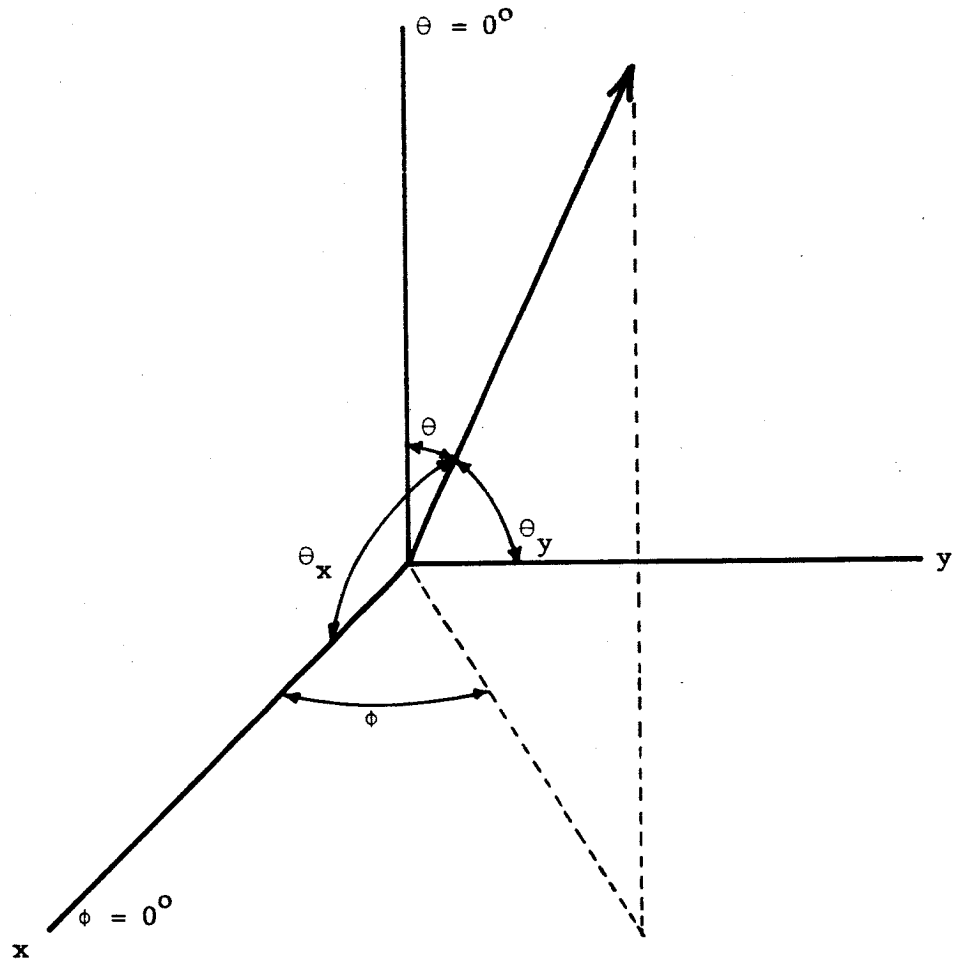


Fig. 2--The coordinate system.

the received signal will, in general, exhibit both of the aforesaid polarizations.

The receiving characteristics of the antenna may be obtained by consideration of the antenna as a transmitting element. The far-zone radiation field is composed of two parts,

$$E_{\theta} = -j\omega\mu \left[ A_x \cos\theta \cos\phi + A_y \cos\theta \sin\phi - A_z \sin\theta \right] \quad (1)$$

and

$$E_{\phi} = -j\omega\mu \left[ -A_x \sin\phi + A_y \cos\phi \right]. \quad (2)$$

The receiving characteristics are seen to depend on the polarization and magnetic vector components  $A_x$ ,  $A_y$  and  $A_z$ .

The theory of the direction finding array may be arrived at by consideration of a four element array of point sources as shown in Figure 3. The following system of simultaneous equations describes the array.

$$\begin{aligned} V_1 &= f_1(\theta, \phi) e^{jk a \cos\theta_x} = I_1 Z_{11} + I_2 Z_{12} + I_3 Z_{13} + I_4 Z_{12} \\ V_2 &= f_2(\theta, \phi) e^{jk a \cos\theta_y} = I_1 Z_{12} + I_2 Z_{11} + I_3 Z_{12} + I_4 Z_{13} \\ V_3 &= f_3(\theta, \phi) e^{-jk a \cos\theta_x} = I_1 Z_{13} + I_2 Z_{12} + I_3 Z_{11} + I_4 Z_{12} \\ V_4 &= f_4(\theta, \phi) e^{-jk a \cos\theta_y} = I_1 Z_{12} + I_2 Z_{13} + I_3 Z_{12} + I_4 Z_{11} \end{aligned} \quad (3)$$



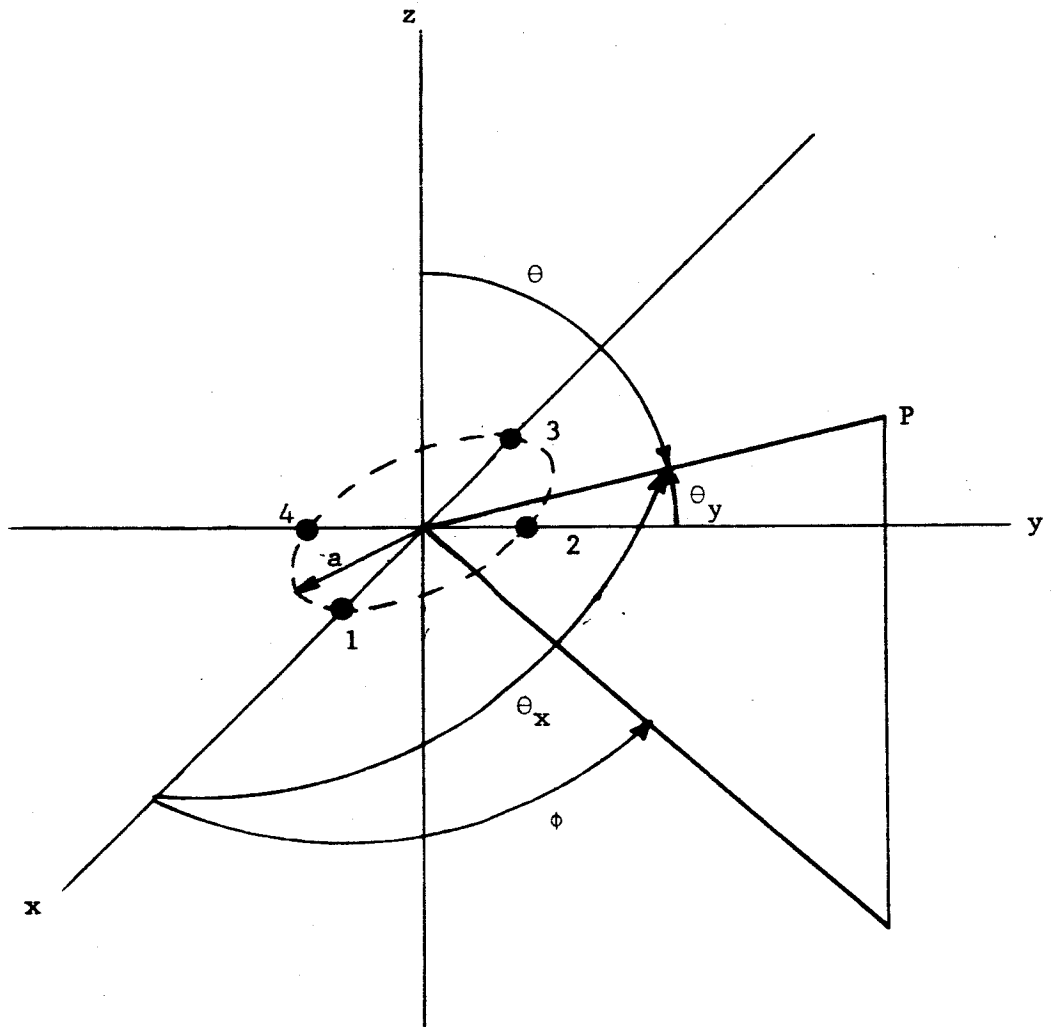


Fig. 3 --A four element array of isotropic antennas.

In these equations  $Z_{11}$  is the sum of the self impedance of each element and the input impedance to the line,  $Z_{12}$  is the mutual impedance between one element and its nearest adjacent antenna, and  $Z_{13}$  is the mutual impedance between one element and the element diametrically opposite. The individual elements of the array must be in the same environment for the system equations above to be valid.

The conditions

$$f_2(\theta, \phi) = f_1(\theta, \phi + \frac{\pi}{2}) \quad (4)$$

$$f_3(\theta, \phi) = f_1(\theta, \phi + \pi) \quad (5)$$

$$f_3(\theta, \phi) = f_1(\theta, \phi + \frac{3\pi}{2}) \quad (6)$$

satisfy this requirement.

In equations (3)<sup>1</sup>

$$k \cos \theta_x = -c\ell \quad (7)$$

$$k \cos \theta_y = -cm \quad (8)$$

where  $c = 12.8^\circ$ . This is determined from the properties of the scanning array. The integers  $\ell$  and  $m$  vary between  $\pm 7$  and govern the beam pointing. Equations (7) and (8) may be substituted into

equations (3). Inspection of these equations reveals  $\ell$  and  $m$  appear as phase angles (with a scale factor  $C$ ) on the antenna terminal voltages. The quantities to be measured include the mutual impedance, but if the elements are identical the equations may be uncoupled. The scheme for accomplishing this depends on forming the sequence voltages  $V_R^{(0)}$ ,  $V_R^{(1)}$  and  $V_R^{(2)}$ . In this notation the superscript indicates the sequence number.

The zero sequence,  $V_R^{(0)}$ , is formed by summing all the terminal voltages across a common load,  $R$ , through equal length transmission lines. This gives:

$$V_R^{(0)} = [I_1 + I_2 + I_3 + I_4] R, \text{ and} \quad (9)$$

$$V [f_1 e^{-jcl} + f_2 e^{-jcm} + f_3 e^{jcl} + f_4 e^{jcm}] = \quad (10)$$

$$[I_1 + I_2 + I_3 + I_4] [Z_{11} + 2Z_{12} + Z_{13}]$$

$$V_R^{(0)} = \frac{VR}{Z_{11} + 2Z_{12} + Z_{13}} [f_1 e^{-jcl} + f_2 e^{-jcm} + f_3 e^{jcl} + f_4 e^{jcm}] \quad (11)$$

The zero sequence impedance,  $Z^{(0)}$ , is defined as:

$$Z^{(0)} = Z_{11} + 2Z_{12} + Z_{13} = |Z^{(0)}| e^{j\phi_0} \quad (12)$$

A consequence of this is

$$V_R^{(0)} = \frac{VR}{|Z^{(0)}|} e^{-j\phi_0} \left[ f_1 e^{-jcl} + f_2 e^{-jcm} + f_3 e^{jcl} + f_4 e^{jcm} \right]. \quad (13)$$

The one-sequence,  $V_R^{(1)}$ , is formed by adding at a common resistance,  $R$ , the antenna voltage  $V_1$ , the antenna voltage  $V_2$  through a  $\frac{3\lambda}{4}$  line, the antenna voltage  $V_3$  through a  $\frac{\lambda}{2}$  line and the antenna voltage  $V_4$  through a  $\frac{\lambda}{4}$  line. This gives

$$V_R^{(1)} = V_1 + jV_2 - V_3 - jV_4.$$

In a similar manner,

$$V_R^{(2)} = V_1 - V_2 + V_3 - V_4, \text{ and}$$

$$V_R^{(3)} = V_1 - jV_2 - V_3 + jV_4.$$

When the indicated operations are carried out, the result is

$$V_R^{(0)} = \frac{VR}{|Z^{(0)}|} e^{-j\phi_0} \left[ f_1 e^{-jcl} + f_2 e^{-jcm} + f_3 e^{jcl} + f_4 e^{jcm} \right]$$

$$V_R^{(1)} = \frac{VR}{|Z^{(1)}|} e^{-j\phi_1} \left[ f_1 e^{-jcl} + jf_2 e^{-jcm} - f_3 e^{jcl} - jf_4 e^{jcm} \right]$$

$$V_R^{(2)} = \frac{VR}{|Z^{(2)}|} e^{-j\phi_2} \left[ f_1 e^{-jcl} - f_2 e^{-jcm} + f_3 e^{jcl} - f_4 e^{jcm} \right] \quad (14)$$

$$V_R^{(3)} = \frac{VR}{|Z^{(3)}|} e^{-j\phi_3} \left[ f_1 e^{-jcl} - jf_2 e^{-jcm} - f_3 e^{jcl} + jf_4 e^{jcm} \right]$$

$$Z^{(0)} = Z_{11} + 2Z_{12} + Z_{13} = |Z^{(0)}| e^{j\phi_0}, \quad (15)$$

$$Z^{(1)} = Z_{11} - Z_{13} = |Z^{(1)}| e^{-j\phi_1}, \quad (16)$$

$$Z^{(2)} = Z_{11} - 2Z_{12} + Z_{13} = |Z^{(2)}| e^{-j\phi_2}, \text{ and} \quad (17)$$

$$Z^{(3)} = Z^{(1)}. \quad (18)$$

Thus, by using phased transmission lines and simple passive combiners it is possible to form the sequence voltages and uncouple the system equations. There is one step remaining before the sequence voltages may be utilized to obtain  $\ell$  and  $m$ . The presence of the sequence impedance in each of the sequence voltages makes the coefficient,  $\frac{VR}{|Z^{(n)}|} e^{-j\phi_n}$  unequal for  $n = 0, 1, 2$  and  $3$ . This difficulty may be removed by a simple normalization process.

The normalized sequence voltages may now be written:

$$\begin{aligned}
V_{RN}^{(0)} &= f_1 e^{-jcl} + f_2 e^{-jcm} + f_3 e^{jcl} + f_4 e^{jcm} \\
V_{RN}^{(1)} &= f_1 e^{-jcl} + jf_2 e^{-jcm} - f_3 e^{jcl} - jf_4 e^{jcm} \\
V_{RN}^{(2)} &= f_1 e^{-jcl} - f_2 e^{-jcm} + f_3 e^{jcl} - jf_4 e^{jcm} \\
V_{RN}^{(3)} &= f_1 e^{-jcl} - jf_2 e^{-jcm} - f_3 e^{jcl} + jf_4 e^{jcm} .
\end{aligned} \tag{19}$$

The voltages for determining  $l$  and  $m$  are now formed in a manner similar to that used in forming the sequence voltages, that is,

$$V_l = \left[ V_{RN}^{(0)} - V_{RN}^{(1)} + V_{RN}^{(2)} - V_{RN}^{(3)} \right], \quad \text{or} \tag{20}$$

$$V_l = 4f_3(\theta, \phi) e^{jcl}, \quad \text{and} \tag{21}$$

$$V_l = \left[ V_{RN}^{(0)} + jV_{RN}^{(1)} - V_{RN}^{(2)} - jV_{RN}^{(3)} \right], \quad \text{or} \tag{22}$$

$$V_m = 4f_4(\theta, \phi) e^{jcm} . \tag{23}$$

A reference signal for phase measurements is needed, and in this case  $V_{RN}^{(0)}$  may be used, therefore,

$$V_{\text{ref}} = V_{RN}^{(0)} = f_1 e^{-jcl} + f_2 e^{-jcm} + f_3 e^{jcl} + f_4 e^{jcm} \tag{24}$$

The three terminal voltages are,

$$V_{\text{ref}} = V_{\text{RN}}^{(0)}$$

$$V_{\ell} = 4f_3 e^{jc\ell}, \text{ and} \quad (25)$$

$$V_m = 4f_4 e^{jcm}.$$

A phase measuring device will now measure  $c\ell$  and  $cm$ . This is the basic scheme of direction finding by a phase measurement.

The problem now becomes one of determining a suitable antenna to use in place of the hypothetical isotropic radiator. A dipole was chosen as the array element. In the vertical position this element will not respond to  $\phi$  polarization and will have a null at  $\theta = 0$  since the pattern factor for the dipole is

$$f_1(\theta, \phi) = \frac{\cos\left(\frac{\pi}{2} \cos\theta\right)}{\sin\theta}. \quad (26)$$

The addition of a horizontal ring of dipole elements will allow the array to respond to  $\phi$  polarization. The problem caused by the dipole factor may not be solved, due to certain properties of the array. (2)

The lack of signal along the polar axis ( $\theta = 0$ ) may be used if properly interpreted by the phase measuring equipment. An array

which appears to incorporate the best features of this type system is shown in Figure 4 . The horizontal part is a four element array of dipoles with their feed points at the same locations as those of the vertical elements.

The system equations previously developed hold, with the exception that the angular dependence of each element (element factor) will have to be substituted into the set.

The sequence voltages may now be formed. The equations are normalized and recombined to yield the following results.

Case I.  $\theta$  Polarization

$$V_{\text{ref},v} = \frac{2\cos(\pi/2\cos\theta)}{\sin\theta} \left[ \cos(\pi/2\sin\theta\cos\phi) + \cos(\pi/2\sin\theta\sin\phi) \right]$$

$$V_{l,v} = \frac{4\cos(\pi/2\cos\theta)}{\sin\theta} e^{jcl} \quad (27)$$

$$V_{m,v} = \frac{4\cos(\pi/2\cos\theta)}{\sin\theta} e^{jcm}$$

$$V'_{\text{ref},h} = 2j \left[ \frac{\cos\theta\sin\phi\cos(\pi/2\sin\theta\sin\phi)\sin(\pi/2\sin\theta\cos\phi)}{1 - \sin^2\theta\sin^2\phi} \right. \\ \left. - \frac{\cos\theta\cos\phi\cos(\pi/2\sin\theta\cos\phi)\sin\pi/2(\sin\theta\sin\phi)}{1 - \sin^2\theta\cos^2\phi} \right] \quad (28)$$

$$V'_{l,h} = \frac{4\cos\theta\sin\phi\cos(\pi/2\sin\theta\sin\phi)}{1 - \sin^2\theta\sin^2\phi} e^{jcl}$$

$$V'_{m,h} = \frac{-4\cos\theta\cos\phi\cos(\pi/2\sin\theta\cos\phi)}{1 - \sin^2\theta\cos^2\phi} e^{jcm}$$



Case II.  $\phi$  Polarization

$$V_{\text{ref},h} = 2j \left[ \frac{\cos\phi \cos(\pi/2 \sin\theta \sin\phi) \sin(\pi/2 \sin\theta \cos\phi)}{1 - \sin^2\theta \sin^2\phi} + \frac{\sin\phi \cos(\pi/2 \sin\theta \cos\phi) \sin(\pi/2 \sin\theta \sin\phi)}{1 - \sin^2\theta \cos^2\phi} \right] \quad (29)$$

$$V_{\ell,h} = \frac{4 \cos\phi \cos(\pi/2 \sin\theta \sin\phi)}{1 - \sin^2\theta \sin^2\phi} e^{jc\ell}$$

$$V_{m,h} = \frac{4 \sin\phi \cos(\pi/2 \sin\theta \cos\phi)}{1 - \sin^2\theta \cos^2\phi} e^{jcm}$$

In these equations v and h refer to the vertical and horizontal elements respectively. Figures 5 thru 8 demonstrate the directional characteristics of the required signal. The ordinary dipole pattern factors  $V_{\ell v}$  and  $V_{mv}$  are shown in Figure 9.

The antenna system is subject to degradation by multipath signal. The performance of a phase measuring system is especially susceptible to multipath since it must measure the direction of an incoming signal. The greatest source of multipath signals is usually the ground surrounding the antenna. The magnitude of the multipath signal will vary with the reflection coefficient of the earth surrounding the antenna. A series of experimental test were performed to determine how the reflection coefficient could be reduced by placing absorbent

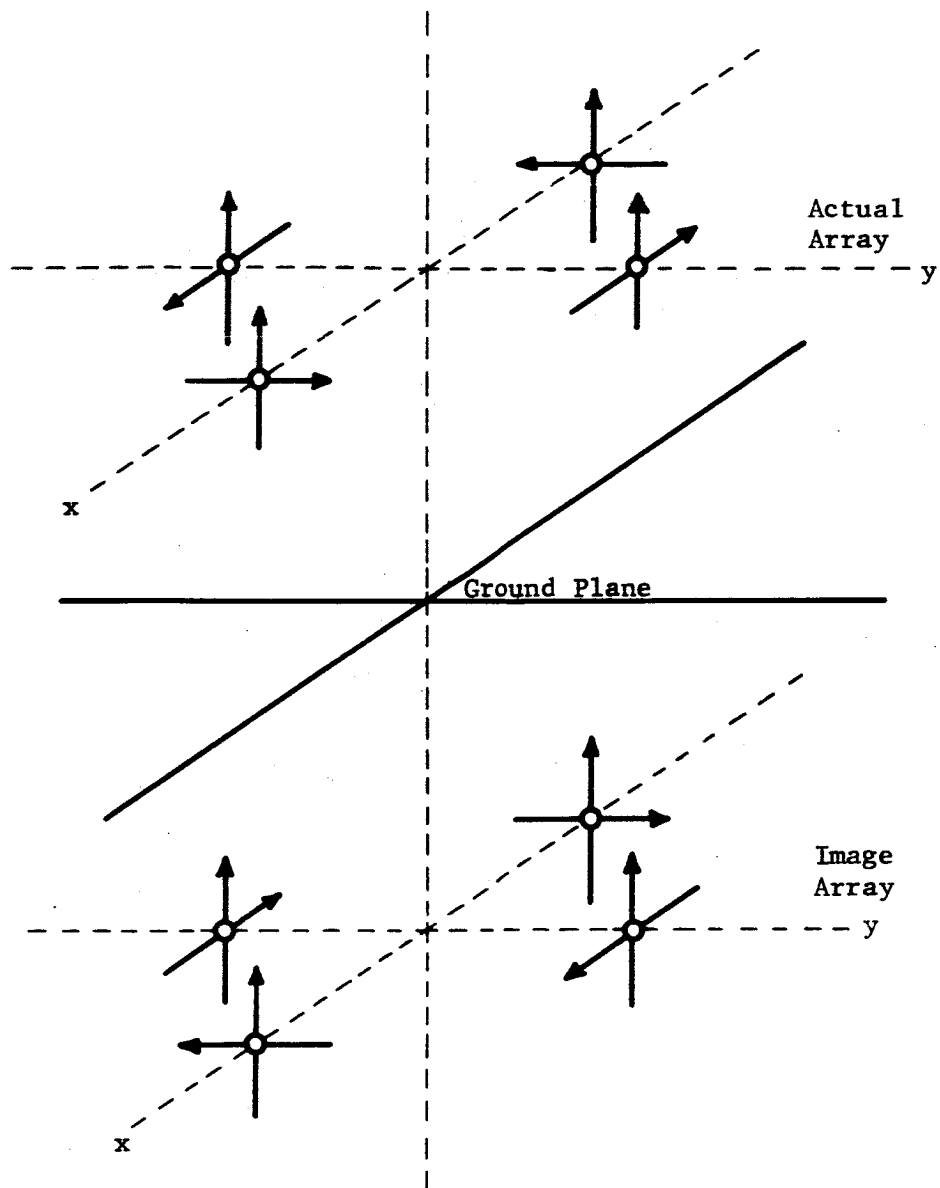


Fig. 4a--The direction finding antenna and its image.



Fig. 4b--Photograph of the VHF direction finder prototype.

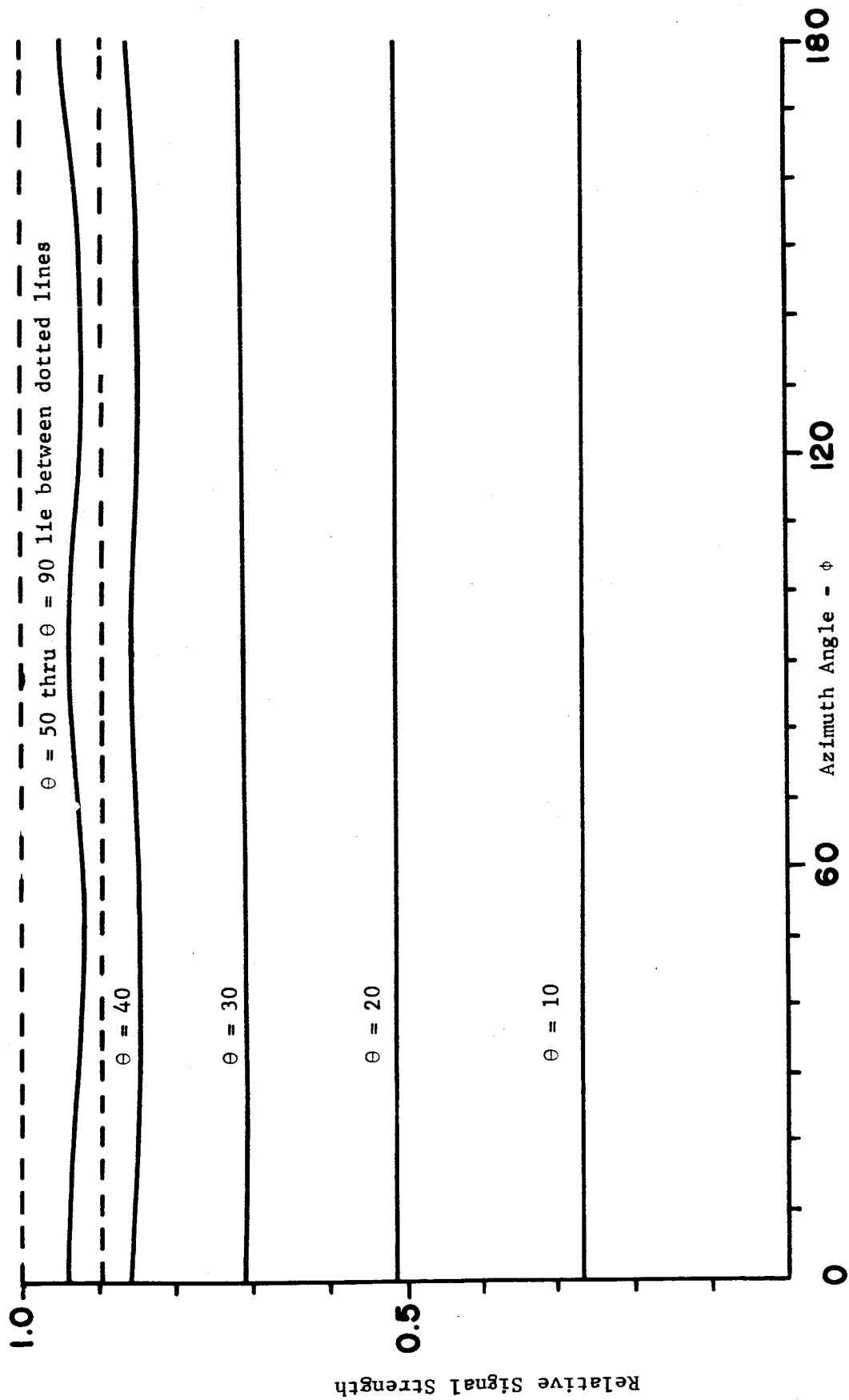


Fig. 5--Directional characteristics of received signal-reference signal from vertical ring,  $V_{ref}, v'$

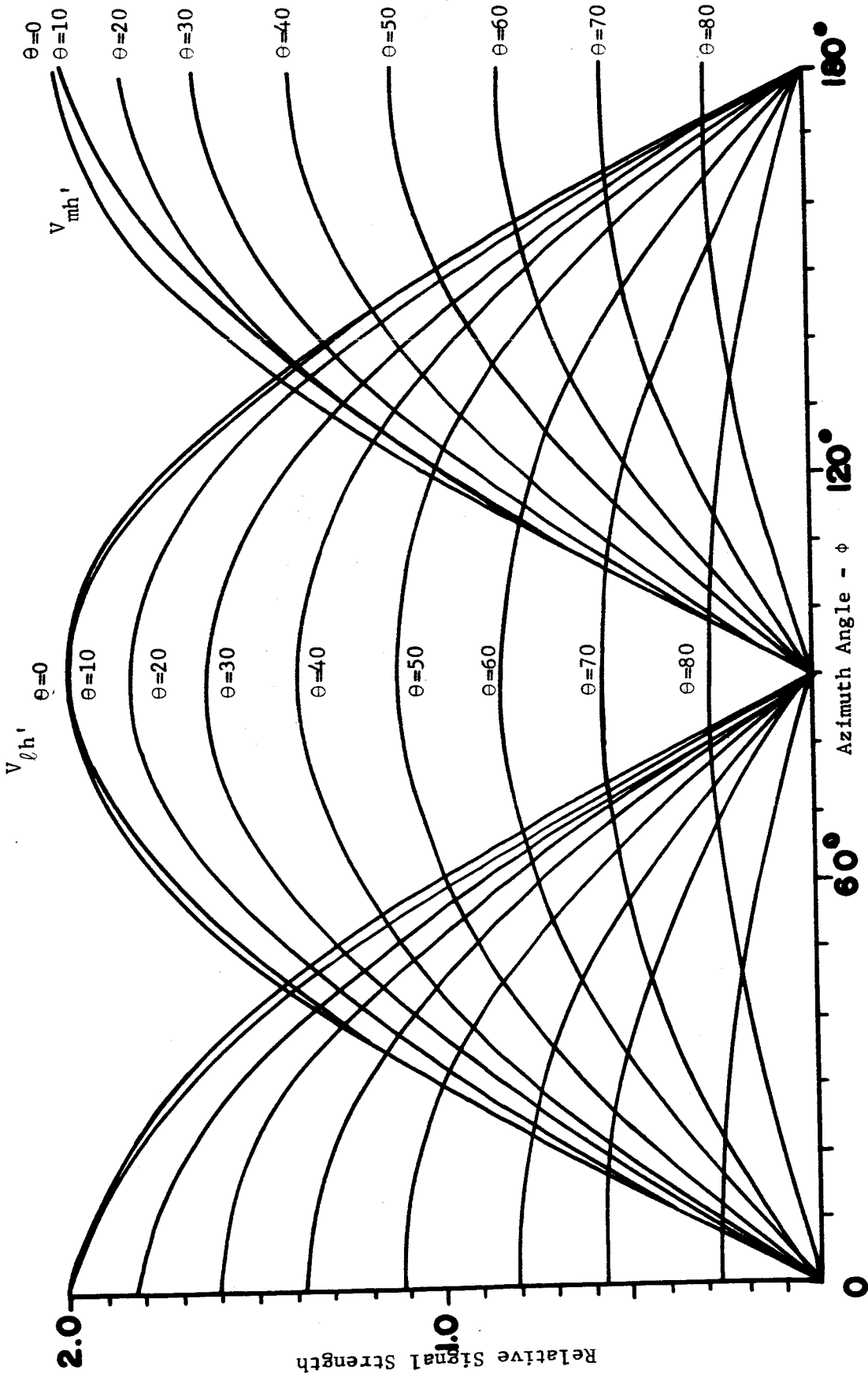


Fig. 6--Directional characteristics of received signal-phase signals from horizontal ring for  $\theta$  polarization  $V'_{oh}$ ,  $V'_{mh}$ .

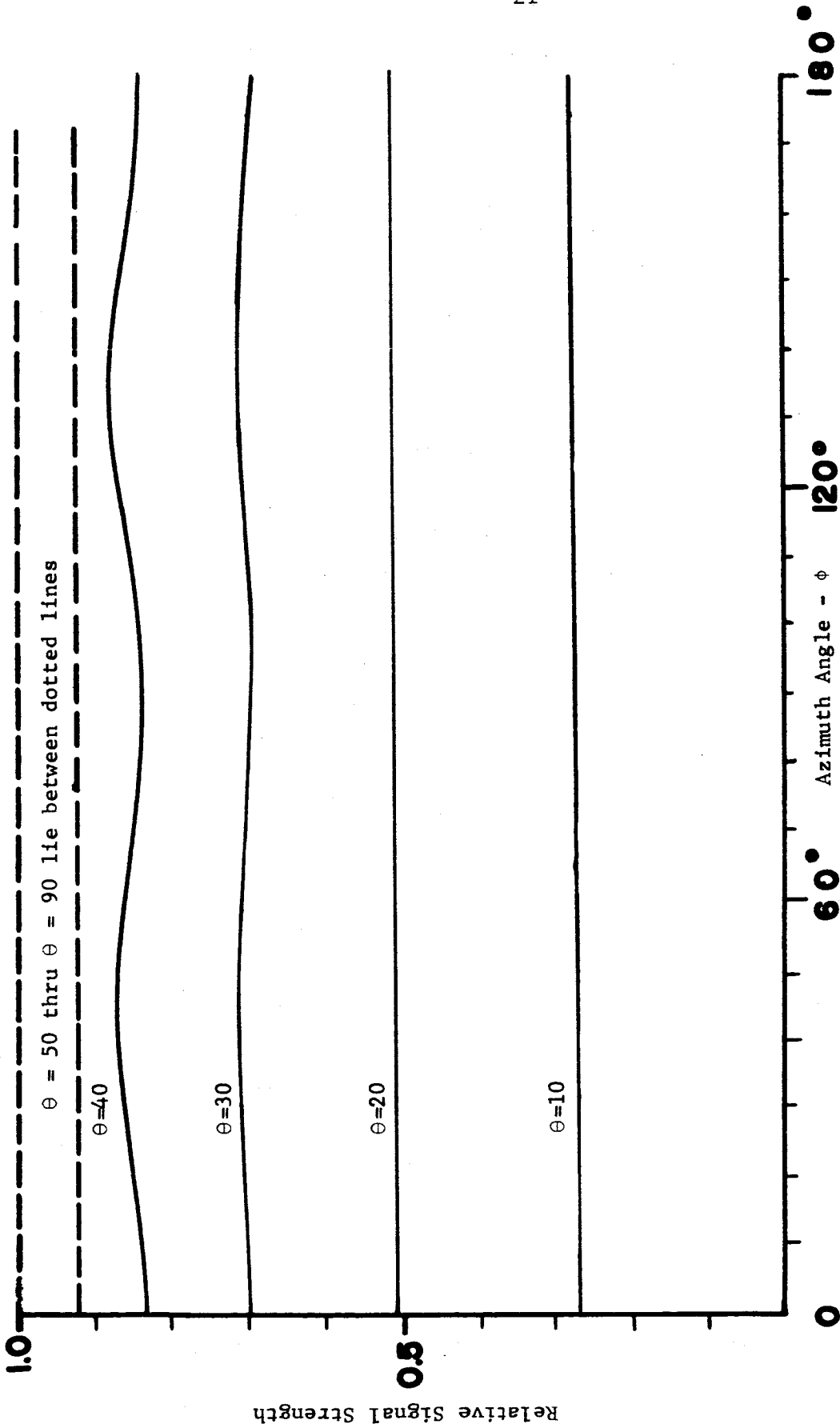


Fig. 7--Directional characteristics of received signal-reference signal from horizontal ring for  $\phi$  polarization -  $V_{ref,h}$ .

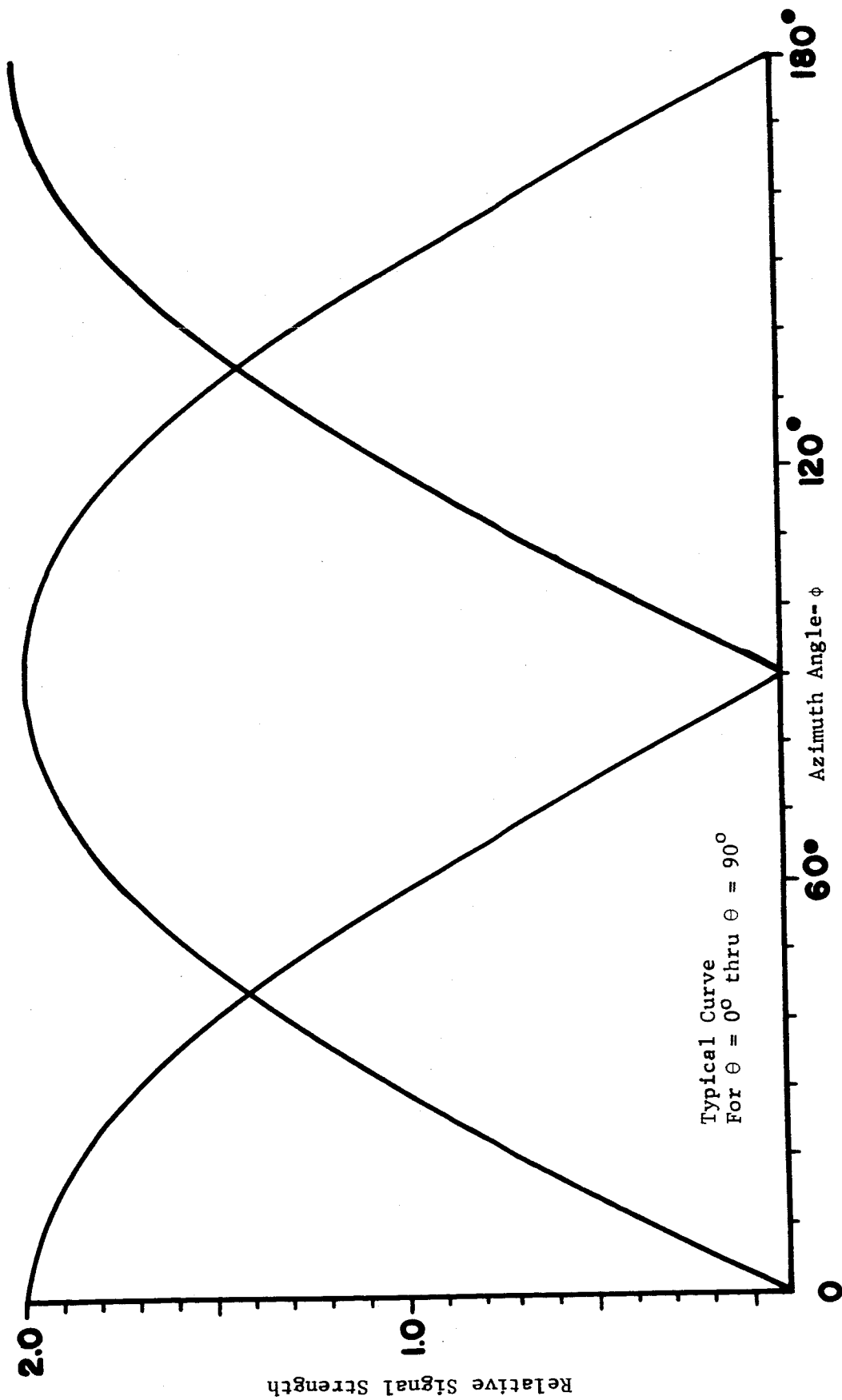
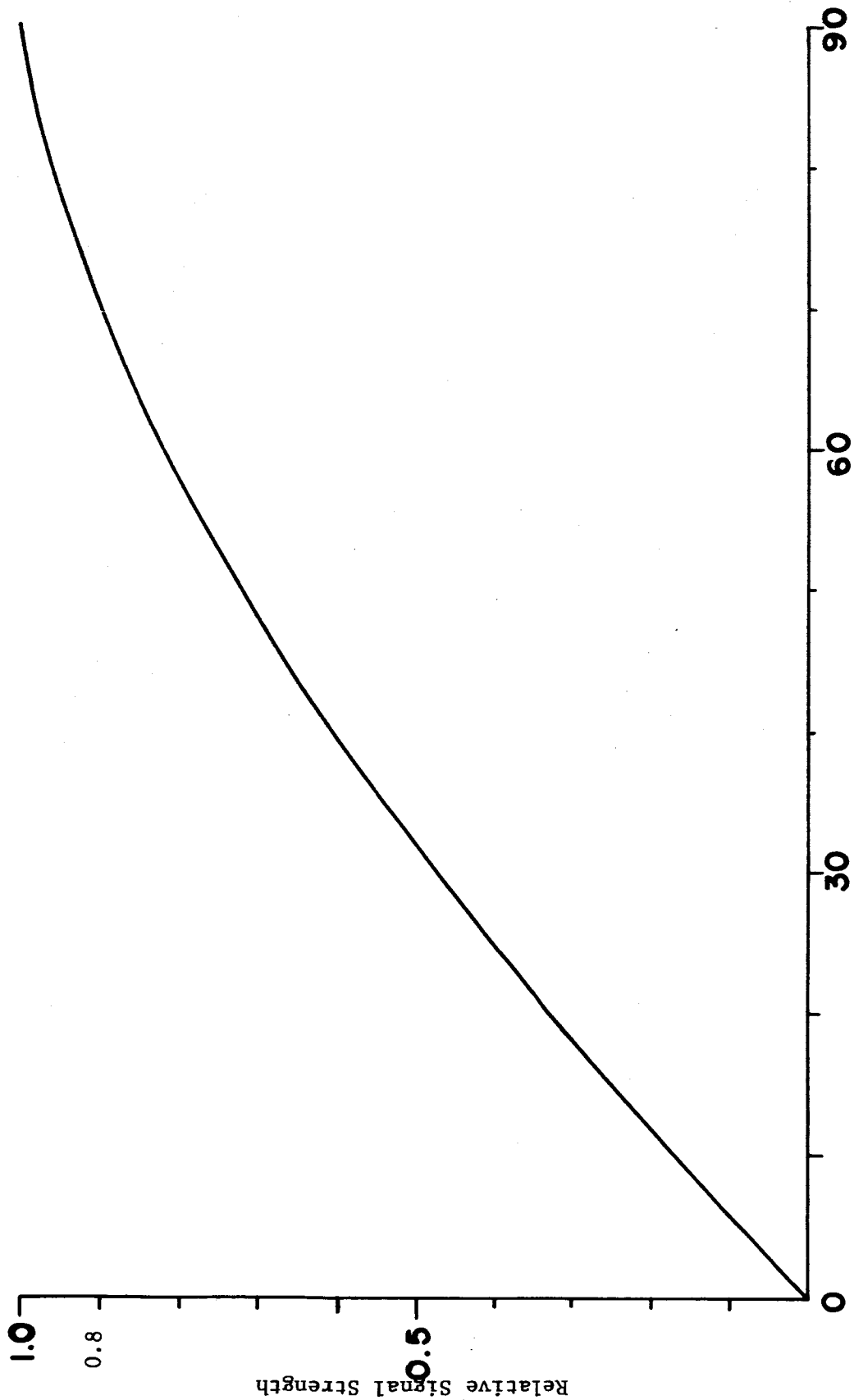


Fig. 8--Directional characteristics of received signal-phase signals from horizontal ring for  $\phi$  polarization -  $V_{\phi h}$ ,  $V_{mh}$ .



Polar Angle -  $\theta$   
Fig. 9 --Half-wave dipole pattern factor



material around the antenna. These test show the reflection coefficient was reduced for some polar angles, but nulls in the radiation patterns occurred at other angles which were not present without the absorbing material.

It was decided the best way to resolve the difficulty in a predictable manner was to build the antenna system above a metallic ground plane. In this manner the reflection coefficient will be known and have a value of approximately unity.

The introduction of the ground plane will result in the forming of a two element array, the D.F. antenna and its image. This effect may be taken into account by multiplying each term in the system equations by an array factor. Figure 10 shows the vertical and horizontal image array factors for  $h = \lambda/4$ . The terms referring to a horizontal element must be multiplied by<sup>3</sup>

$$F_{ih} = 2j\sin(kh\cos\theta)e^{-jkh\cos\theta} \quad (30)$$

and the vertical elements by

$$F_{iv} = 2\cos(kh\cos\theta)e^{jkh\cos\theta}, \quad (31)$$

where  $h$  is the height above the ground plane. Figure 11 shows the angle  $\alpha$  as a function of antenna height above ground. These terms are introduced into equations (27), (28) and (29) accompanied by an angle  $\alpha$ . This angle is used to distinguish the cases of  $\theta$ -polarization and  $\phi$ -polarization. For  $\theta$  polarization alone  $\alpha=0$ , and for  $\phi$ -polarization only,  $\alpha = \frac{\pi}{2}$ . The resulting equations for an antenna height of  $\lambda/4$  are:

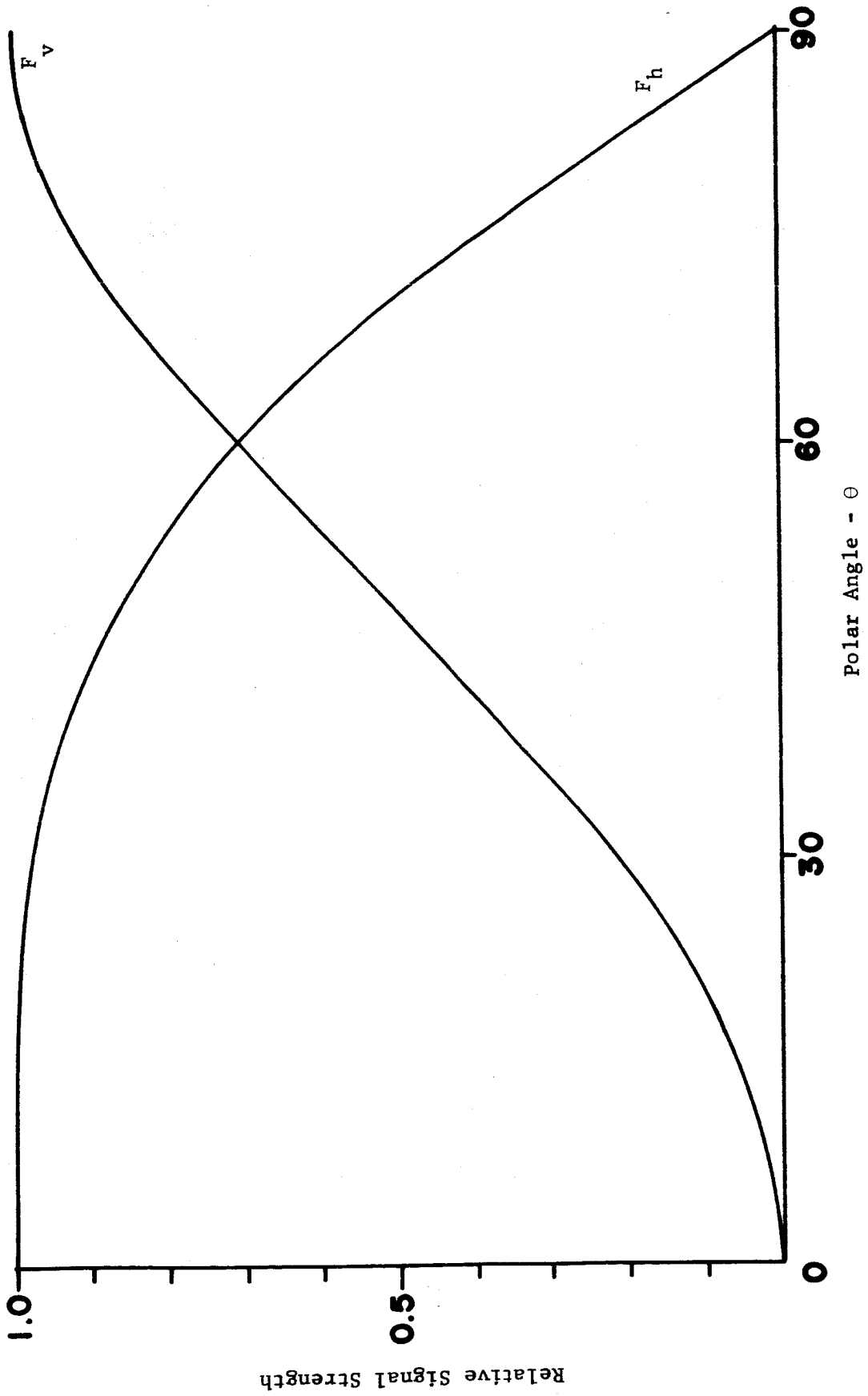


Fig. 10--Horizontal and vertical image array factors,  $h = \lambda/4$ .

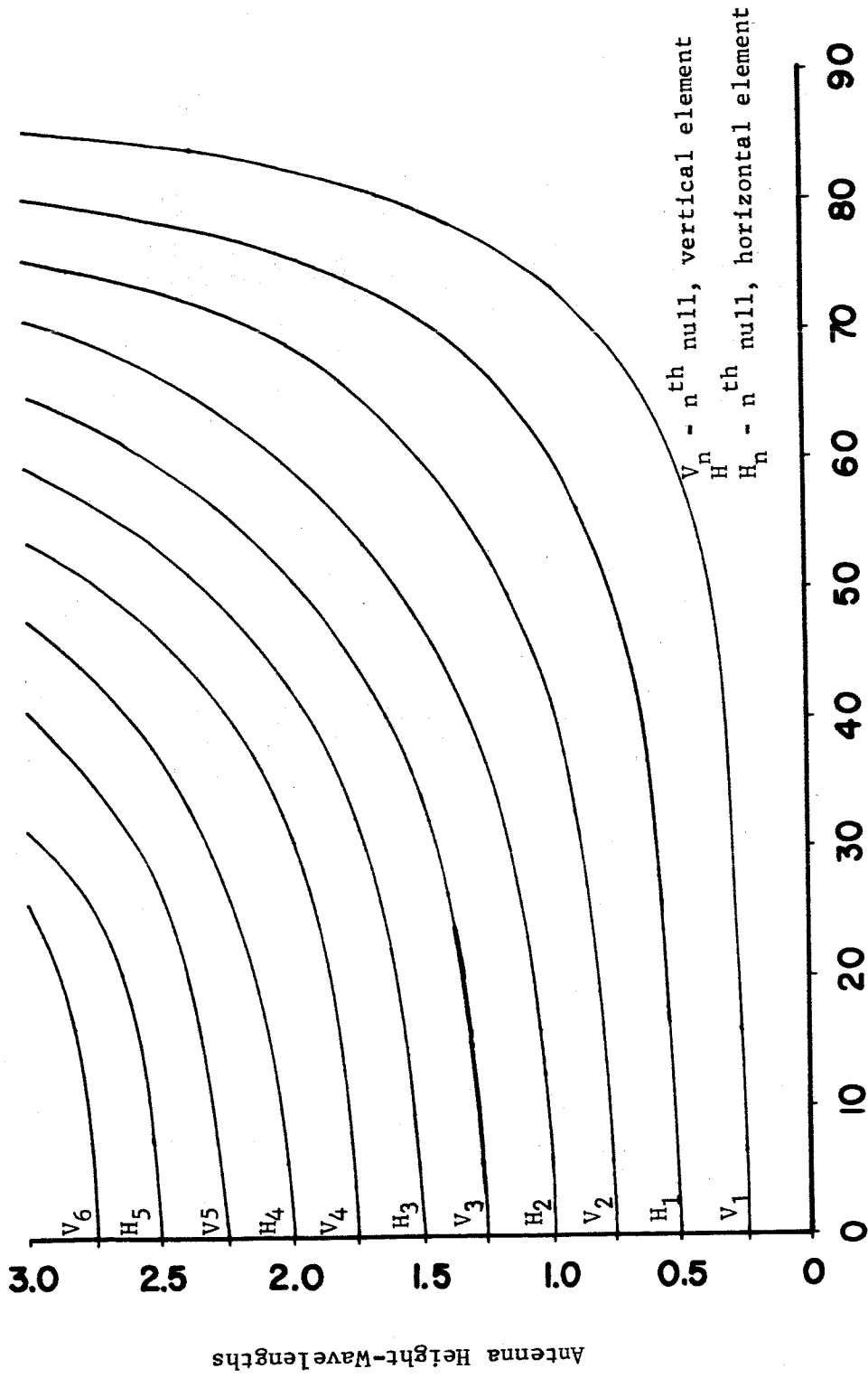


Fig. 11-Null angles as a function of antenna height above a perfectly conducting ground plane for both  $\theta$  and  $\phi$  polarization.

$$\begin{aligned}
 V''_{\text{ref},v} &= 4\cos\alpha\cos(\pi/2\cos\theta)e^{-j\pi/2\cos\theta} V_{\text{ref},v} \\
 V''_{l,v} &= 8\cos\alpha\cos(\pi/2\cos\theta)e^{-j\pi/2\cos\theta} V_{l,v} e^{jcl} \\
 V''_{m,v} &= 8\cos\alpha\cos(\pi/2\cos\theta)e^{-j\pi/2\cos\theta} V_{m,v} e^{jcm}
 \end{aligned} \tag{32}$$

$$\begin{aligned}
 V''_{\text{ref},h} &= -4\sin(\pi/2\cos\theta)e^{-j\pi/2\cos\theta} \left[ \cos\alpha V'_{\text{ref},h} + \sin\alpha V_{\text{ref},h} \right] \\
 V''_{l,h} &= 8j\sin(\pi/2\cos\theta)e^{-j\pi/2\cos\theta} \left[ \cos\alpha V'_{l,n} + \sin\alpha V_{l,h} \right] e^{jcl} \\
 V''_{m,h} &= 8j\sin(\pi/2\cos\theta)e^{-j\pi/2\cos\theta} \left[ \cos\alpha V'_{m,h} + \sin\alpha V_{m,h} \right] e^{jcm}
 \end{aligned} \tag{33}$$

where (32) applies to the ring of vertical elements and (33) applies to the ring of horizontal elements.

An inspection of equations (32) shows that the vertical ring performs as desired. This result obviously occurs due to the fact that the radiation functions are independent of  $\phi$ . Equations (33) are more complicated, requiring the use of a computer. In order to determine the performance of the horizontal ring the equations were calculated with  $\phi$  as the independent variable and with  $\theta$  and  $\alpha$  as parameters.

The direction finding system is also required to furnish a signal for the station control receiver. This signal should be

derived from the particular antenna radiation functions which are independent of direction. In this manner the signal will have a hemispherical characteristic insofar as direction is concerned. Of course, as in any antenna system mounted above a ground plane, there will be a null in the received signal at  $\theta = \pi/2$  for  $\phi$  polarization. The other polarization ( $\theta$ ) will provide a signal at this angle. A combination of the voltages already derived in the system will serve as the station control receiver signal. This is a linear combination of the zero-sequence voltage from the vertical ring and the one-sequence voltage from the horizontal ring. The resulting signal will approximate that described above.

A block diagram of the direction finding system is shown in Figure 12. The signal from each antenna element is amplified in an r.f. amplifier and divided into phase lines and combiners. This is the matrix system which forms the sequence voltages. The sequence voltages are normalized, as mentioned earlier, and then recombined in another matrix system to form the signals whose phase is to be measured. In each case the phase lines are coaxial transmission lines whose lengths differ by one quarter wavelength at the operating frequency (138 MC). The combiners and dividers are actually the same device, constructed from passive elements. Transmission line type diode switches are employed to switch the desired signals into the phase measuring equipment. To insure proper operation of the phase

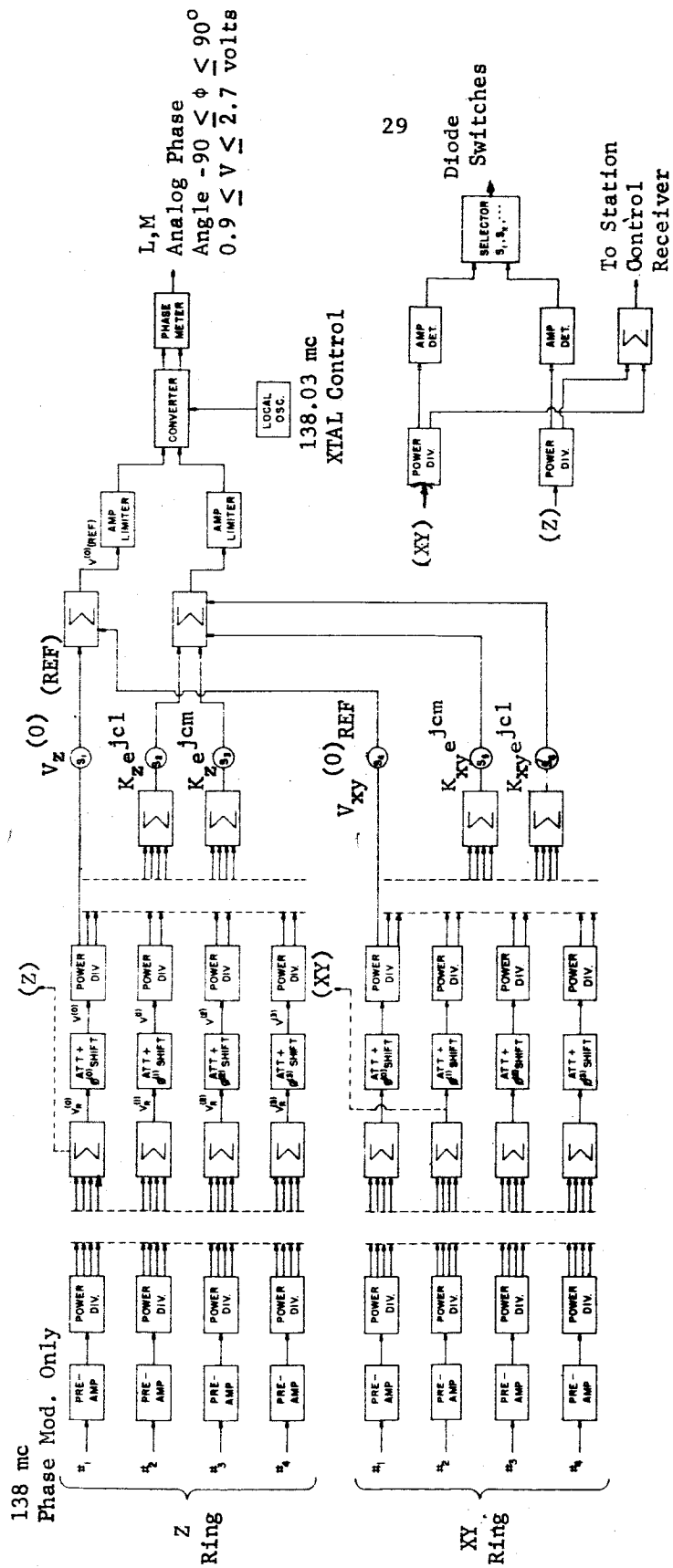


FIG. 12--THE VHF DIRECTION FINDING SYSTEM

measuring equipment, amplifier-limiters are used ahead of the converter. In order to operate at frequencies within the bandwidth of the phase meter, a two-channel converter-local oscillator is employed at this point in the system. The phase meter produces an analog output. The complete system timing is controlled by clock pulses formed in the logic circuitry mentioned elsewhere in this report.

## B. Digital Switching System

### 1. The System in General

The processing of the information from the direction finder to the drivers of the phase-shifting array is accomplished with the use of the digital switching system shown in Figure (13). The quantities  $\ell$  and  $m$  are multiplied in the direction finder so that the output of the phase meter represents their values, alternatingly, with an analog voltage range of 0.0 volts to -1.8 volts. The digitized values of  $\ell$  and  $m$  are produced at the output of the analog-to-digital converter in dc output registers with outputs ABCD and EFGH for  $\ell$  and  $m$  respectively.

With ABCDEFGH as inputs, the combinational switching network provides the  $y_1$  through  $y_{140}$  outputs that are required to control the phase-shifting array. To supply coincident inputs to the phase-shifting array and the required switching time, an output hold network is used with fast switching elements that advances  $Y_1$  through  $Y_{140}$  to  $Z_1$  through  $Z_{140}$ , respectively, with each clock pulse received from the system clock. The values of  $Z_1$  through  $Z_{140}$  are held until new values of  $y_1$  through  $y_{140}$  are available at the output of the combinational switching network. These new values of  $y_1$  through  $y_{140}$  are advanced through the hold network to up-date  $Z_1$  through  $Z_{140}$  coincidentally with the next clock pulse from the system clock.



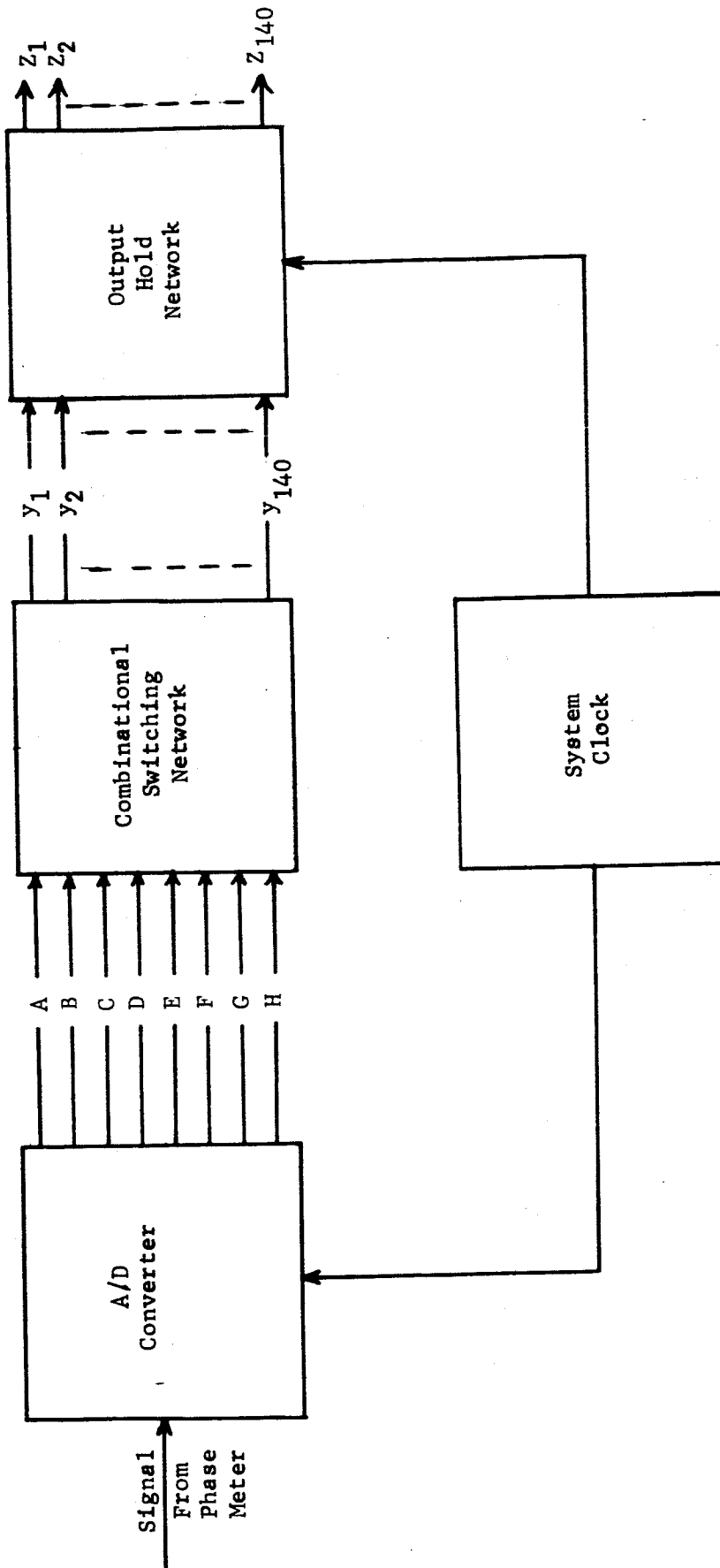


Fig. 13--The digital switching system.

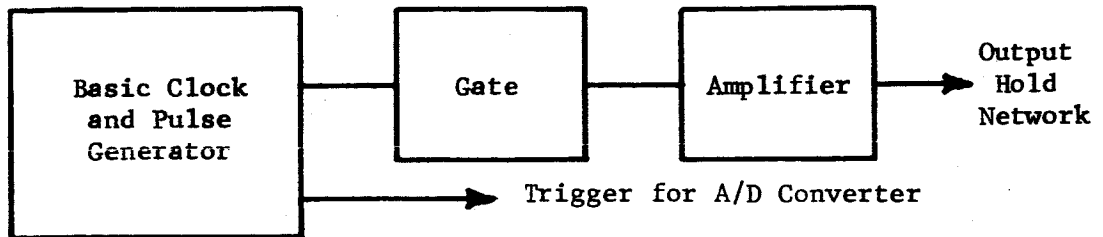


Fig. 14--System clock.

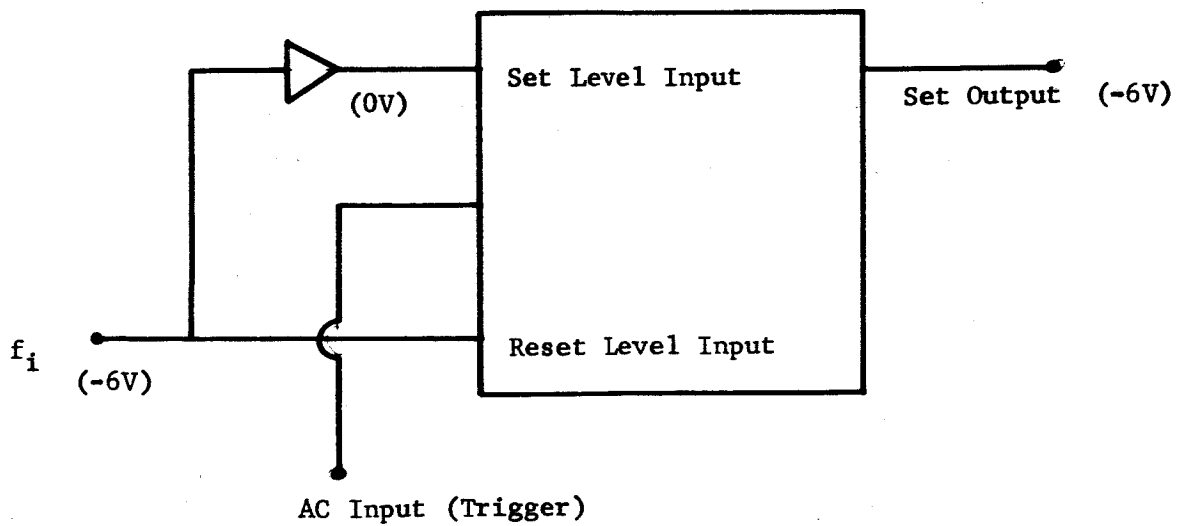


Fig. 15--An Output hold circuit.

## 2. System Clock

The system clock consists of three components that are shown in Figure 14. The basic component is a clock which includes a self starting multivibrator circuit, a pulse shaper, and pulse amplifiers. The frequency of operation is adjustable with a particular frequency obtained by selection of an appropriate capacitor. Assertion and negation pulse outputs are provided. In this case an output pulse occurs at 1/2 second intervals. The second component shown in Figure 14, and labeled "Gate" consists of a counter and a logic AND-gate. The AND-gate is inhibited for alternate pulses so that every other pulse from the basic clock is passed through to the amplifier. The amplifier just mentioned is the third component in the system clock, and consists of eight non-inverting power amplifiers. Each amplifier output is connected to supply a trigger signal to a group of flip-flops. The flip-flops that require a trigger signal are in the output hold circuits for the over all system.

Characteristics of the basic clock are given in this paragraph. There are two outputs from the basic clock. At the assertion output terminal there is a negative six volt pulse occurring at 1/2 second intervals with a pulse width of 10 milliseconds. The rise time (typical value) is 0.025 microseconds and a typical value for fall time is 0.05 microseconds. The trailing edge of alternate pulses from the assertion terminal is used to trigger the output hold circuits. The negation output waveform is a series of pulses rising from (-6)

volts to zero volts. The pulse interval and width is the same as the interval and width at the assertion output. The leading edge (positive transition) of each pulse from the negation output is used to trigger the analog-to-digital converter.

The "Gate" component of the system clock is used to transmit only alternate pulses from the assertions output to the amplifier. A multi-purpose flip-flop is used to count pulses from the basic clock. The set output terminal of the flip-flop is alternately at logic one (-6V) or logic zero (0V). A two input AND-gate, having one input from the set output of the counter and the other input from the basic clock, transmits only alternate pulses.

The amplifier section is used to supply trigger signals to each of the output hold circuits of the overall system. Each individual amplifier has an output capability (maximum) to drive 14 of the output hold flip-flops. The output waveform of these amplifiers can have typical values for rise time of 0.025 microsecond and a fall time of 0.04 microsecond. The fast output transition is obtained by using the "totem pole" configuration.

### 3. Output Hold Network

There are seventy logic functions which must be connected to a set of one hundred-forty output terminals. The logic functions are derived from a combinational circuit during an interval. At the end of the interval the logic functions are switched to the output ter-

minals. Two pulse intervals from the system clock are taken to derive the logic functions with switching taking place at the end of each second pulse. A typical hold circuit is shown below in Figure 15.

The hold circuit shown includes an inverter and a flip-flop. An a.c. trigger signal applied to the a.c. input will change the output of the flip-flop only in case the input signal  $f_i$  is different from the existing output. For example, if the output is a logic one (-6V) and  $f_i$  is a logic zero (0V), the output will change to a logic zero (0V) when an a.c. signal is applied. This means that the output is held at which ever logic input is present when an a.c. signal is applied. The output is held until the next alternating current signal is applied. The inverter is needed because a logic zero (0V) is required at a level input to cause a change in state of the flip-flop when an a.c. trigger signal is applied. The delay of the inverter in one of the inputs to the flip-flop is of no consequence. This is because the delay is very much less than the interval between the trigger inputs. The output waveform of the flip-flop has typical values for rise time of 0.025 microsecond and for fall time 0.05 microsecond.

### C. Electronic Phase Shifter

#### 1. Analysis of the Hybrid Ring

At present there are two methods of achieving phase control at microwave frequencies. One is by making use of the phase properties of ferrites and the second by using diode switches. At higher frequencies, ferrites seem, at present, to have distinct advantages. At S-band frequencies (1.55GHz to 5.2GHz) the advantage is not so pronounced and diode methods are more competitive. Due to system requirements of 100 n sec. switching speed, and phase control in discrete increments, the diode method was selected.

The diode method has three different configurations by which phase can be controlled in steps. One method is actually switching in and out of the transmission line, sections of line whose length differentials result in a phase shift. A switched line phase shifter is shown in Figure 16a. It must be noticed in this scheme that each switch acts as an on-off device and four diodes are necessary for each phase increment.

A second method makes use of periodic loading of the transmission line at quarter wave intervals. In this case, reactances are switched in and out with diode pairs. A schematic is shown in Figure 16b. Two diodes are required for each phase increment; however, the phase differentials are relatively small ( $\approx 22.5^\circ$ ) so that a large number of pairs are necessary for  $360^\circ$  shift capability.

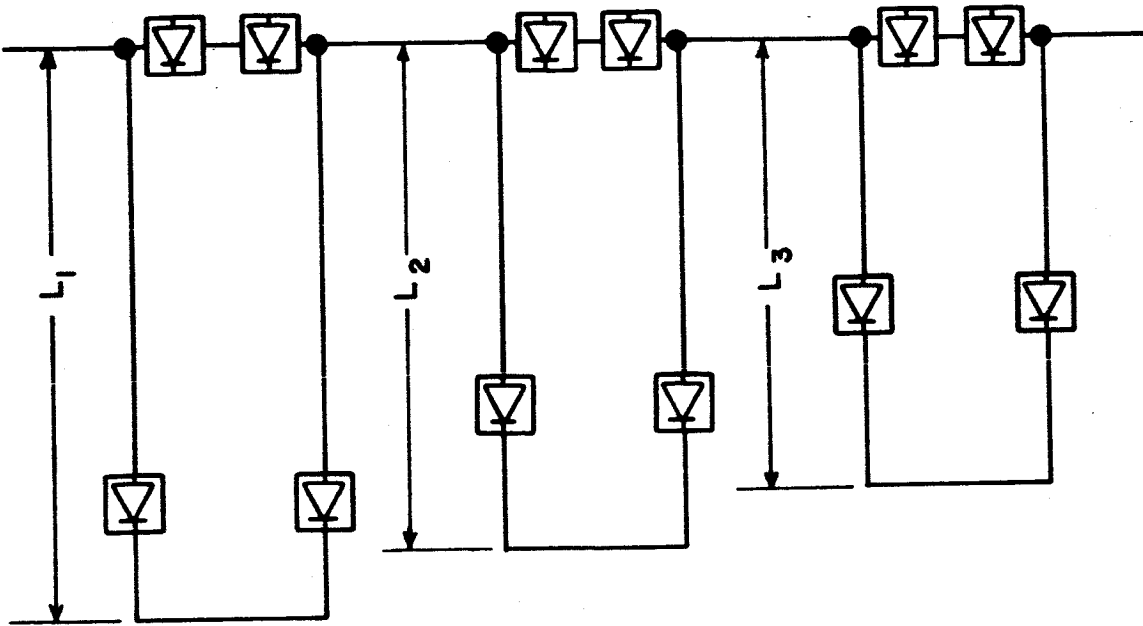


Fig. 16a--Three-bit switched line phase shifter.

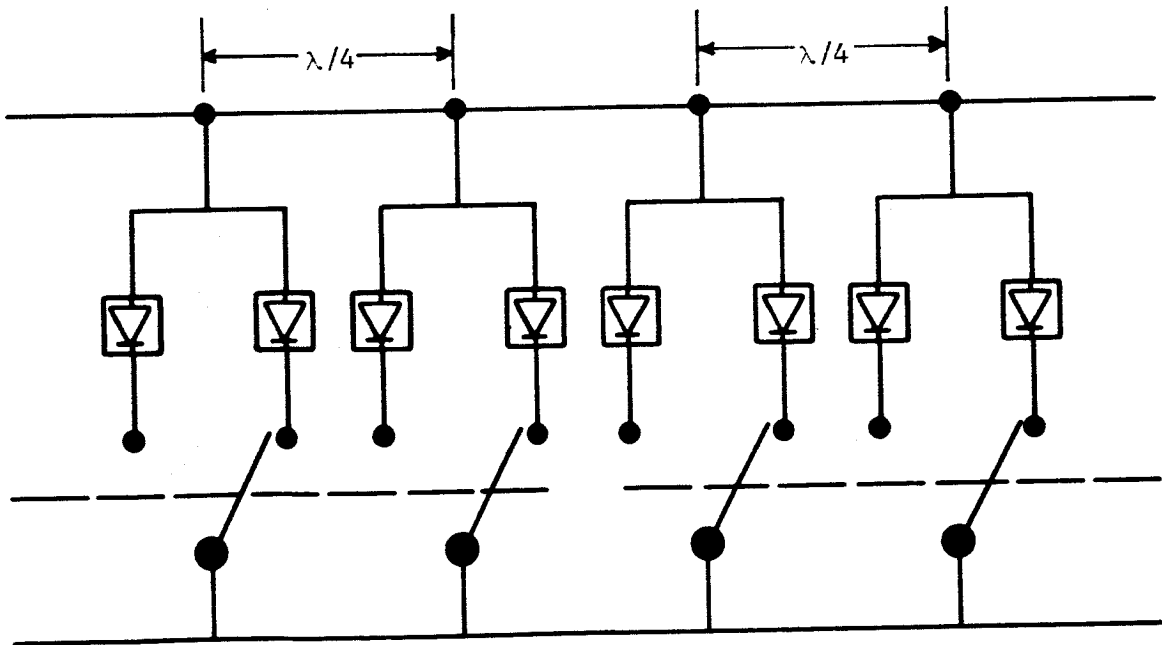


Fig. 16b--Periodically loaded transmission line phase shifter.

A third method is usually referred to as the reflection method. Phase control by the reflection method is achieved by control of the effective terminating load impedance of a transmission line. In order to make use of the reflected energy and at the same time maintain a matched input, it is necessary to decouple incident from reflected energy. Decoupling can be achieved with a hybrid ring.

It is advantageous to introduce a normalized incident wave,  $a$ , and normalized reflected wave,  $b$ . The proportionality constants,  $a$  and  $b$ , relate the magnitude of the incident transverse electric field and the magnitude of the reflected transverse electric field. They are chosen such that  $1/2 a_i a_i^*$  is equal to the power incident at port  $i$  and  $1/2 b_i b_i^*$  is the power flow out of port  $i$ . The relation between  $a$  and  $b$  at a junction is given by the scattering matrix. For example, the outward traveling wave,  $b$ , at the  $i^{\text{th}}$  port of a  $n$ -line junction is

$$b_i = S_{i1} a_1 + S_{i2} a_2 + S_{i3} a_3 + \dots + S_{in} a_n, \quad (34)$$

where  $s_{ij}$  is the contribution to the outward wave on the  $i^{\text{th}}$  line due to the incident wave,  $a$  at the  $j^{\text{th}}$  line. Clearly the reflection coefficient at the  $i^{\text{th}}$  line is

$$S_{ii} = \Gamma_i \quad (35)$$



Equation (34) can be extended to a set of equations. These may be represented in matrix notation as

$$b = [S] a, \quad (36)$$

where  $S_{ij}$  are called the scattering coefficients.

In the hybrid shown in Figure 17, all loads are external to the ring and all ports are completely matched, therefore as indicated by equation (35)

$$S_{11} = S_{22} = S_{33} = S_{44} = 0 \quad (37a)$$

In addition, there is no coupling between ports 1 and 3 or 2 and 4; hence

$$S_{13} = S_{31} = S_{24} = S_{42} = 0 \quad (37b)$$

and the matrix equation

$$\begin{bmatrix} b_1 \\ b_2 \\ b_3 \\ b_4 \end{bmatrix} = \begin{bmatrix} 0 & S_{12} & 0 & S_{14} \\ S_{21} & 0 & S_{23} & 0 \\ 0 & S_{32} & 0 & S_{34} \\ S_{41} & 0 & S_{43} & 0 \end{bmatrix} \begin{bmatrix} a_1 \\ a_2 \\ a_3 \\ a_4 \end{bmatrix}$$

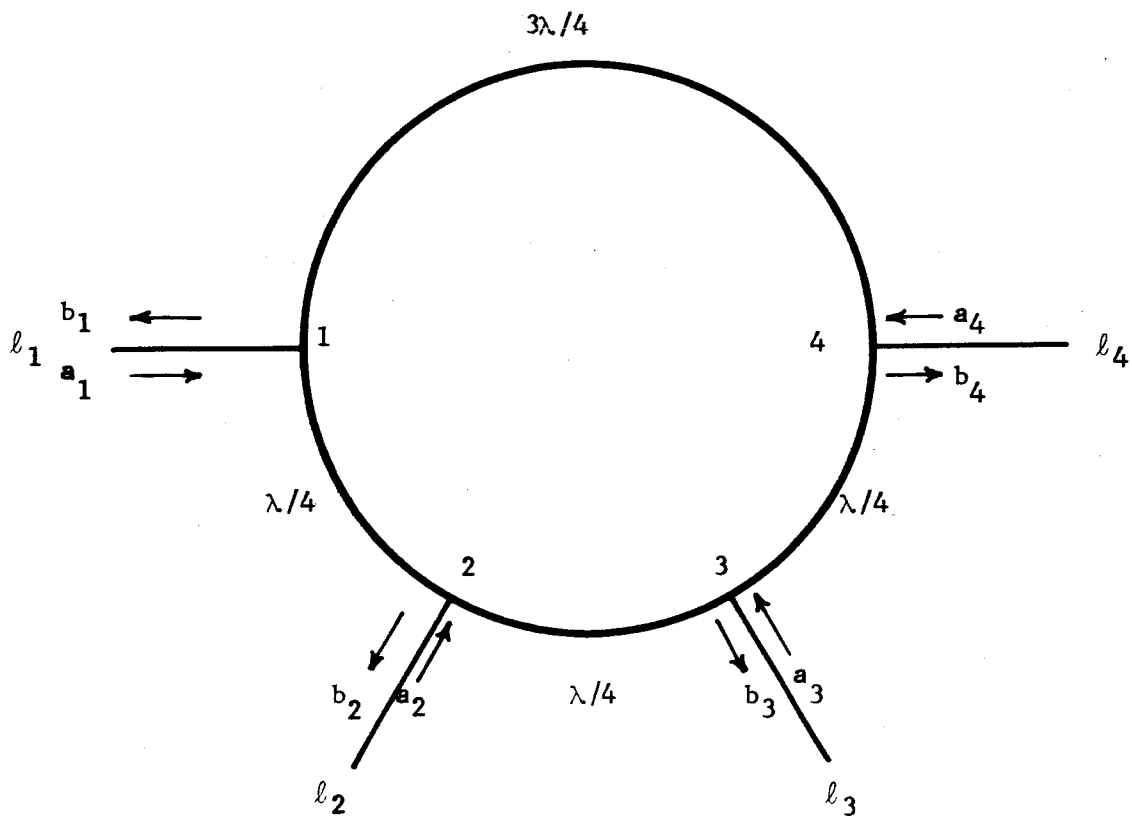


Fig. 17--A schematic of the hybrid ring.

may be written for the junction. Assuming sinusoidal excitation at port 1, Figure 17 shows the expressions

$$S_{12} = S_{21} = S_{32} = S_{23} = \frac{1}{\sqrt{2}} e^{-j(B\ell_2 + \pi/2)} \quad (38)$$

$$S_{14} = S_{41} = \frac{1}{\sqrt{2}} e^{-j(B\ell_4 + 3\pi/2)} \quad (39)$$

$$S_{34} = S_{43} = \frac{1}{\sqrt{2}} e^{-j(B\ell_4 + \pi/2)} \quad (40)$$

describe the scattering elements. Equations (39) and (40) may be combined with the result;

$$S_{34} = S_{14} e^{-j\pi} \quad (41)$$

In equations (38), (39), and (40) the lengths  $\ell_1$  and  $\ell_3$  were arbitrarily taken to be zero since  $\ell_1$  and  $\ell_3$  are not pertinent to the differential phase shift. If the input (port 1) and the output (port 3) are to be properly matched, then  $b_1$  and  $a_3$  must be zero. Under these conditions, the expanded matrix yields the following set of equations:

$$b_1 = S_{12}a_2 + S_{14}a_4 = 0, \quad (42)$$

$$b_2 = S_{21}a_1, \quad (43)$$

$$b_3 = S_{23}a_2 + S_{34}a_4, \quad (44)$$

and

$$b_4 = S_{41}a_1, \quad (45)$$

which describe the junction. Let  $a_2 = \Gamma_2$  and  $a_4 = \Gamma_4$  where  $\Gamma_2$  and  $\Gamma_4$  are the reflection coefficient of port 2 and 4 terminations. Utilizing these equations in conjunction with equation (43) and (45),

$$a_2 = \Gamma_2 S_{21}a_1 \quad (46)$$

$$a_4 = \Gamma_4 S_{41}a_1 \quad (47)$$

result. Equation (44) becomes, after combining with equations (46) and (47),

$$b_i = \Gamma_2 S_{12}S_{21}a_1 + \Gamma_4 S_{14}S_{41}a_1 = 0 \quad (48)$$

For the nontrivial solution of equation (48), that is  $a_1 \neq 0$ , equation (48) becomes

$$\Gamma_2 S_{12}S_{21} = -\Gamma_4 S_{14}S_{41} \quad (49)$$

Let the condition  $\Gamma_2 = \Gamma_4$  be imposed. Combining equations (38), (39) and (49),

$$e^{-2j(B\ell_2 + \pi/2)} = -e^{-2j(B\ell_4 + 3\pi/2)} \quad (50)$$

In the last equation a necessary criterion for equality is  $\ell_4 - \ell_2 = \lambda/4 + n\lambda/2$ , where  $n$  is an integer. If both  $\ell_2$  and  $\ell_4$  are terminated in identical loads ( $\Gamma_2 = \Gamma_4$ ), subject to the condition that the difference in length of  $\ell_2$  and  $\ell_4$  is  $\lambda/4$ , then the input is matched.

The expression for the output of port 3 may be obtained by combining equations (44), (46) and (47). The equation

$$b_3 = \Gamma_2 S_{32} S_{12} a_1 + \Gamma_4 S_{41} S_{34} a_1 \quad (51)$$

describes  $b_3$  in terms of the reflection coefficient of port 2 and 4 and the scattering coefficients. Imposing the condition  $\Gamma_2 = \Gamma_4$ , yields

$$b_3 = \Gamma \left[ S_{32} S_{12} + S_{41} S_{34} \right] \quad (52)$$

Combining equations (38) and (41) with equation (52), gives the result;

$$b_3 = \Gamma \left[ S_{21}^2 + S_{41}^2 e^{-j\pi} \right] a_1 \quad (53)$$

It is evident from equation (50) that

$$S_{21}^2 = - S_{41}^2 \quad (54)$$

This may be used in equation (53) to yield:

$$b_3 = \Gamma_2 S_{21}^2. \quad (55)$$

The scattering coefficient  $S_{21}$  is described in terms of the junction parameters by equation 40, therefore, the combination of equations (40) and (55) will result in

$$b_s = \Gamma e^{-2j(B\ell_2 + \pi/2)} a_1 \quad (56)$$

This equation expresses the output ( $b_3$ ) in terms of the reflection coefficients of ports 2 and 4 and the arbitrary length of line  $\ell_2$ . It is evident that the differential output phase of  $b_3$  depends exclusively on the reflection coefficient .

## 2. Diode Characteristics

The success of this type phase shifter depends upon the control of the reflection coefficient  $\Gamma$ . With this in mind, an examination of switching diodes is in order.

A PIN (P-layer, intrinsic layer, N-layer) diode was chosen as the switching diode. Shown in Figure 18a is a lumped circuit representation of the PIN diode. In this figure  $C_p$  is the package capacitance;  $L_p$  is the package inductance;  $C_i$  is the capacitance across the I-layer;  $R_s$  is the contact resistance;  $R_i$  is the resistance of the I-layer.<sup>4</sup> Figures 18b and 18c show the equivalent circuit for the forward and back biased states respectively. Differential phase shift is obtained by proper tuning of the diode switches.

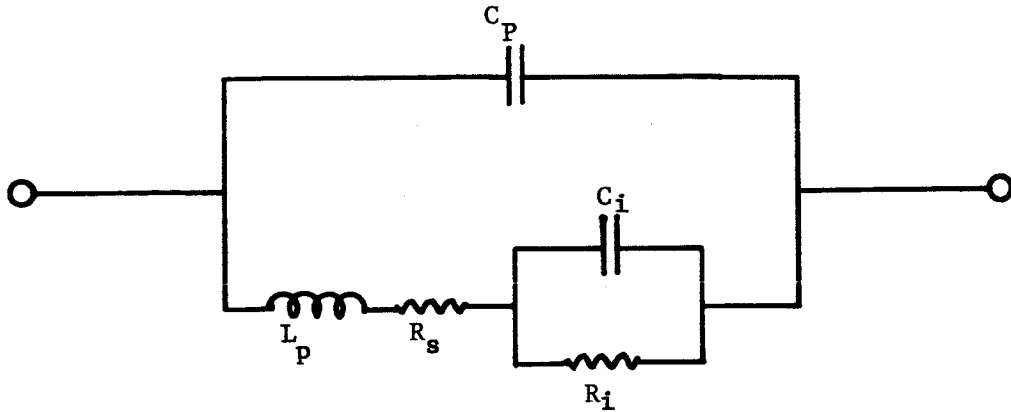


Fig. 18a--PIN-diode equivalent circuit.

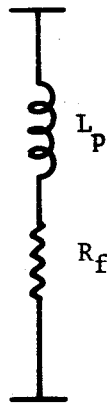


Fig. 18b--Simplified PIN-diode equivalent in forward bias state.



Fig. 18c--Simplified PIN-diode equivalent in reverse bias state.

### 3. Phase-Bit Design

To produce a phase differential of  $180^\circ$ , it is desired to have a short circuit ( $Z_T = 0$ ) in one diode state and an open circuit ( $Z_T = \infty$ ) in the other diode state. Diodes are not perfect elements and therefore actual short circuits and open circuits can not be produced. Since imperfections are present, a desirable procedure would be to minimize the losses and make the losses equal in each state. This eliminates amplitude variation between different phase shifts. A theoretical evaluation can be made to determine practical limitations of diode switching. One approach is to tune the diode in the forward bias to series resonance and tune the back biased diode to parallel resonance. Consider first the series resonance where the impedance is real and equal to  $R_f$ . The reflection coefficient in this case would be

$$\Gamma_f = \frac{R_f - Z_o}{R_f + Z_o} \quad (57)$$

and the voltage standing wave ratio is

$$S = \frac{Z_o}{R_f} \quad (58)$$

where  $Z_o$  is the characteristic impedance of the line. For the parallel resonance case, the impedance is approximately  $Q^2 R_R$  and reflection coefficient is



$$\Gamma_r = \frac{Q^2 R_R - Z_0}{Q^2 R_R + Z_0}, \quad (39)$$

and the standing wave ratio is

$$S = \frac{Q^2 R_R}{Z_0} \quad (60)$$

where  $Q$  is defined by the equation

$$Q = \frac{1}{\omega C_i R_R} \quad (61)$$

Equal loss is desired, therefore, equations (58) and (60) may be equated to solve for  $Z_0$ . The result is

$$Z_0 = Q \sqrt{R_R \cdot R_f} \quad (62)$$

This equation gives the characteristic impedance of the line in terms of the diode parameters. To compute the loss for the  $180^\circ$  bit, it is desirable to use  $Z_0$  as found in (62) in the expression (59). This substitution yields,

$$\Gamma = \frac{Q^2 R_R - Q \sqrt{R_R R_f}}{Q^2 R_R + Q \sqrt{R_R R_f}} \quad (63)$$

If  $\omega_c$  is defined as<sup>5</sup>

$$\omega_c = \frac{1}{C_i \sqrt{R_r R_f}} \quad (64)$$

Then equation (63) may be reduced to

$$\Gamma = \frac{\frac{\omega_c}{\omega} - 1}{\frac{\omega_c}{\omega} + 1} \quad (65)$$

$\frac{\omega_c}{\omega}$  may be recognized as the standing wave ratio. For high standing wave ratios, as in the case in question, the losses can be approximately by<sup>6</sup>

$$\text{loss db} = \frac{17.4}{S} = 17.4 \frac{\omega}{\omega_c} \quad (66)$$

The development thus far has furnished a method of obtaining a  $180^\circ$  phase bit and the expected losses in terms of the diode parameters. It is conceptually simple once the  $180^\circ$  bit is designed to obtain smaller bits. For example, a  $180^\circ$  bit is essentially an on-off switch. It is evident that the  $180^\circ$  bit could be used to switch in or out an appropriate length of shorted transmission line. In spite of the simplicity, this method is not satisfactory. Due to the reactance of the shorted

transmission line, the resonant conditions of the switch are disturbed; thus, unequal and excessive losses occur in this method. A superior method, in so far as that the losses are equal, is obtained by use of transformers and tuning elements. Smaller increments of phase shift may be obtained with this method. Examination of the expression for reflection coefficient shows the greatest loss will occur in the  $180^\circ$  bit and the losses decrease as the bit angle is decreased. Due to the decrease in losses in the smaller bits, this method yields the lowest insertion loss; however, it does not necessarily offer the highest power handling capabilities. The latter will not be a major concern in this system as each bit will more than adequately handle expected powers.

#### 4. Experimental Results

Four phase bits ( $180^\circ, 90^\circ, 45^\circ, 22.5^\circ$ ) were constructed using strip transmission line with diodes as the reflecting elements. To obtain a approximately equal losses in each state, the characteristic impedances of the transmission lines are higher than  $50 \Omega$  and open circuit transmission lines are used as tuning elements. In each case, all lines are ultimately transformed to  $50 \Omega$  so that the input and output of the phase shifter is at the  $50 \Omega$  level. The diodes are backed with low impedance capacitors to facilitate dc control and are biased with 85 volts, 0.0 amperes in the back bias state and 1.0 volts, 100 ma in the forward bias state. Figures 19 and 20 show diode loss and phase shift

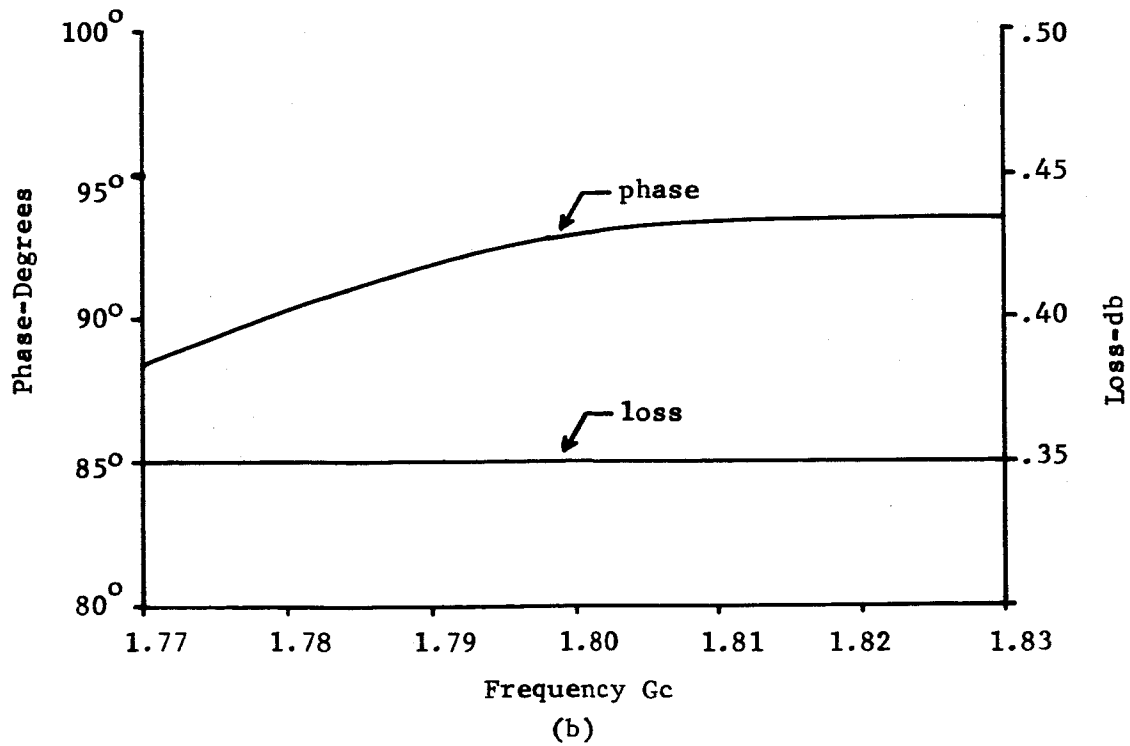
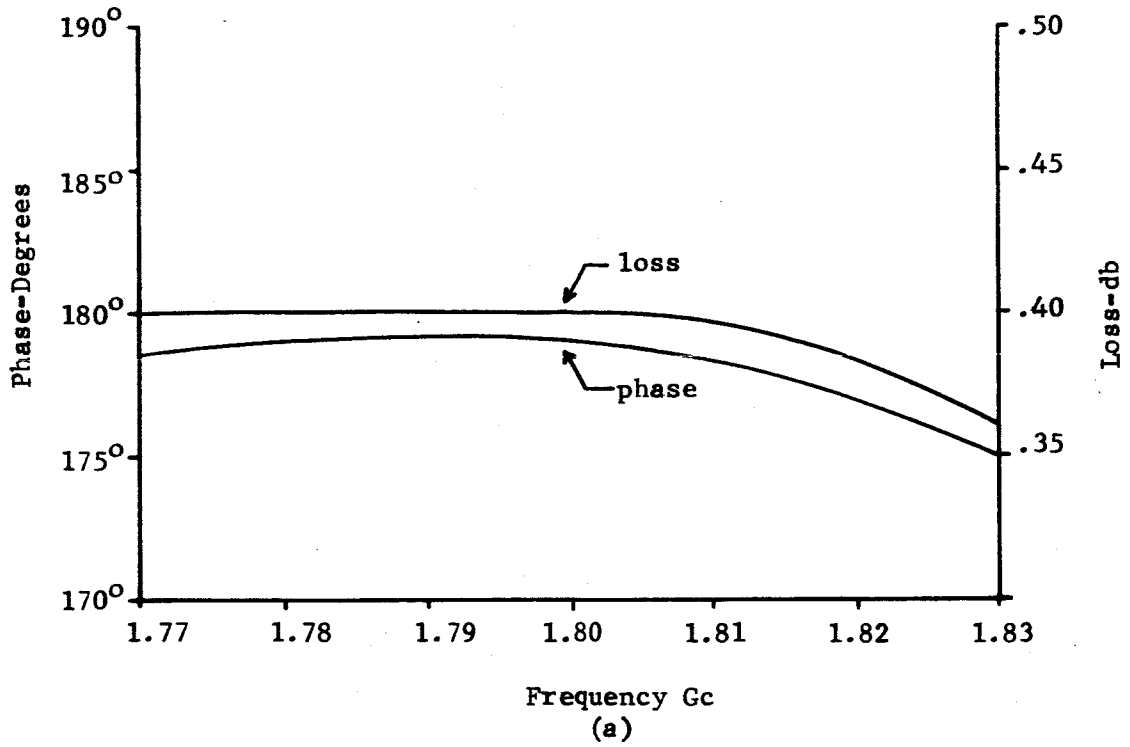


Fig. 19a,b--Phase and loss characteristics of (a) 180° (b) 90° phase bits.

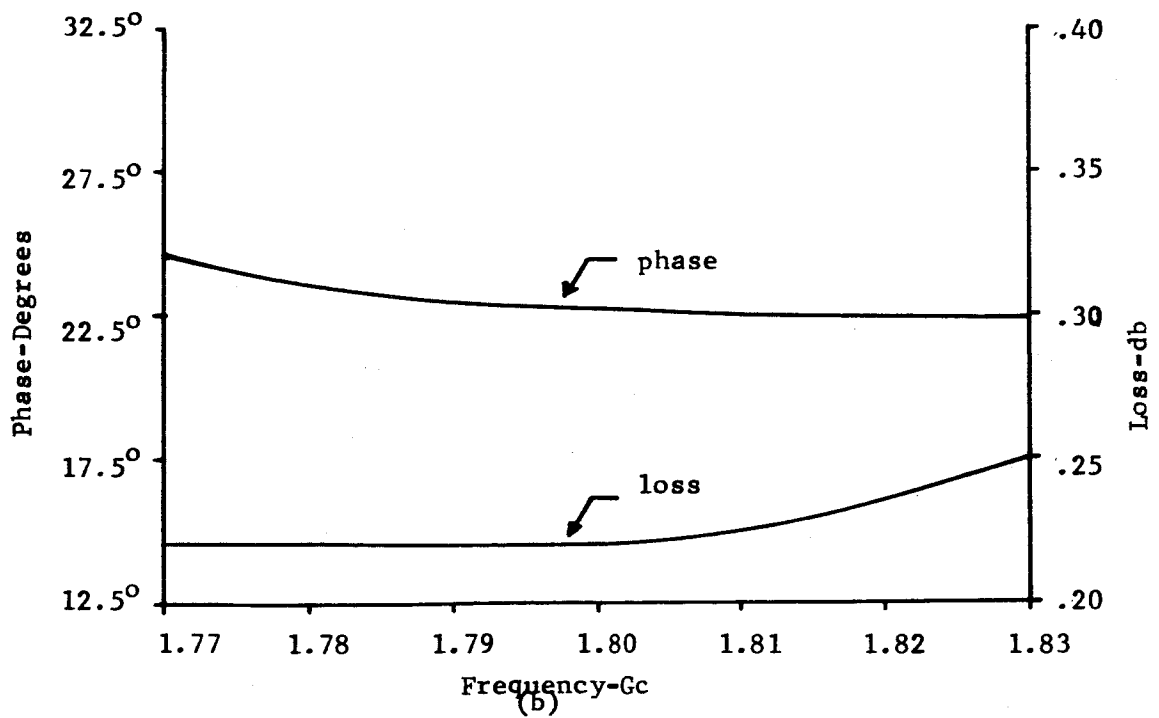
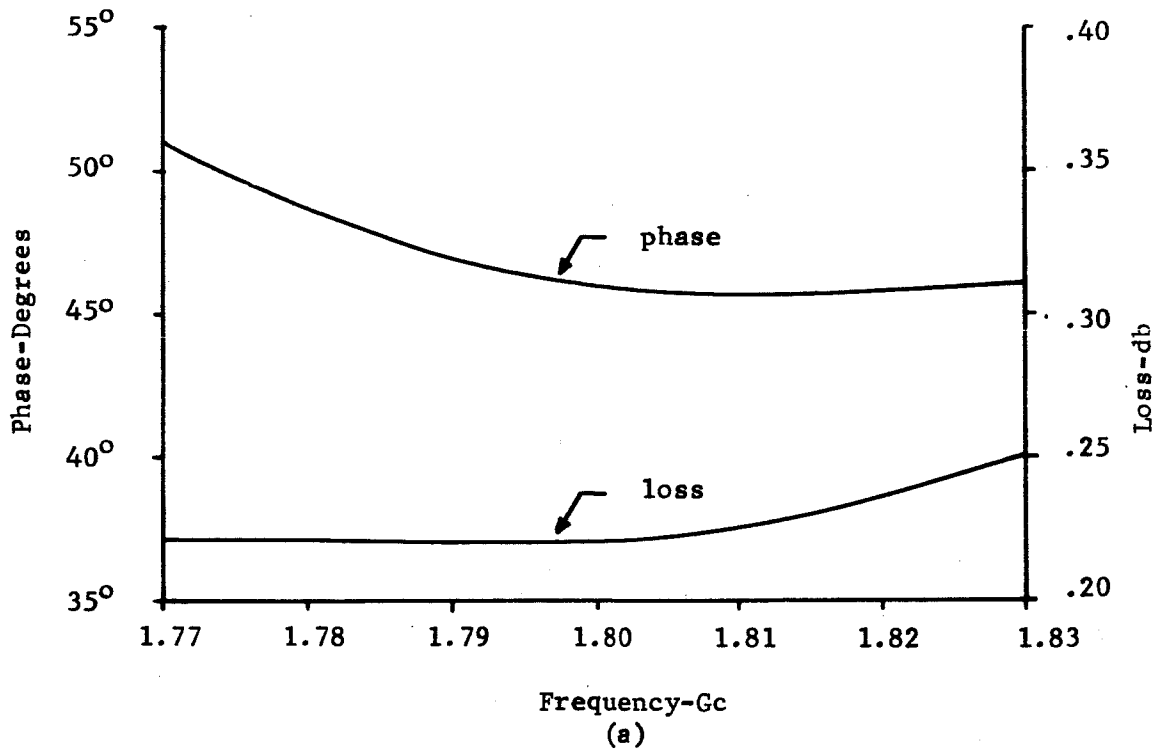


Fig. 20--Phase and loss characteristics of (a) 45°, (b) 22.5 phase bits.

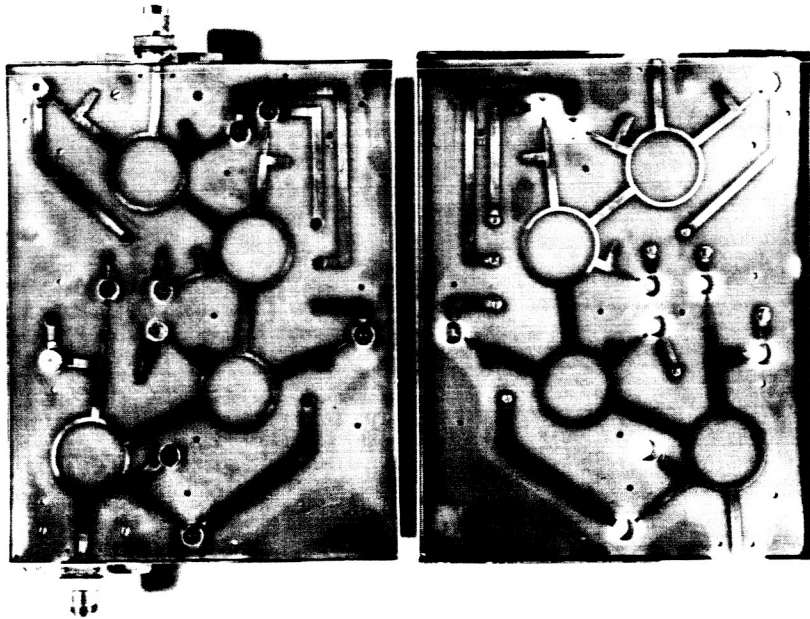


Fig. 21--A photograph of a four bit, hybrid phase shifter.

TABLE 1

INSERTION LOSS AND VOLTAGE STANDING WAVE RATION MEASUREMENTS  
FOR VARIOUS PHASE SHIFTS<sup>1</sup>

Phase Shift Degrees	Voltage Standing Wave Ratio	Insertion Loss db
0	1.23	1.1
22.5	1.25	1.2
45	1.28	1.2
67.5	1.35	1.2
90	1.20	1.0
112.5	1.25	1.1
135	1.05	1.0
157.5	1.06	1.0
180 <sup>o</sup>	1.18	1.0
202.5	1.21	.95
225	1.06	.95
247.5	1.09	.95
270	1.13	.95
292.5	1.19	.95
315	1.17	.95
337.5	1.24	.95

<sup>1</sup> Measurements were taken at 1.8 Gc.

versus frequency for the band 1.77 - 1.83 GC. The phase shift and loss data were obtained by measured minimum shifts and reflection coefficient data taken on a slotted line. Examination of the curves will show that the phase is within  $3^\circ$  over a 30 MC band width centered at 1.8GC, with losses approximately .40, .35, .22 and .22 db for the  $180^\circ$ ,  $40^\circ$ ,  $45^\circ$ ,  $22.5^\circ$ , bits respectively. This would correspond to a total insertion loss of 1.2 db for the cascaded sections.

The composite phase shifter was constructed again using strip transmission line techniques (Figure 21). Table 1 shows the voltage standing wave ratio and insertion loss for each phase increment through  $360^\circ$ . It is noted that the first few standing wave measurements are a little high. This is due to the problem of coupling between adjacent bits and efforts will be made to correct this in subsequent models.

## 5. Solid State Driver

### (a) Theory

The design of a solid state driver is required for operation of the phase shifter. The phase shifter is constructed of four bits, each requiring a separate driver. The physical structure of this device is such that each bit contains two PIN diodes which operate in parallel when viewed from the input driver terminals. For proper operation each diode requires approximately 100 ma at 1 volt in the forward state and 0 ma at -85 volts in the reverse state. Since the diodes in each bit are in parallel, the driver must be capable of supplying 200 ma at approximately 1 volt in the forward state and 0 ma at -85 volts in the reverse state.



According to system specification, incremental phase shifts must be accomplished in 100 nanoseconds or less. Therefore, in addition to the above requirements, the driver must have a rise time and a fall time in the order of 100 nanoseconds. To gain insight into the difficulty of attaining the above requirements consider the circuits of Figures 22a and 22b.

Devices A and B in Figures 22a and 22b are switches having resistances  $R_A$  and  $R_B$  respectively.  $C_{eq}$  is the equivalent capacitance of the diode and diode holder in the phase shifter. Experimentally,  $C_{eq}$  for the two parallel diodes in each bit of the phase shifter is found to be much larger than the capacitance associated with devices A and B. Device capacitance shall therefore be neglected in the following approximate analysis.

Consider the diode as shown in the circuit of Figure 22a. In this condition the diode is in the forward state when steady state conditions are reached. Suppose at time  $t = 0$  switches A and B are activated to positions as shown in Figure 22b. If the voltage drop across the diode biased in the forward state is assumed to be small, then

$$e(t) = -E_2 \left[ 1 - \exp \left( \frac{-1}{R_B C_{eq}} t \right) \right], \quad t \geq 0. \quad (67)$$

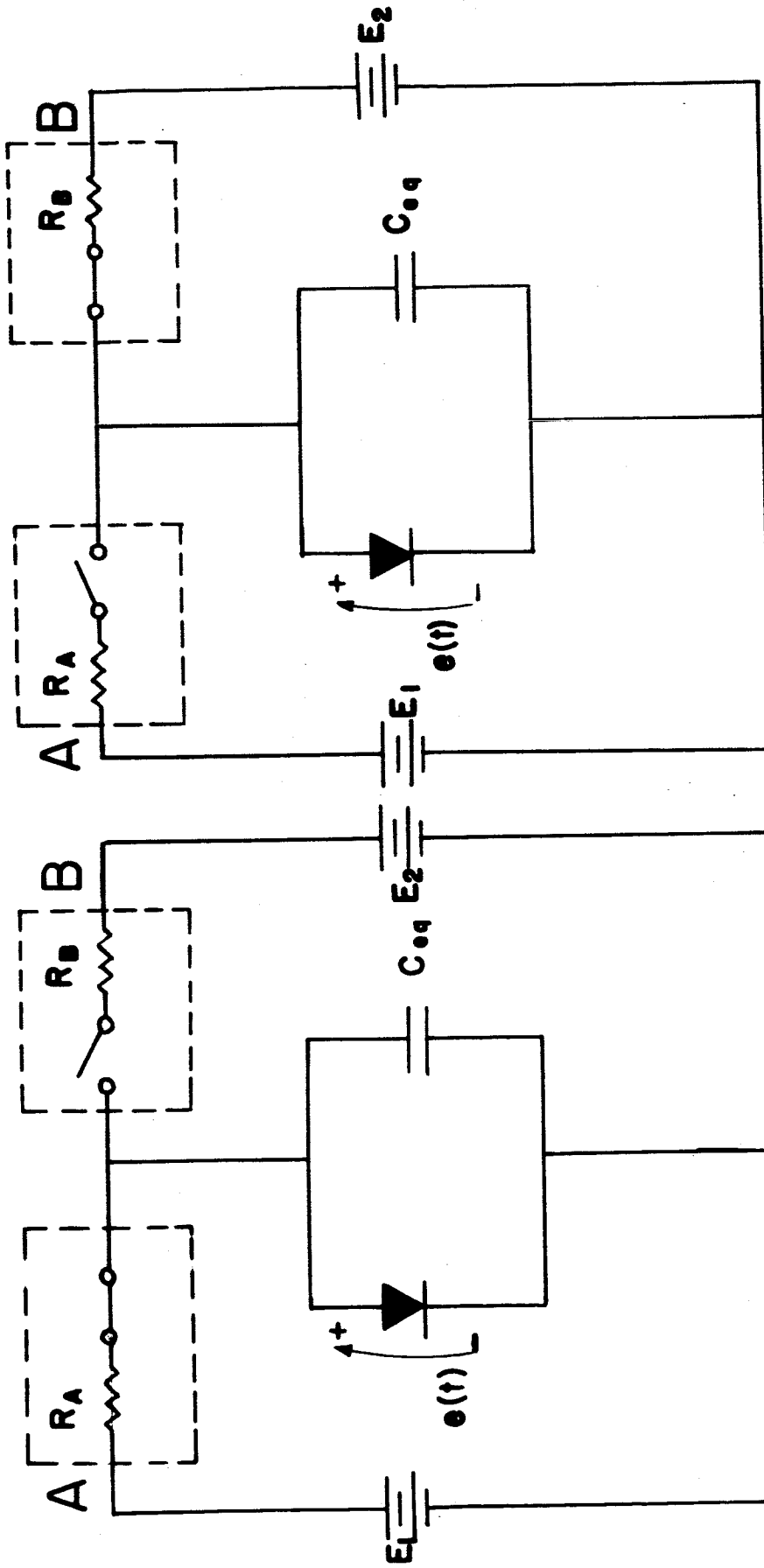


Fig. 22b--Diode in reverse state.

Fig. 22a--Diode in forward state.

A rise time of 100 nanoseconds requires that the time constant

$$\tau_1 = R_B C_{eq} = 45 \times 10^{-9} \text{ seconds.} \quad (68)$$

Typical values of  $C_{eq}$  are found to be in the order of 300 picofarads. Equation (68) requires that  $R_B$  should be of the order of 150 ohms for a rise time of 100 nanoseconds from a forward bias condition to a reverse bias condition.

Consider the diode as shown in the circuit of Figure 22b. In this condition the diode is in the reverse state under steady state conditions. At this time it is observed from equation (67) that  $e(t) = -E_2$ . At time  $t = t_1$  let switches A and B be activated to the positions depicted in Figure 22a. Let  $t = t_2$  represent the time at which  $e(t) = 0$ . Then

$$e(t) = (E_1 + E_2) \left[ 1 - \exp\left(\frac{-1}{R_A C_{eq}}\right)(t - t_1) \right] - E_2, \quad t_1 \leq t \leq t_2. \quad (69)$$

If  $E_1 = 6$  volts,  $E_2 = 90$  volts and  $t_2 - t_1 = 100$  nanoseconds, from equation (69) the time constant

$$\tau_2 = R_A C_{cq} = 36 \times 10^{-9} \text{ seconds.} \quad (70)$$

Equation (70) requires, for  $C_{eq}$  in the order of 300 pico-farads, that  $R_A$  be of the order of 120 ohms. It is noted that this is the maximum value of  $R_A$  permissible for the reverse bias to be completely removed from the diode in 100 nanoseconds. At this time the diode is driven into the forward bias condition.

Consider the circuit of Figure 23 as a method of obtaining the above mentioned requirements. Transistors  $T_A$  and  $T_B$  represent devices A and B, respectively, of Figures 22a and 22b. An understanding of the operation of this circuit is obtained by the following approximate analysis.

Consider an input voltage  $e_{in} = 0$  volts. This requires transistor  $T_A$  be in an off state, that is,

$$I_1 + I_3 = 0$$

For  $E_2 > E_1$ , the presence of the diode in the loop of  $I_1$  requires  $I_1 = 0$ , regardless of the state of transistor  $T_B$ . This requires

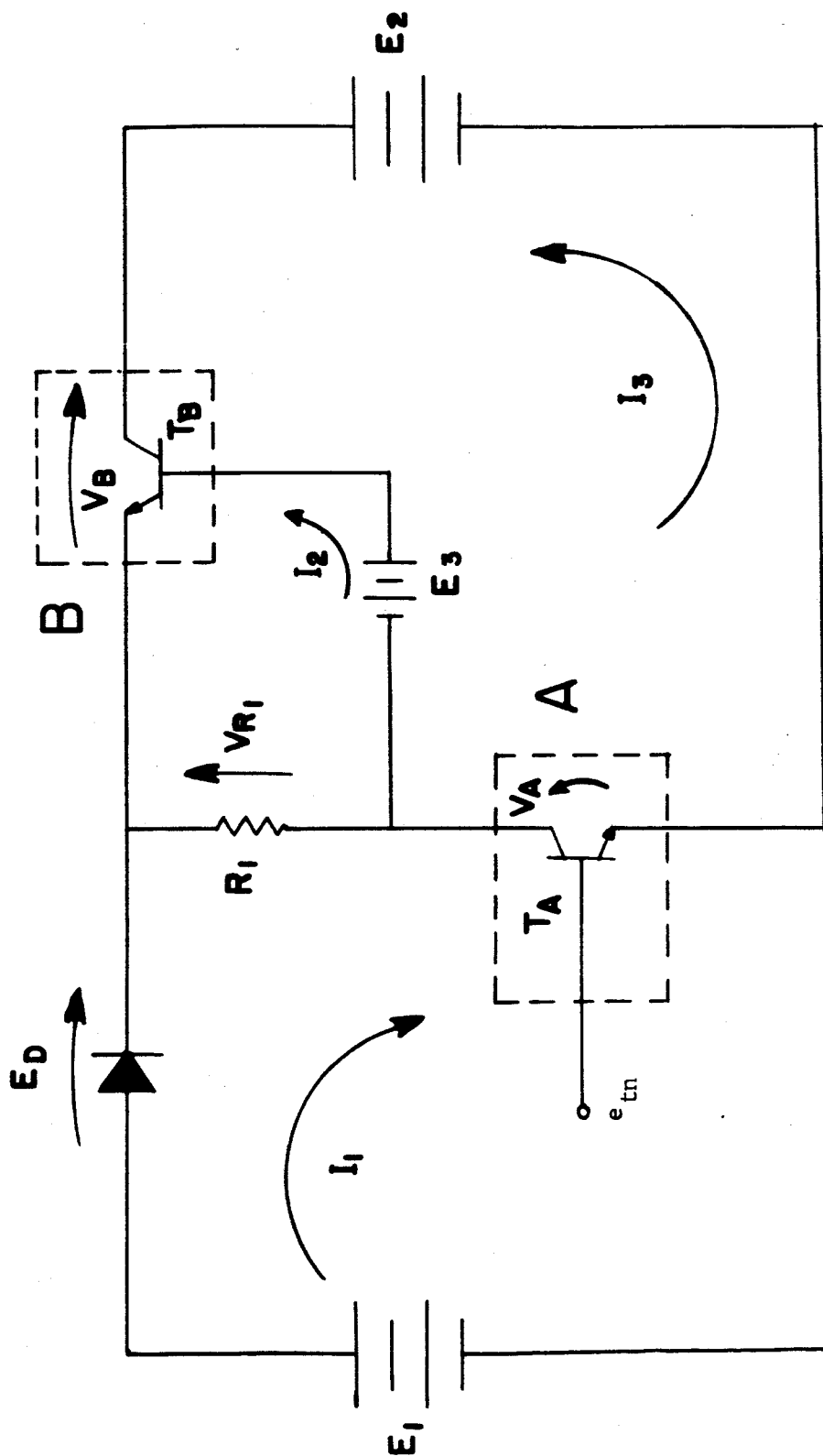


Fig. 23--Basic circuit of transistor switch.

that  $I_3 = 0$ . From Figure 23 and the above conditions,

$$V_{R_1} = R_1 I_2 = E_3 - V_{be} < E_3,$$

where  $V_{be}$  is the voltage drop from base to emitter of  $T_B$ . If the above equation is rearranged, it is observed that

$$V_{be} = E_3 - V_{R_1} . \quad (71)$$

Since  $V_{be} > 0$ , transistor  $T_B$  is in an on condition and the reverse bias on the diode is

$$E_D = E_2 - E_1 - V_B.$$

$V_b \approx 0$  for  $T_B$  in a saturated condition. In this case  $E_D \approx E_2 - E_1$  and  $V_A \approx E_2$ .

Consider an input voltage  $e_{in}$  being applied to  $T_A$  such that  $T_A$  is driven into saturation. At this instant voltage  $V_A$  approaches 0 volts and  $V_{R_1}$  approaches  $E_2$ . If  $E_2 \gg E_3$ , then from equation (71)

$$V_{be} = E_3 - E_2 < 0.$$

This results in  $T_B$  being driven into an off condition causing

$V_B = E_2$ . At this time

$$V_{1R} = E_1 - V_A - E_D ,$$

where  $E_D$  is now the forward voltage drop of the diode. For  $E_1 > E_3$ , proper selection of  $R_1$  results in  $V_{1R} > E_3$ . Equation (71) now yields

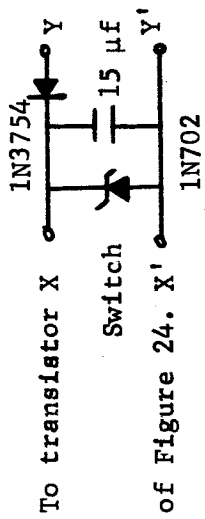
$$V_{be} = E_3 - V_{R_1} < 0$$

and  $T_B$  is in an off condition. This is required for proper operation of the switch, since  $T_B$  must remain in the off state when the diode is biased in the forward state.

#### (b) Circuit Design

The circuit developed for driving each bit of the phase shifter is shown in Figures 24 and 25. The circuits of these figures are divided into sections. In Figure 24 are indicated the inverter, amplifier, transistor switch and phase shifter. Figure 25 is the bias supply denoted by  $E_3$  in Figure 23. An explanation of the function of each section is given in the following discussion.

The inverter section of Figure 24 is employed to invert the input signal from the logic. This section consists of a PNP common emitter stage driving an NPN common base stage. The input signal from the logic consists of 0 volts or -6 volts. The inverter is designed so that the application of 0 volts to the input yields 0 volts output and -6 volts input yields 6 volts output in series with a 1000 ohm resistance.



of Figure 24. X'

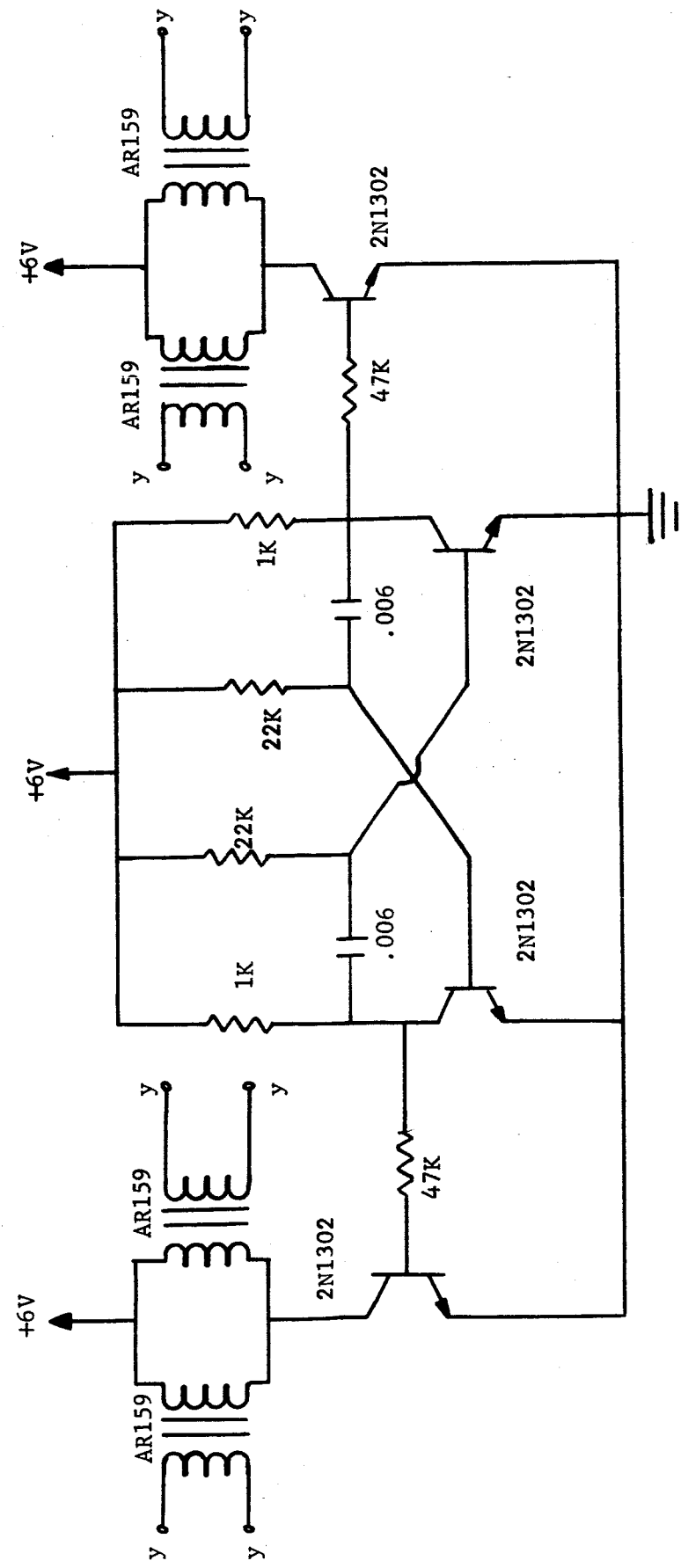


Fig. 25--Circuit diagram for 2 volt d.c. bias supply.



Note: All capacitors .006 uf.

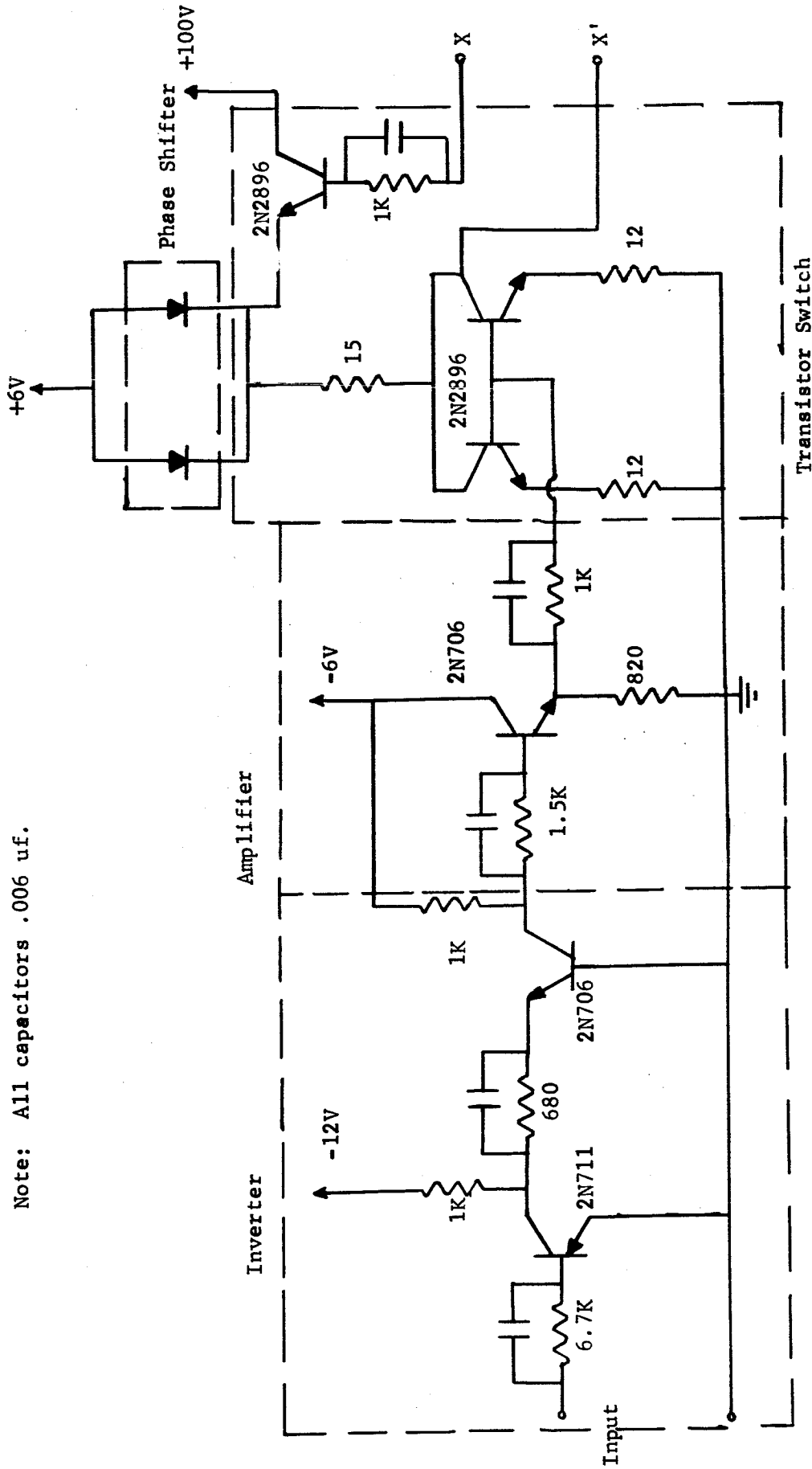


Fig. 24--Circuit diagram of driver for 1 bit of phase shifter.

The amplifier section consists of an NPN emitter follower. From the preceding paragraph it is noted that 0 volts input from the logic results in no base current to this transistor causing no activation of the transistor switch. Application of -6 volts from the logic to the input places 6 volts in series with a 1000 ohm resistance to the amplifier input resulting in activation of the transistor switch. In this state the amplifier is designed to yield 4 ma output current into the transistor switch.

The transistor switch of Figure 24 corresponds to the circuit of Figure 23. From the preceding analysis the requirements of  $T_A$  are as follows:

- (a)  $T_A$  must be able to withstand the reverse diode voltage.  
For the circuit of Figure 24 this voltage is 85 volts:
- (b)  $T_A$  must have the capacity to pass the forward diode current.  
For the circuit of Figure 24 this current is 200 ma;
- (c)  $T_A$  must have a gain-bandwidth product which is as large as economically feasible. This requirement is a direct consequence of equation (70). Resistance  $R_A$  for transistor  $T_A$  is small for  $T_A$  in saturation. Therefore, the time required to saturate  $T_A$  becomes the important factor.

In Figure 24,  $T_A$  is simulated by two NPN transistors operated in a parallel connection. This particular type of connection is required to satisfy conditions (b) and (c) above with commercial components available at the present time.

The requirements of  $T_B$  are as follows:

- (i)  $T_B$  must have the capacity to withstand the reverse diode voltage. For the circuit of Figure 24 this voltage is 85 volts;
- (ii)  $T_B$  must have a gain-bandwidth product which is as large as economically feasible. This requirement is a direct consequence of equation (68). Resistance  $R_B$  for  $T_B$  is small for  $T_B$  in saturation. Therefore, the time required to saturate  $T_B$  becomes the important factor.

The operation of the transistor switch of Figure 24 is identical to that described above for Figure 23.

The function of the 2 volt d.c. bias supply of Figure 25 is identical with that of  $E_3$  in Figure 23. Since this supply has no common terminal to the system ground, isolation of this supply from ground is necessary. This is obtained by means of transformer coupling to the rectifier circuit supplying each driver as indicated by Figure 25. The voltage applied to each rectifier circuit is obtained from a free-running multivibrator. The rectifier circuit is then regulated by a zener diode placed in parallel with the output of the supply.

#### (c) Experimental Results

The driver constructed for operation of the phase shifter is shown pictorially in Figure 26. In this figure is shown the mechanical mounting of the driver to the phase shifter. Electrical con-

tinuity to the diodes within the phase shifter is made by means of the mounting bolts securing the printed circuit board to the phase shifter.

The block diagram of Figure 28 illustrates the circuit constructed for testing the driver and phase shifter. The r-f energy from the klystron is divided into two paths by means of a power divider. In the line of one path is placed the phase shifter and in the other a line stretcher. These paths are then terminated into a hybrid ring. The line stretcher is adjusted such that a minimum response occurs from the detector for a given state of the diodes in the phase shifter. A change to the opposing state for the diodes results in a change of response from the detector. Therefore, a change in the d.c. voltage from the detector represents the phase shift associated with the two states of the diodes.

The waveforms of a typical phase shift and the corresponding input voltage to the driver are shown in Figure 27. This figure displays the response of the phase shifter to a 1 KHz square wave applied to the input. The rise times associated with the waveforms of Figure 27 are shown in Figure 29 and the fall times in Figure 30. From these figures it is observed that the phase shifts occur in less than 100 nanoseconds.

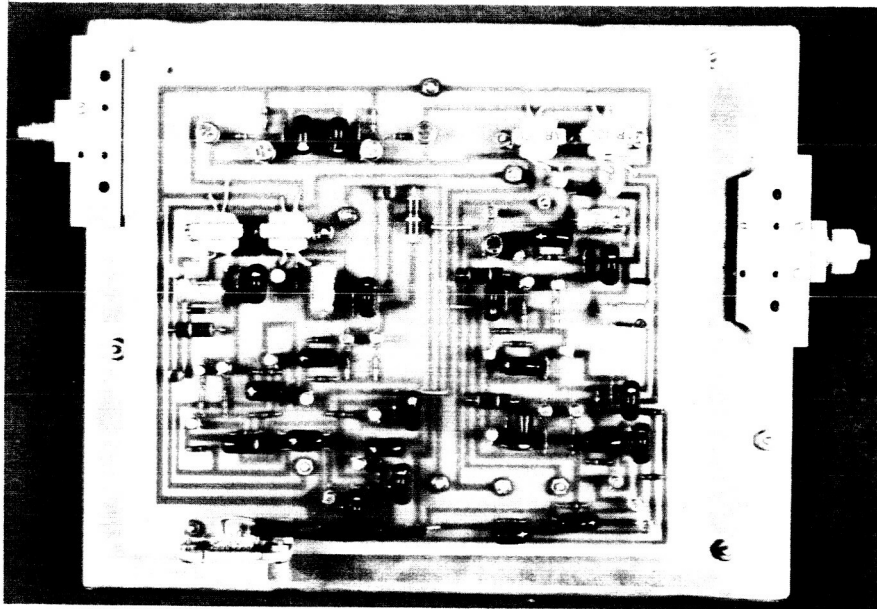


Fig. 26--Driver and phase shifter.

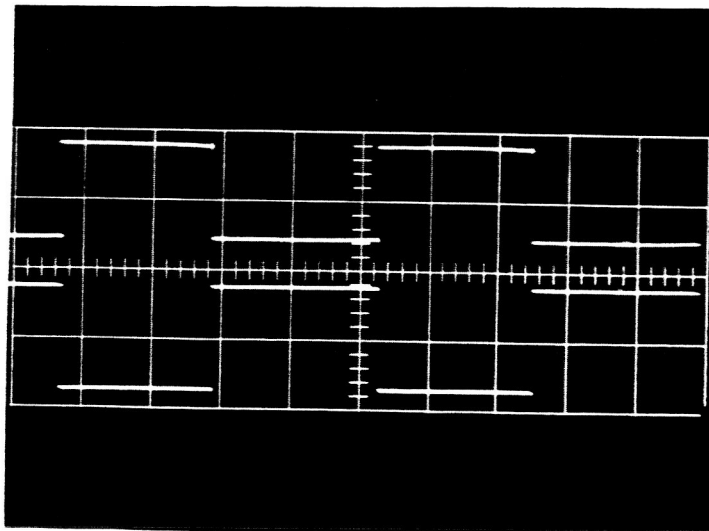


Fig. 27--Waveforms of a typical phase shift (upper waveform) and input voltage to the driver (lower waveform). (horizontal scale: 0.2ms/div.)

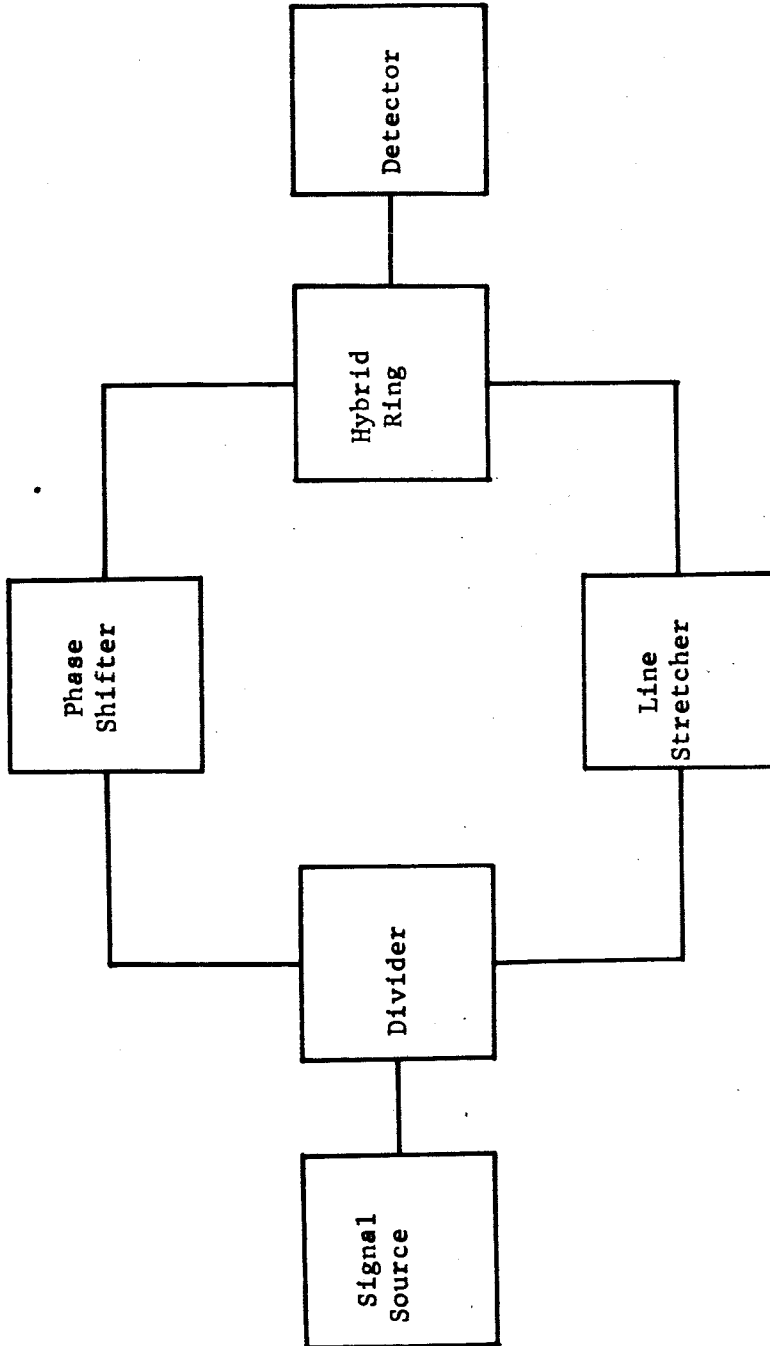
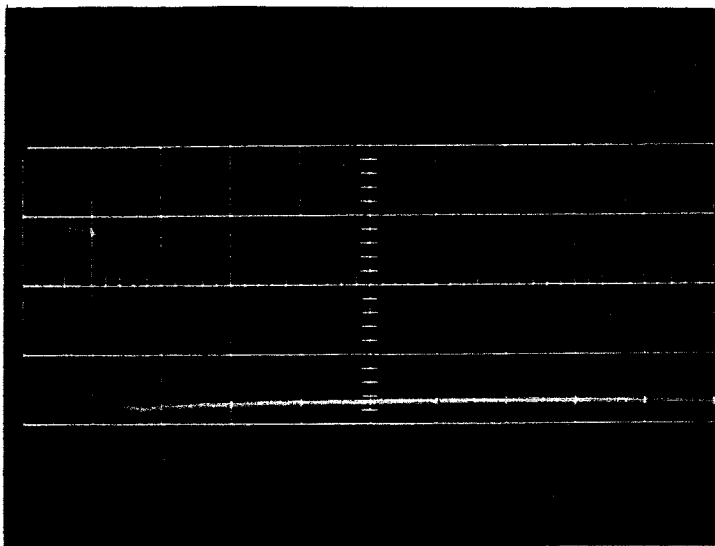
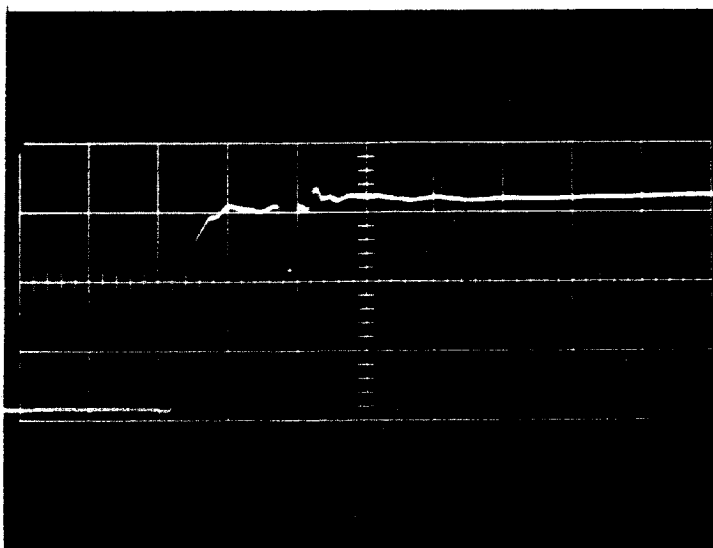


Fig. 28--A block diagram of the circuit employed for testing the driver and phase shifter.

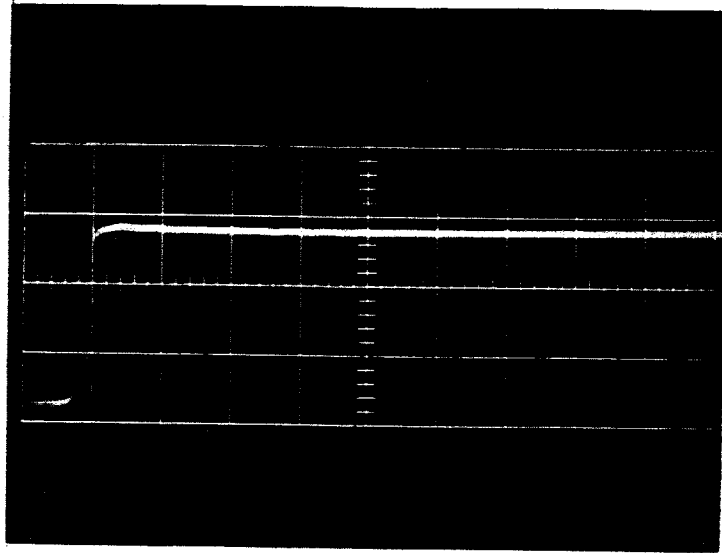


(a) Input voltage to driver (horizontal scale: 0.1 us/div.)

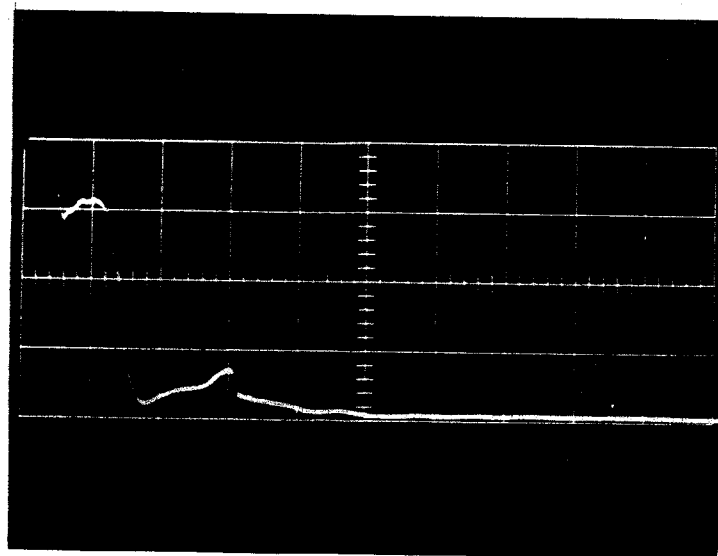


(b) Phase shift (horizontal scale: 0.1 us/div.)

Fig. 29--Rise time waveforms.



(a) Input voltage to driver (horizontal scale: 0.1 us/div.)



(b) Phase shift (horizontal scale: 0.1 uses/div.)

Fig. 30--Fall time waveforms.



## D. Electronically Scanned Antenna Arrays

### 1. Tracking Antenna Arrays

The receiving and transmitting antenna arrays will be of identical construction except for the frequency of operation. Each array will produce an elliptically polarized pattern that is capable of being electronically scanned over a full hemisphere. An antenna array will be composed of 36 identical cavity-backed, crossed-slot antennas as shown in Figure 31. A full description including theoretical and measured results for a single isolated crossed-slot antenna is described in section 4. Technical Report No. 3 reported the original work on this antenna. The basic array dimensions (not including the ground plane) are given in Figure 32. The receiving array will operate at a center frequency of 2.214 GHz with a bandwidth of 30 MHz. The feed system for both antennas utilizes 50 ohm coaxial transmission lines that will exhibit a maximum VSWR of 1.2:1 at the input to the respective array and a total gain (including phase shifters) of from 11 to 13 db.

The following is a description of the theoretical study of the tracking antenna array, described in greater detail in Technical Report No. 4, in which gain and patterns are computed for various beam pointings. Comparison of the theoretical patterns with actual measured patterns are made for two pointings.

The pattern for an array with the geometry shown in Figure 33 as a function of  $\theta$  and  $\phi$  may be expressed as

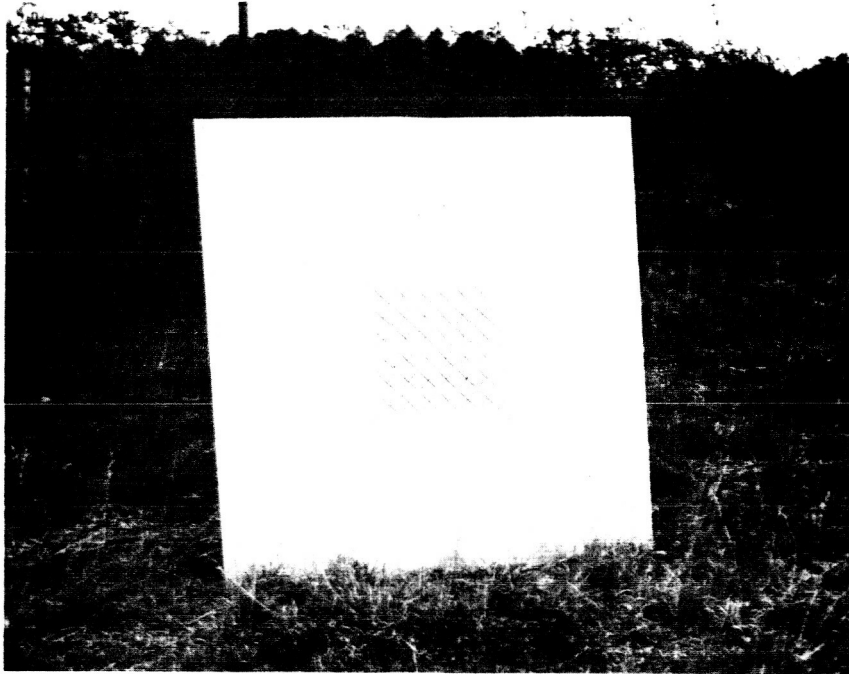


Fig. 31a--A front view of the 36 element, crossed-slot receiving array mounted on a 4 x 4 ground plane.

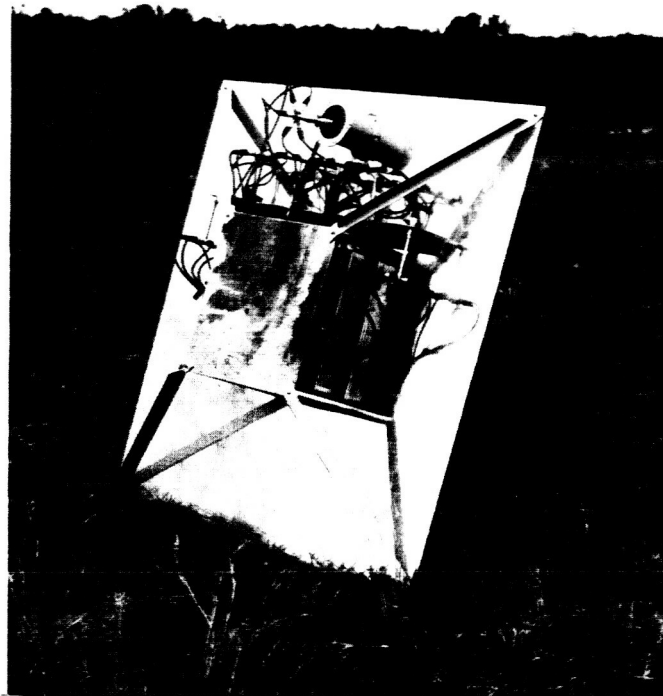


Fig. 31b--A back view of the 36 element, crossed-slot receiving array mounted on a 4 x 4 foot ground plane.

Transmitter (1.800GHz)  
 A = 13 1/4 inches  
 B = 4 1/16 inches  
 C = 17 1/4 inches

Receiver (2.214GHz)  
 A = 15 1/4 inches  
 B = 3 9/16 inches  
 C = 14 1/4 inches

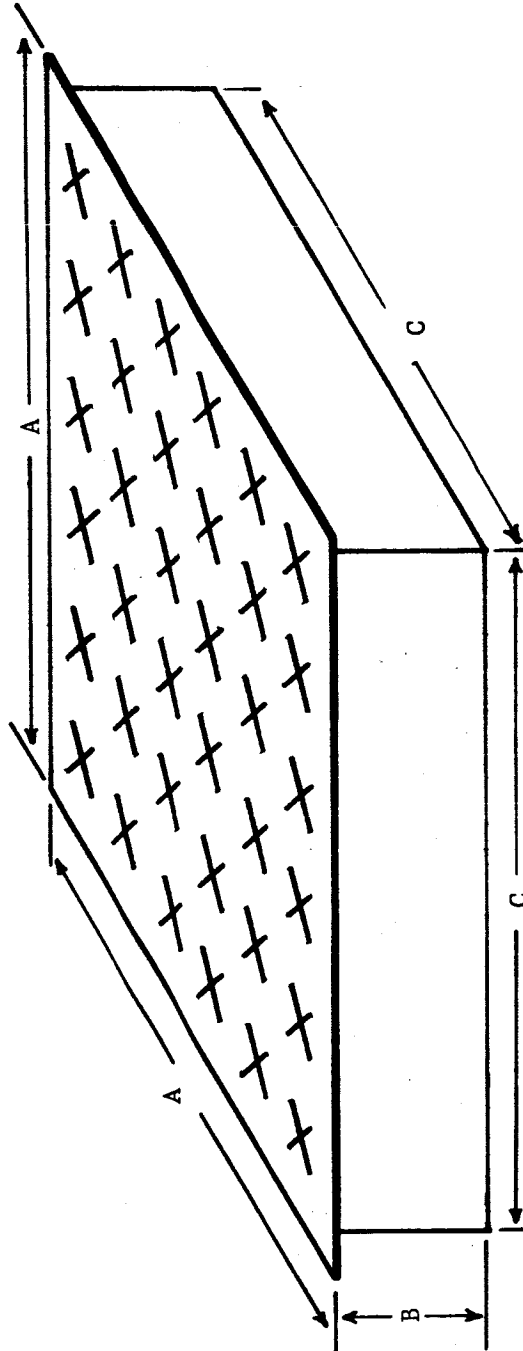


Fig. 32--6 X 6 array dimensions.

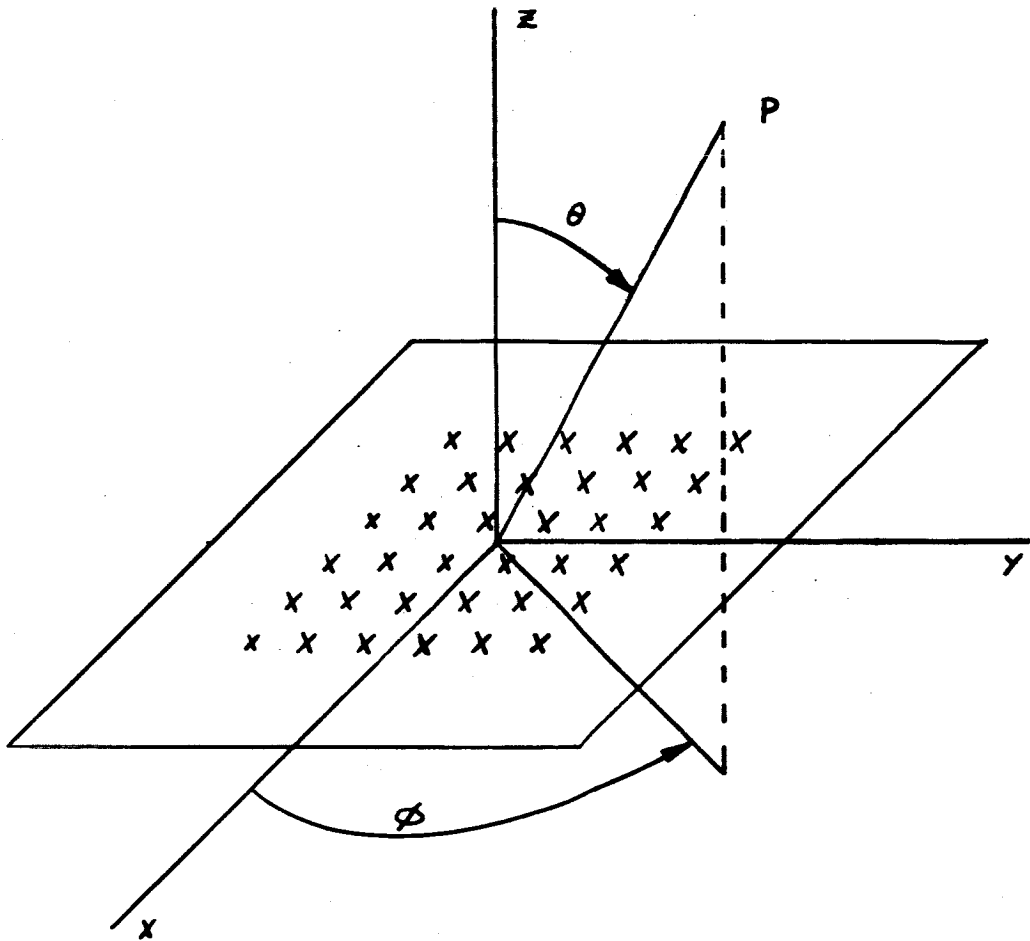


Fig. 33--Array Geometry.

$$F(\theta, \phi) = \sum_{i=1}^N V_i e^{-jk(r-r_i)} \quad (72)$$

or using Euler's identity,

$$F(\theta, \phi) = \sum_{i=1}^N V_i \left[ \cos k(r-r_i) - js \sin k(r-r_i) \right] \quad (73)$$

where

$N$  = the number of elements in the array

$V_i$  = the complex voltage at the  $i^{\text{th}}$  element obtained by solution of the simultaneous equations described below

$$k = \frac{2\pi}{\lambda}$$

$r$  = the distance from the phase center of the array to the field point under consideration

$r_i$  = the distance from the  $i^{\text{th}}$  element to the field point under consideration

$$\text{or } r_i = r - x_i \sin \theta \cos \phi - y_i \sin \theta \sin \phi - z_i \cos \theta$$

Once the value of  $V_i$  has been determined the array pattern for any array can be easily determined with the aid of a computer. The system equations for the array are

$$\begin{aligned}
 I_1 &= Y_{11}V_1 + Y_{12}V_2 + \dots + Y_{1N}V_N \\
 I_2 &= Y_{21}V_1 + Y_{22}V_2 + \dots + Y_{2N}V_N \\
 &\vdots \\
 I_N &= Y_{N1}V_1 + Y_{N2}V_2 + \dots + Y_{NN}V_N
 \end{aligned}
 \tag{74}$$

or

$$\begin{aligned}
 I_1 &= \sum_{i=1}^N Y_{1i}V_i \\
 I_2 &= \sum_{i=1}^N Y_{2i}V_i \\
 I_N &= \sum_{i=1}^N Y_{Ni}V_i
 \end{aligned}
 \tag{75}$$

Since  $I$ ,  $Y$  and  $V$  are complex numbers it is necessary to separate the real part from the imaginary

$$\begin{aligned}
 I_{1R} + jI_{1Q} &= \sum_{i=1}^N (G_{1i} + jB_{1i})(V_{iR} + jV_{iQ}) \\
 I_{2R} + jI_{2Q} &= \sum_{i=1}^N (G_{2i} + jB_{2i})(V_{iR} + jV_{iQ}) \\
 &\vdots \\
 &\vdots \\
 &\vdots
 \end{aligned}
 \tag{76}$$

$$I_{NR} + jI_{NQ} = \sum_{i=1}^N (G_{Ni} + jB_{Ni})(V_{iR} + jV_{iQ}),$$

where  $G$  is the conductance and  $B$  the susceptance. Expanding these equations and setting the real parts equal and the imaginary parts equal yields the following set of equations

$$\begin{aligned} I_{1R} &= \sum_{i=1}^N (G_{1i}V_{iR} - B_{1i}V_{iQ}) \\ I_{2R} &= \sum_{i=1}^N (G_{2i}V_{iR} - B_{2i}V_{iQ}) \\ &\quad \vdots \\ I_{NR} &= \sum_{i=1}^N (G_{Ni}V_{iR} - B_{Ni}V_{iQ}) \end{aligned} \tag{77}$$

$$\begin{aligned} I_{1Q} &= \sum_{i=1}^N (G_{1i}V_{iQ} + B_{1i}V_{iR}) \\ I_{2Q} &= \sum_{i=1}^N (G_{2i}V_{iQ} + B_{2i}V_{iR}) \\ &\quad \vdots \\ I_{NQ} &= \sum_{i=1}^N (G_{Ni}V_{iQ} + B_{Ni}V_{iR}) \end{aligned} \tag{78}$$

In matrix form the equations are

$$\begin{array}{ccccccc}
 & G_{11} & -B_{11} & G_{12} & -B_{12} \cdots & G_{1N} & -B_{1N} & V_{1R} \\
 I_{1R} & & & & & & & V_{1Q} \\
 & G_{21} & -B_{21} & G_{22} & -B_{22} \cdots & G_{2N} & -B_{2N} & V_{2R} \\
 I_{2R} & & & & & & & V_{2Q} \\
 \cdot & & & & & & & \cdot \\
 \cdot & & & & & & & \cdot \\
 I_{NR} & & & & & & & V_{NR} \\
 & & & & & & & V_{NQ} \\
 I_{1Q} & & & & & & & V_{1Q} \\
 & & & & & & & V_{1R} \\
 I_{2Q} & & & & & & & V_{2Q} \\
 \cdot & & & & & & & \cdot \\
 \cdot & & & & & & & \cdot \\
 I_{NQ} & & & & & & & V_{2R} \\
 & & & & & & & \cdot \\
 & & & & & & & V_{NQ} \\
 & G_{N1} & -B_{N1} & G_{N2} & -B_{N2} \cdots & G_{NN} & -B_{NN} & V_{NR}
 \end{array} \tag{79}$$

Thus, when mutual coupling is considered the above  $2N \times 2N$  matrix results and for the array of 36 crossed slots each slot must be considered separately so a  $144 \times 144$  matrix results. The above matrix can easily be solved on a computer by inverting the augmented matrix. However, limitations of the available computer do not permit the inversion of a matrix larger than  $90 \times 90$ . Since the mutual coupling between parallel slots is much greater than for any other orientation, a good approximation to the array may be obtained by considering an array composed of 36 parallel slots as shown in Figure 34. The other 36 perpendicular



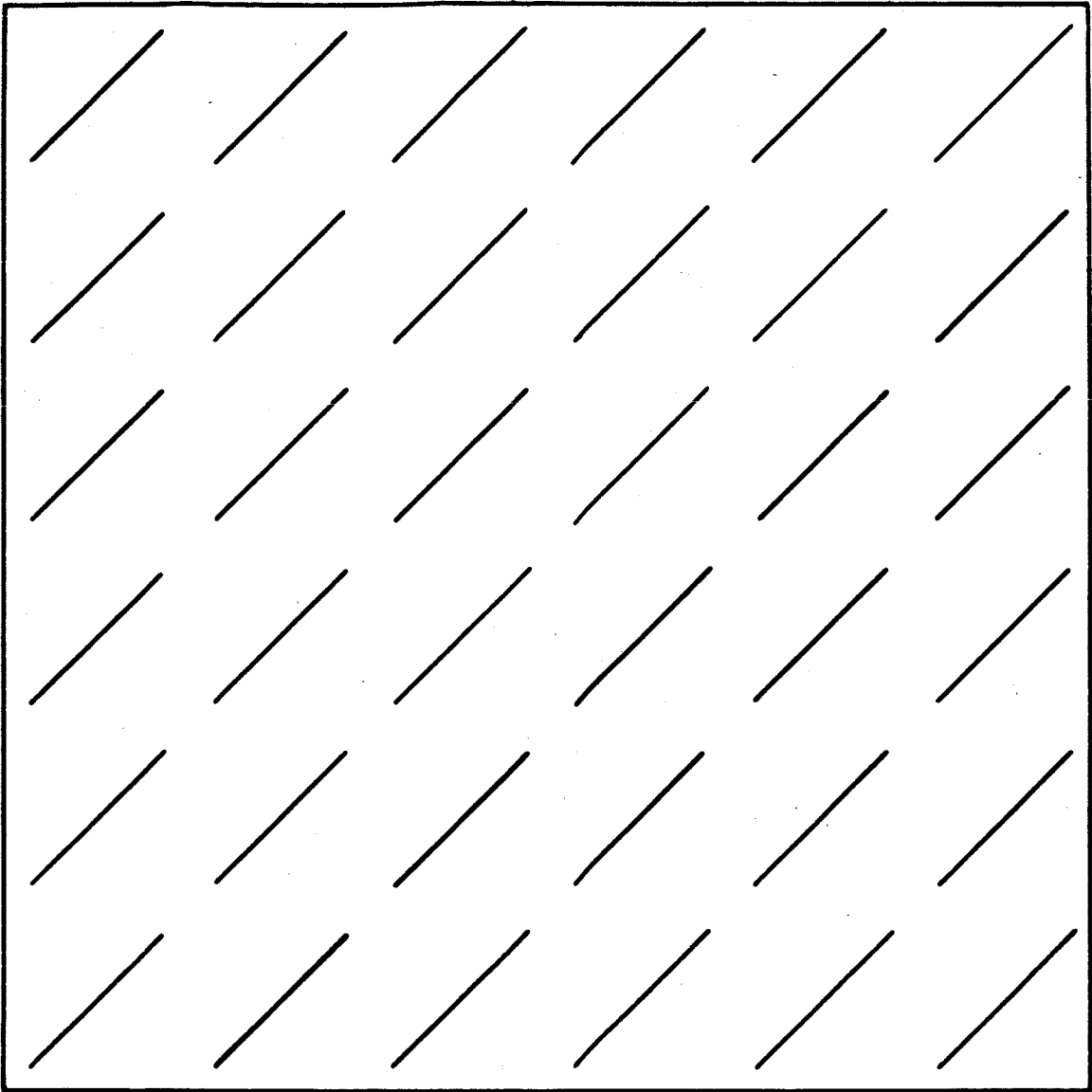


Fig. 34--A simplified array consisting of parallel slots.

slots contribute only to the polarization characteristics so the results will represent the field strength corresponding to alignment parallel to the model array only. A simplification based upon the assumption that the element patterns are hemispherical necessitates adjustment of the computed patterns to account for the actual element patterns. See, for example, the element patterns for the  $E_{\theta}$  and  $E_{\phi}$  components shown in Figures 46 and 47.

The currents for a  $K \times K$  planar array may be expressed in the form

$$\begin{aligned}
 I_1 &= I_{(11)} = |I_{(11)}| \delta_{11} \\
 I_2 &= I_{(12)} = |I_{(12)}| \delta_{12} \\
 I_i &= I_{(pq)} = |I_{(pq)}| \delta_{pq} \\
 I_N &= I_{(KK)} = |I_{(KK)}| \delta_{KK}
 \end{aligned} \tag{80}$$

where  $\delta_{pq} = (pM + qL) 22.5^\circ =$  input phase to  $pq^{\text{th}}$  element. The  $p$  designates the row and  $q$  the column. The above expression is appropriate for a phase scanned array in which the phase is changed in integral multiples of  $22.5^\circ$ . The array can thus be scanned only to those beam pointings that correspond to some combination of  $L$  and  $M$ .  $L$  and  $M$  may assume any integer from  $-7$  to  $+7$ . The upper limit on  $L$  and  $M$

is due to the element spacing, i.e. L or M equal to 7 corresponds to the end fire position. Figure 35 is a photograph of a hemisphere on which a number of beam pointings have been indicated by an "x" with the corresponding L, M value. Several 3 db contours are also shown illustrating that this number of pointings is more than adequate to cover the hemisphere.

A derivation of the mutual admittance between two slots for use in computing the voltages obtained from equations (79) is described in the next section.

## 2. Theoretical Gain and Array Patterns

With the aid of a computer, an arbitrary input current of 0.25 milliamperes at a phase  $\delta_{pq} = (pM + qL) 22.5^\circ$  was assumed and the admittance of each element in the 6 x 6 array was computed for an element spacing of  $0.44\lambda$ . The values were computed for five representative beam pointings where  $(L,M) = (0,0), (0,7), (-2,-2), (-3,-4)$  and  $(-3,-6)$ . These admittance values are tabulated in Appendix A of Technical Report No. 4 for comparison with the isolated value of  $1.19 \times 10^{-2}$  milliohms. The corresponding voltages for the assumed current input are also tabulated in Appendix A. The isolated voltage of the pqth element is  $V_{pq} = .210 \delta_{pq} - 30.2^\circ$  volts. The relative gain and patterns are shown in Appendix B of the same report. The theoretical beam pointings and gain are tabulated below.

where

$$\frac{\delta_0}{kd} = \frac{1}{7.04}$$

These patterns clearly show that the pattern shape is relatively unaffected by mutual coupling. However, the gain is affected to some extent. It should be pointed out that the element pattern has been assumed uniform over the hemisphere. It is clearly seen from Figure 46 that this is a good approximation to the  $E_\theta$  component except near the ground plane. A good approximation to the pattern for the  $E_\phi$  component should be obtained from multiplication of the  $E_\phi$  element pattern shown in Figure 47. Good pattern correspondence was obtained for the only two pointings that have been measured so far as shown in Figure 36 and 37. Since a full set of phase shifters is not available yet, these patterns were obtained by the use of a set of coaxial feed lines cut to lengths required to give the  $(L = 0, M = 0)$ ,  $(L = 0, M = -2)$ ,  $(L = 0, M = -4)$ ,  $(L = 0, M = -6)$  and  $(L = 0, M = -7)$  beam pointings. These patterns are shown in Figures 38 thru 42. At  $L = 0, M = -6$  and  $L = 0, M = -7$  the beam appears to have considerable pointing error. However, this is due to the reduction of the  $E_\phi$  component in the element pattern at angles approaching  $90^\circ$ . This apparent error should not be appreciable for the  $E_\theta$  component. Future test work will include the measurement of the  $E_\theta$  component.

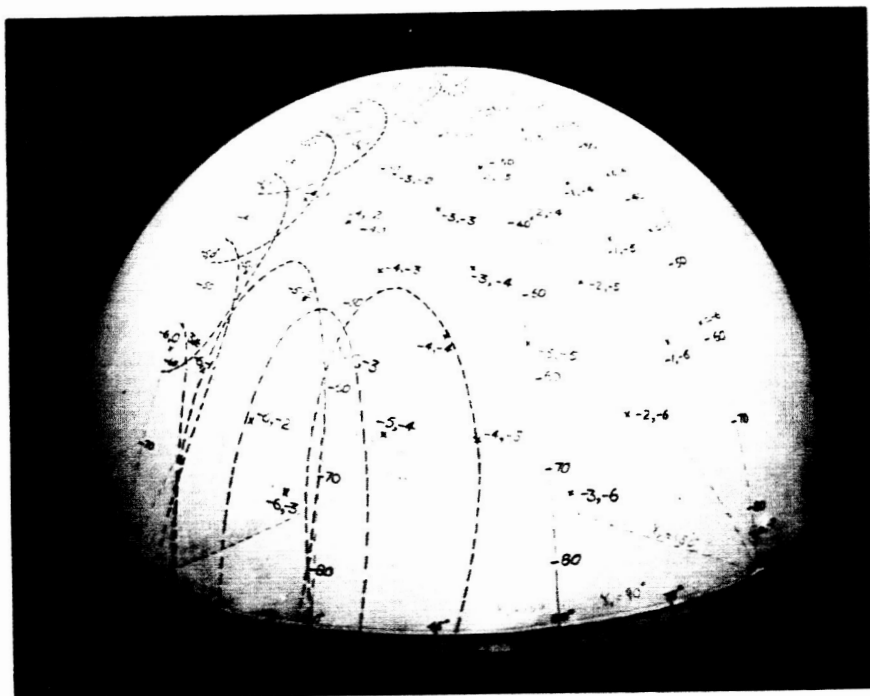


Fig. 35--A photograph of the hemisphere on which the possible beam pointings for the 36 element, crossed-slot receiving and transmitting arrays have been plotted.

<u>L,M</u>	<u>Theoretical Beam Pointing</u>	<u>*Gain (db)</u>
0,0	$\phi = 0^\circ$ and $\theta = 0^\circ$	-1.7
0,-7	$\phi = 90^\circ$ and $\theta = 84^\circ$	-2.7
-2,-2	$\phi = 45^\circ$ and $\theta = 24^\circ$	-0.2
-3,-4	$\phi = 53^\circ$ and $\theta = 45^\circ$	+2.1
-3,-6	$\phi = 63^\circ$ and $\theta = 72^\circ$	+1.4

The positions of the beam maxima were obtained from the simultaneous solution of the following expressions for phase in an array

$$\begin{aligned} k d \cos \alpha_x + L \delta_o &= 0 \\ k d \cos \alpha_y + M \delta_o &= 0 \end{aligned} \quad (81)$$

where

$$k = \frac{2\pi}{\lambda}$$

$$d = 0.44\lambda$$

$$\delta_o = 22.5^\circ \text{ or } \frac{\pi}{8} \text{ radians}$$

The appropriate equations are then

$$\sin \theta = \frac{\delta_o}{k d} \sqrt{L^2 + M^2} \quad (82)$$

$$\sin \phi = - \frac{M}{\sqrt{L^2 + M^2}}$$

---

\*Relative to the maximum of the uncoupled 0,0 beam pointing.

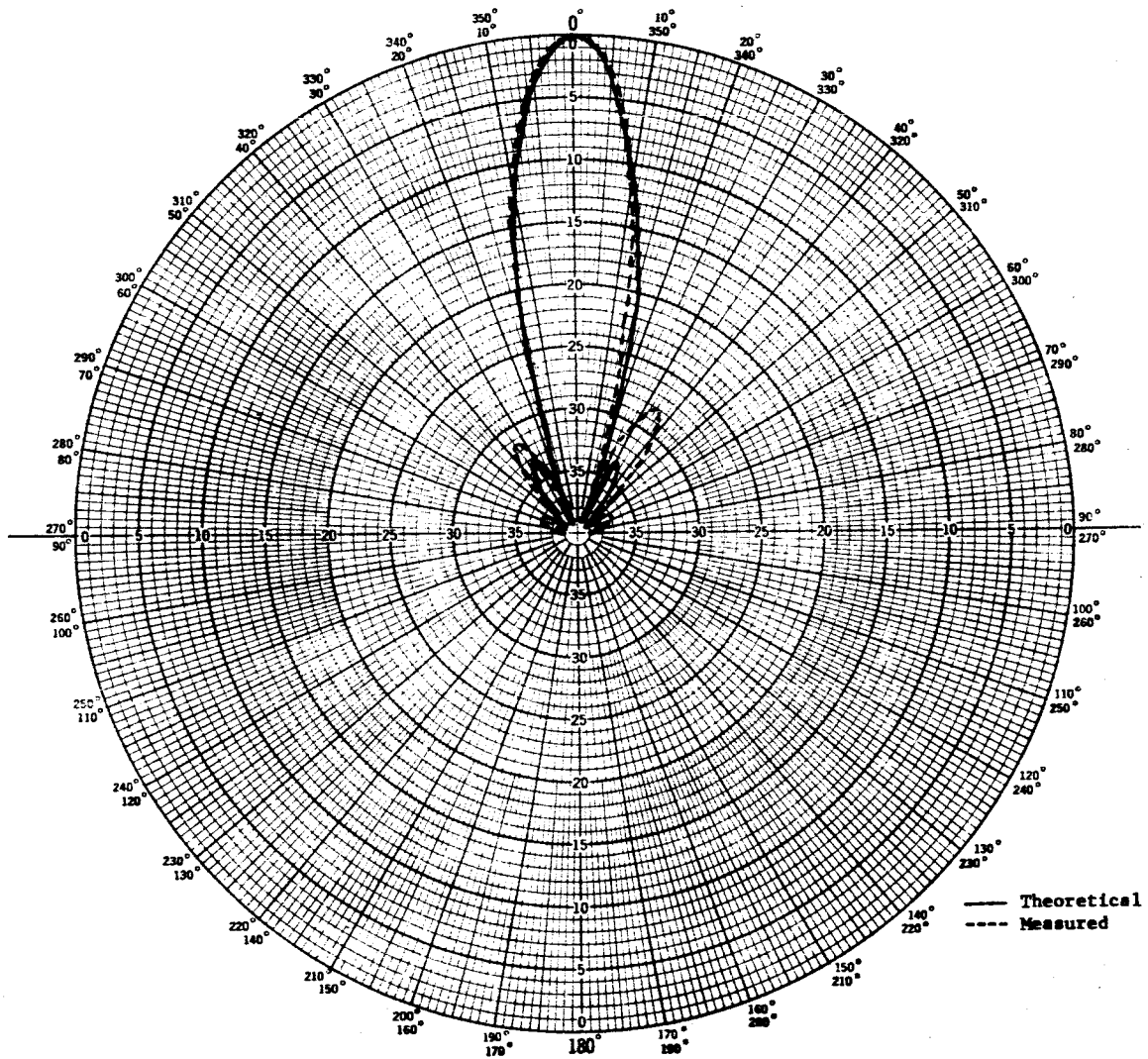


Fig. 36--A  $\theta$ -cut\* of the  $E_\theta$  component for the 36 element receiving array for the  $L = 0$ ,  $M = 0$  beam pointing.

\* $\theta$  as defined in figure 33 with  $\phi = 0^\circ$ .

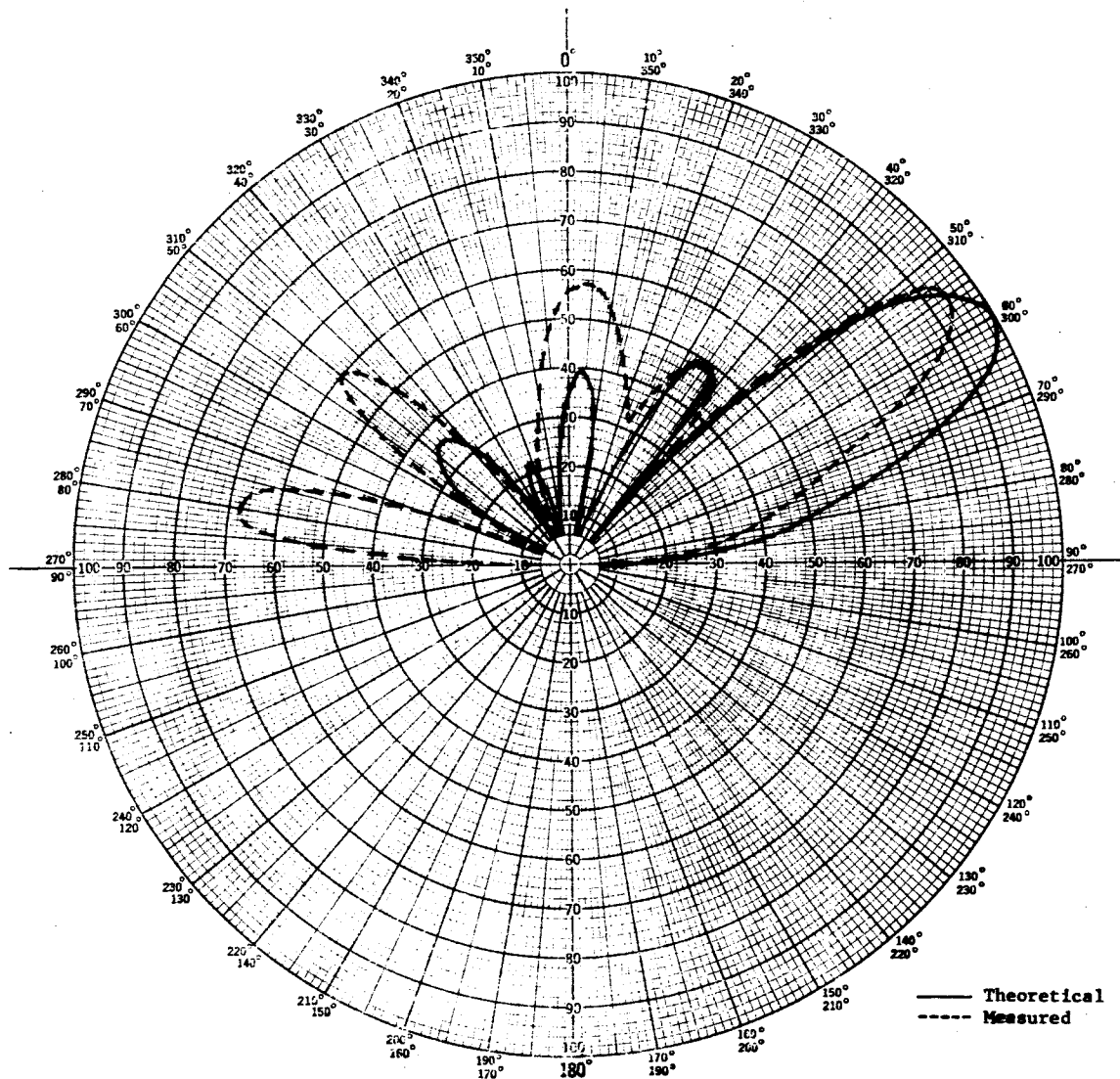


Fig. 37--A  $\theta$ -cut\* of the  $E_\theta$  component for the 36 element receiving array for the  $L = 0$ ,  $M = -7$  beam pointing.

\* $\theta$  as defined in figure 33 with  $\phi = 0^\circ$ .



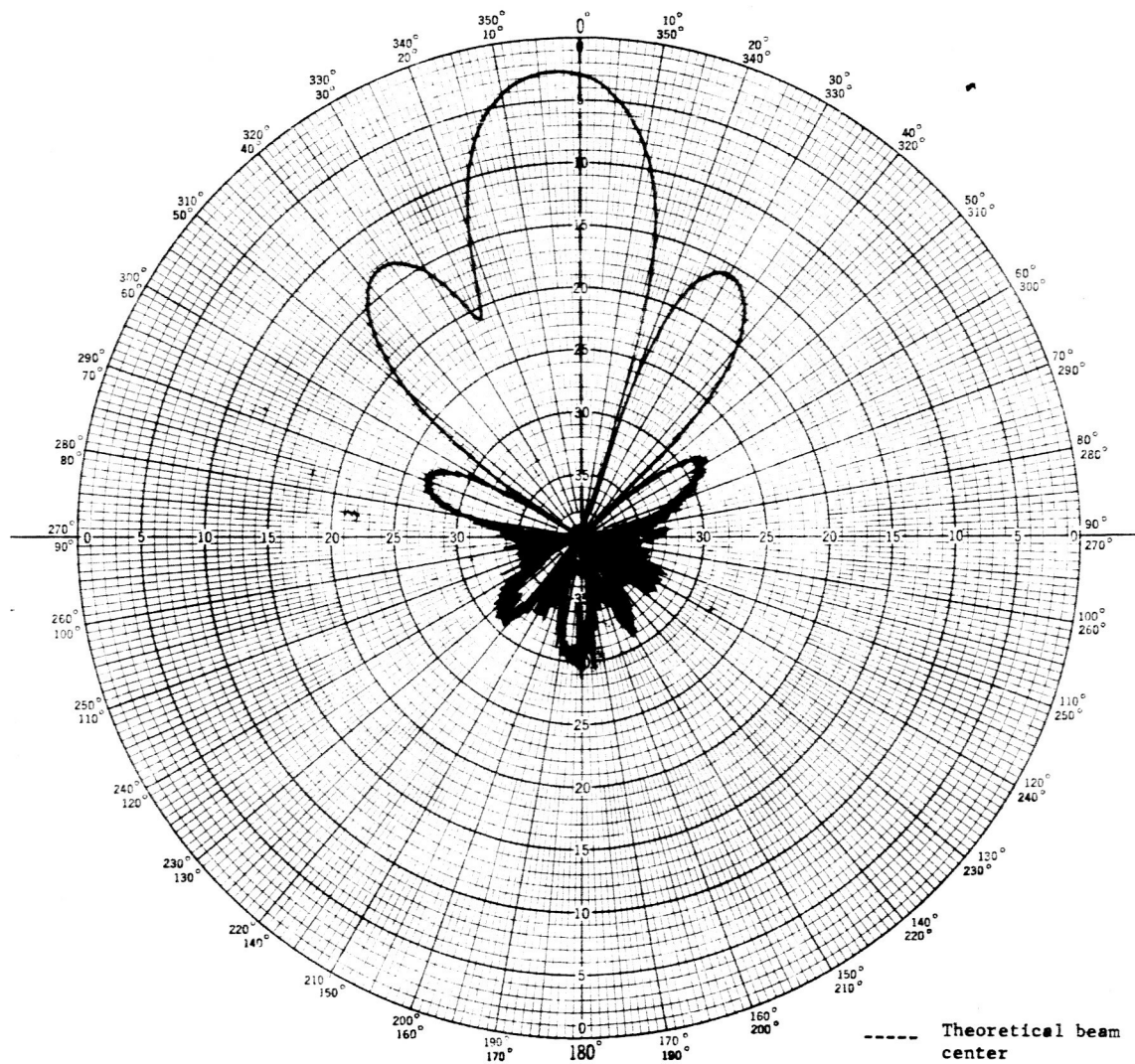


Fig. 38--A  $\theta$ -cut\* of the  $E_0$  component for the 36 element receiving array for the  $L = 0$ ,  $M = 0$  beam pointing.

\* $\theta$  as defined in figure 33 with  $\phi = 0^\circ$ .

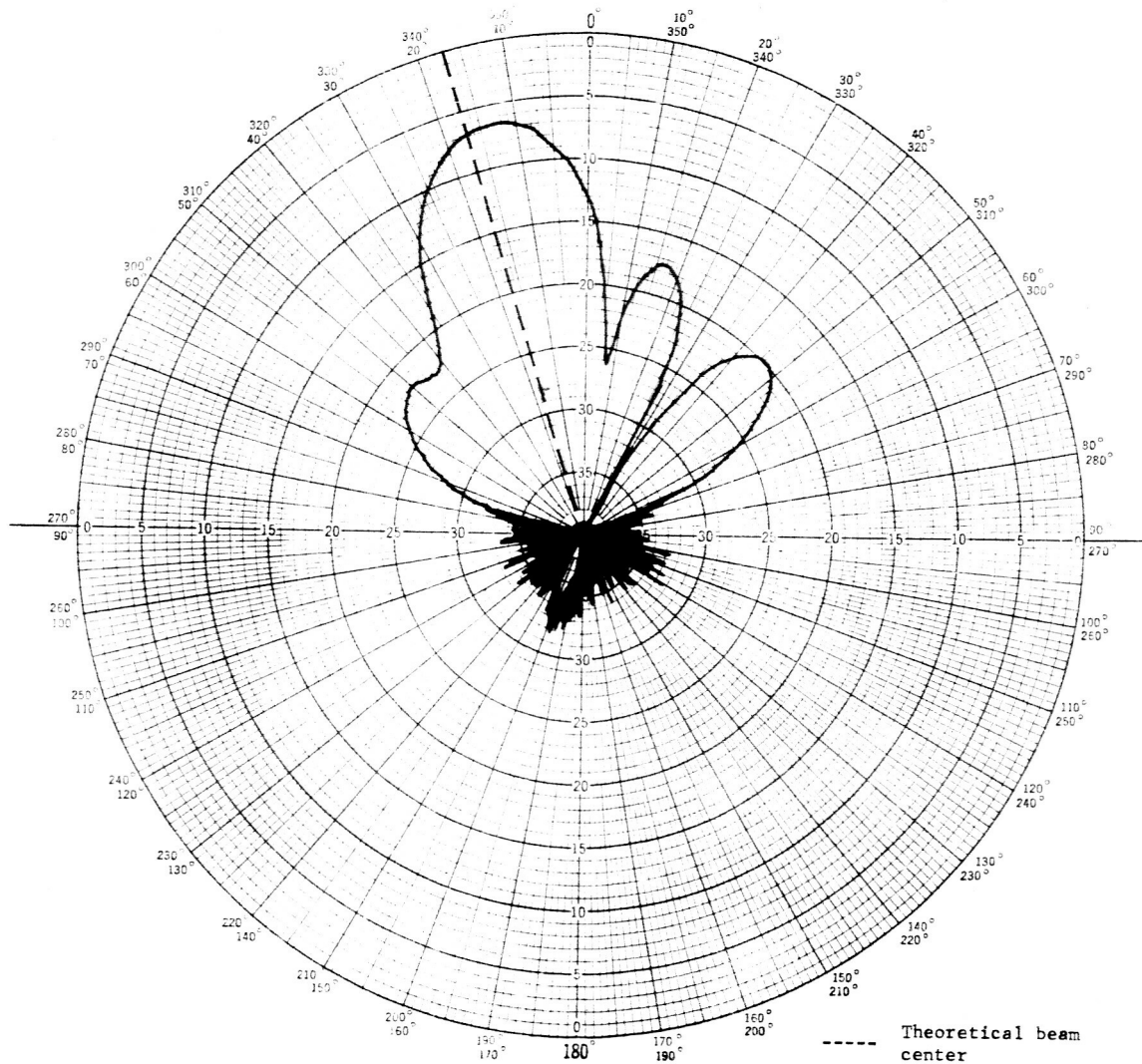


Fig. 39--A  $\theta$ -cut\* of the  $E_\phi$  component for the 36 element receiving array for the  $L = 0$ ,  $M = -2$  beam pointing.

\* $\theta$  as defined in figure 33 with  $\phi = 0^\circ$ .

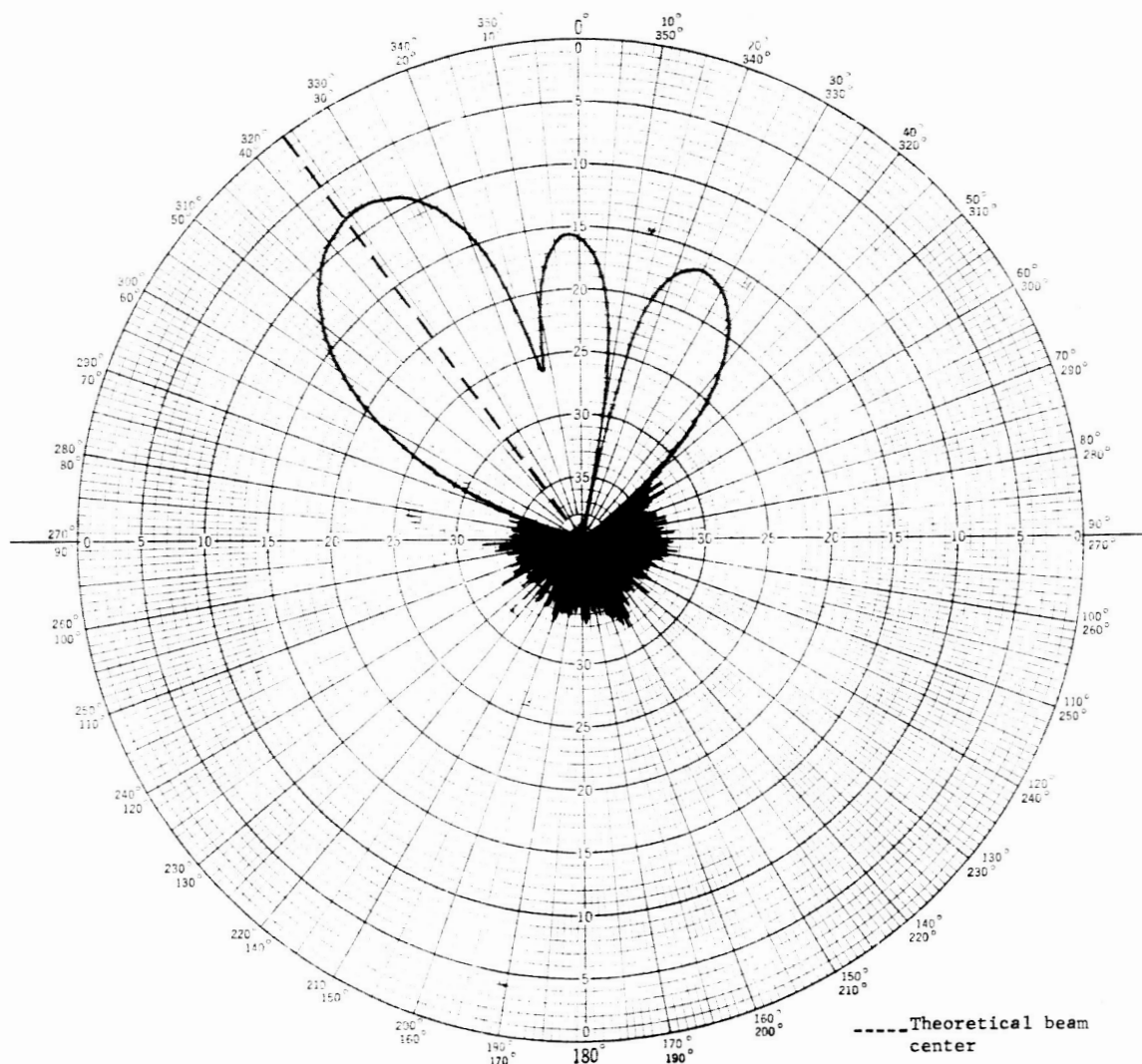


Fig. 40--A  $\theta$ -cut\* of the  $E_0$  component for the 36 element receiving array for the  $L = 0$ ,  $M = -4$  beam pointing.

\* $\theta$  as defined in figure 33 with  $\phi = 0^\circ$ .

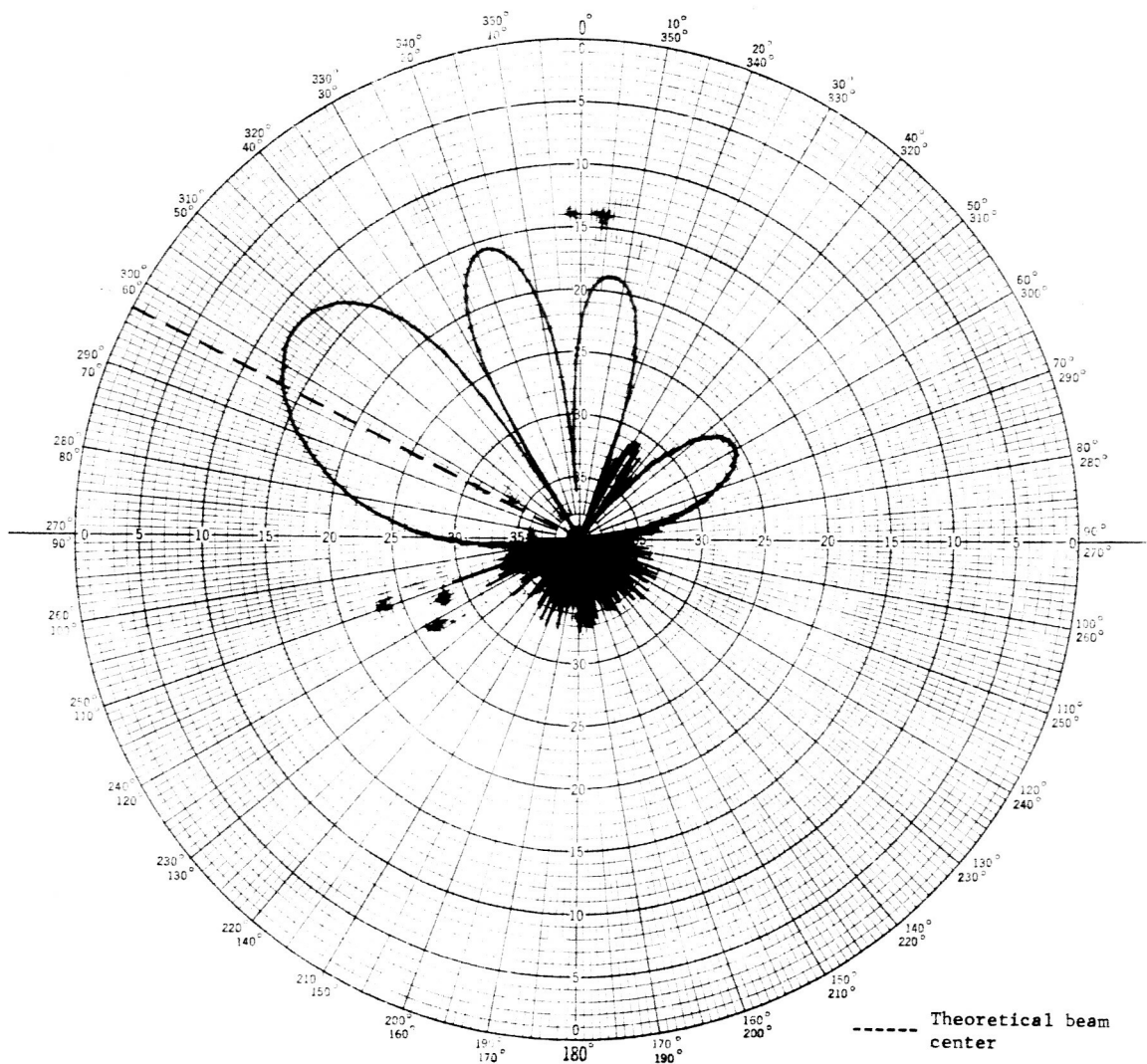


Fig. 41--A  $\theta$ -cut\* of the  $E_\theta$  component for the 36 element receiving array for the  $L = 0$ ,  $M = -6$  beam pointing.

\* $\theta$  as defined in figure 33 with  $\phi = 0^\circ$ .

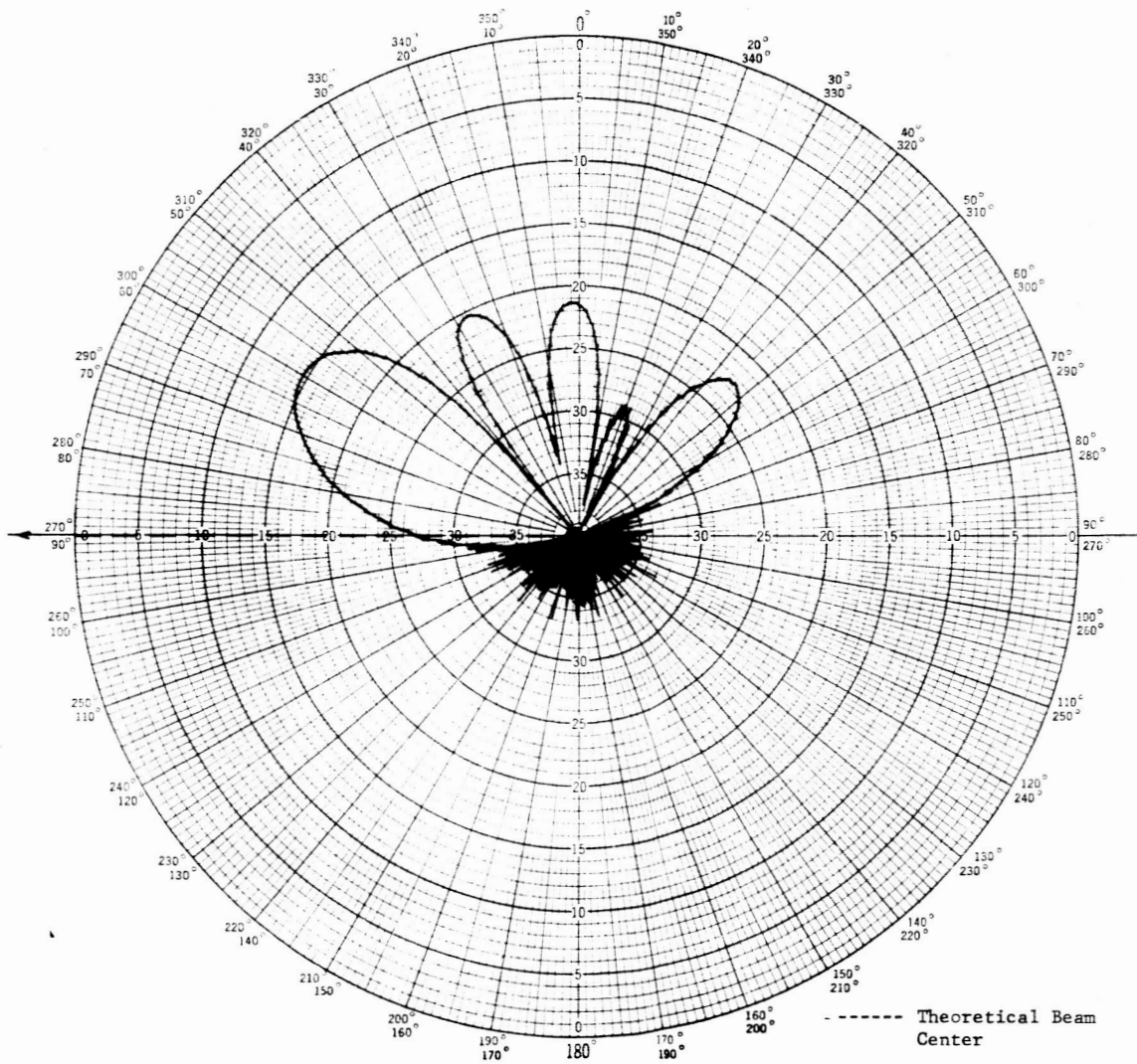


Fig. 41--A  $\theta$ -cut\* of the  $E_0$  component for the 36 element receiving array for the  $L = 0$ ,  $M = -7$  beam pointing.

\* $\theta$  as defined in figure 33 with  $\phi = 0^\circ$ .

The total input power to the array may be expressed as

$$P_T = \sum_{p=0}^5 \sum_{q=0}^5 |V_{pq}|^2 G_{pq} \quad (83)$$

where  $G_{pq}$  is the real part of the terminal admittance of the  $pq^{\text{th}}$  element. From this equation the power gain of the array can be obtained for each pointing. Choosing a single slot in an infinite ground plane as a reference antenna the reference power is

$$P_{\text{ref}} = |V|^2 G_{11} \quad (84)$$

where  $G_{11}$  is the real part of the input admittance to a single half wavelength slot. The field pattern of the reference slot may be expressed as

$$F(\theta, \phi)_{\text{max}} = V \left[ \cos k(r-r_1) - j \sin k(r-r_1) \right] \quad (85)$$

and obviously

$$F(\theta, \phi)_{\text{max}} = V \text{ for a single slot} \quad (86)$$

also,

$$P_{\text{ref}} = |F(\theta, \phi)_{\text{max}}|^2 G_{11} \quad (87)$$

Now, if the  $F(\theta, \phi)_{\text{max}}$  for the single slot is made equal to the  $F(\theta, \phi)_{\text{max}}$  of the array, the ratio of the  $P_{\text{ref}}$  required to accomplish this to the total input power to the array,  $P_T$ , is equal to the power gain of the array, that is

$$G = \frac{|F(\theta, \phi)_{\text{max}}|^2 G_{11}}{P_T} \quad (88)$$

where  $F(\theta, \phi)_{\text{max}}$  has been obtained in accordance with equation (72) and  $G_{11}$  is obtained from equation (107).

For the uncoupled case, let  $P_s$  be the power input to each slot, then  $P_T = 36P_s$  is the total power input to the array and  $P_s = |V_s|^2 G_{11}$ . The field maximum will be proportional to  $36 V_s$ . Now,  $P_{\text{ref}} = |V|^2 G_{11}$  and the field maximum will be proportional to  $V$  in this case. If  $V$  is made equal to  $36 V_s$  then  $P_{\text{ref}} = |36 V_s|^2 G_{11}$ . As before,

$$G = \frac{P_{\text{ref}}}{P_T} \quad (89)$$

or

$$G = \frac{|36 V_s|^2 G_{11}}{36 |V_s|^2 G_{11}} = 36 \quad (90)$$

The uncoupled slot array gain above a single slot antenna is  $10 \log_{10} G$  or 15.55 db. The element gain added to this will give the total gain. The measured gain of the receiving array was 11.7 db above an isotropic source. This corresponds to an element gain of -3.85 db below an isotropic source. The directivity of an isolated slot antenna is approximately 1.33 (or 1.24 db above an isotropic source) obtained from the relation

$$D = \frac{4\pi F(\theta, \phi)_{\max}}{\int \int F(\theta, \phi) d\Omega} \quad (91)$$

and the gain is related to the directivity by

$$G = KD \quad (92)$$

where  $k$  = the antenna efficiency factor.

The relative gain of -3.85 db, corresponds to a power ratio of 0.41, therefore,  $K = 0.308$  or 30.8% efficiency. Most of the efficiency loss is due to the method of achieving circular polarization. This is discussed in more detail in Section 4. It should be possible to improve the efficiency of the slot element somewhat by further optimization of the slot width and slot length.

### 3. Derivation of the Mutual Admittance Between Two Slots

Consider the slot shown in Figure 43, the electric field intensity in the slot is given by



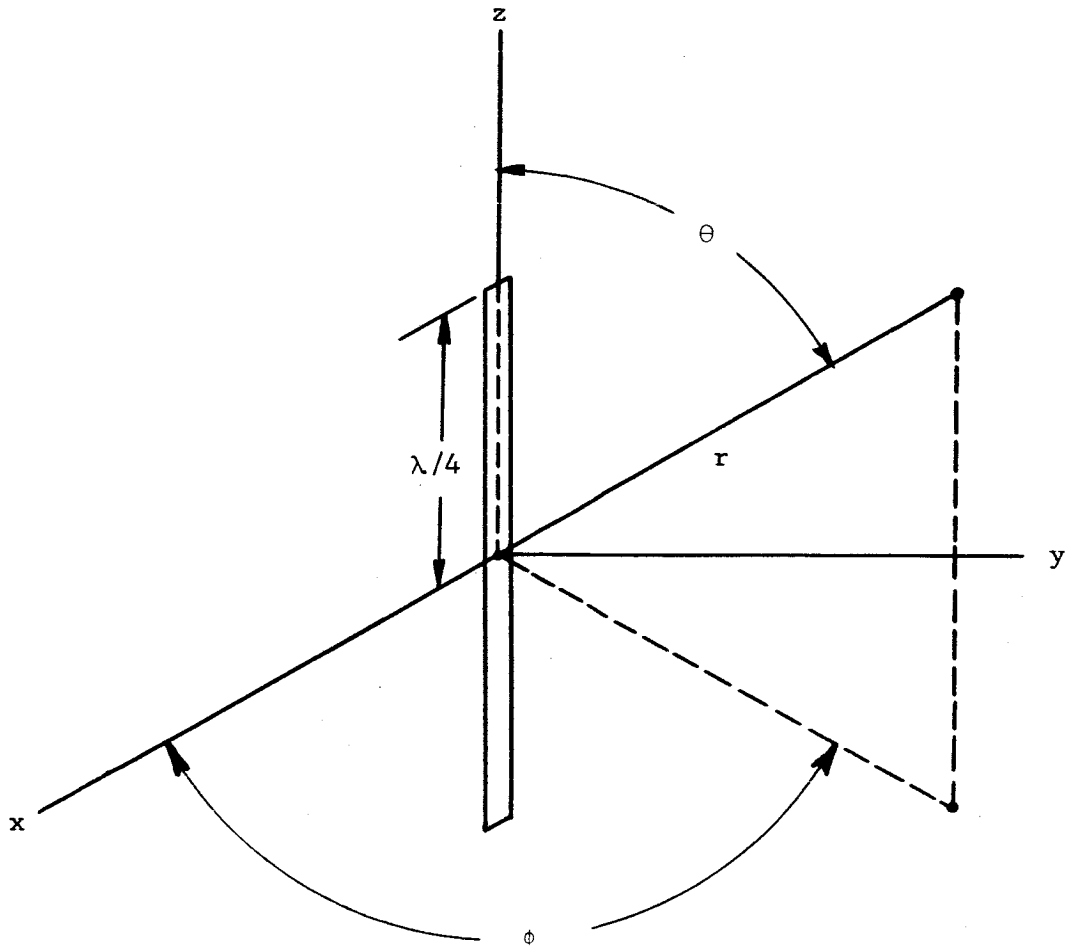


Fig. 43-Single slot geometry.

$$E_x(z) = \frac{V_T}{2a} \cos(kz) \quad (93)$$

where  $V_T$  is the gap voltage at the center of the slot. The time average pointing vector is

$$\langle \vec{s} \rangle_P = \frac{1}{2} \vec{E} \times \vec{H}^* = \frac{-1}{2} E_x H_z^* \vec{n}, \quad (94)$$

where  $\vec{n}$  is normal to and directed outward from the plane of the slot.

Equation (94) may also be written

$$\langle \vec{s} \rangle_P = \frac{-V_T}{4a} \cos(k_z) H_z^*(z) \vec{n}, \quad (95)$$

The complex power is the integral of (95) over the total surface and may be written as

$$P_c = V_T \int_{-\lambda/4}^{\lambda/4} H_z^*(z) \cos(kz) dz \quad (96)$$

For a cavity-backed slot, the complex power is halved due to the halving of the physical aperture and is

$$P_c = \frac{1}{2} V_T \int_{-\lambda/4}^{\lambda/4} H_z^*(z) \cos(kz) dz \quad (97)$$

The complex power may also be expressed as

$$P_c = \frac{1}{2} V_T V_T^* Y_T \quad (98)$$

Combining (97) and (98) yields

$$Y_T = \frac{1}{V_T} \int_{-\lambda/4}^{\lambda/4} H_z^*(z) \cos(kz) dz, \quad (99)$$

$H_z^*(z)$  can be obtained by duality from the expression derived for the  $E(z)$  component for dipoles and is described in Technical Report No. 4. Note that  $Y_T = Y_{11}$  since  $Y_T$  was derived for a single isolated slot antenna. The magnetic field component in the  $z$ -direction is

$$H_z(z) = -j \frac{V_T}{2\pi\eta} \left[ \frac{e^{-jkr_{t1}}}{r_{t1}} + \frac{e^{-jkr_{b2}}}{r_{b2}} \right], \quad (100)$$

where  $\eta$  is replaced by  $1/\eta$  and the multiplication by 2 occurs due to the magnetic current relationship on a conductor  $M_s = \bar{E} \times \bar{n}$ . The use of symmetrical and antisymmetrical inputs yields

$$\begin{aligned} Y_s &= Y_{11} + Y_{12} \\ Y_z &= Y_{11} - Y_{12} \end{aligned} \quad (101)$$

and, thus,

$$Y_{12} = \frac{1}{2} (Y_s - Y_a) \quad (102)$$

It is seen that  $Y_s$  is the terminal admittance of each slot when the two slots are symmetrically fed, that is  $Y_s = Y_T$ , and from expression (99)

$$Y_s = \frac{1}{V_T} \int_{-\lambda/4}^{\lambda/4} H_z^*(z) \cos(kz) dz \quad (103)$$

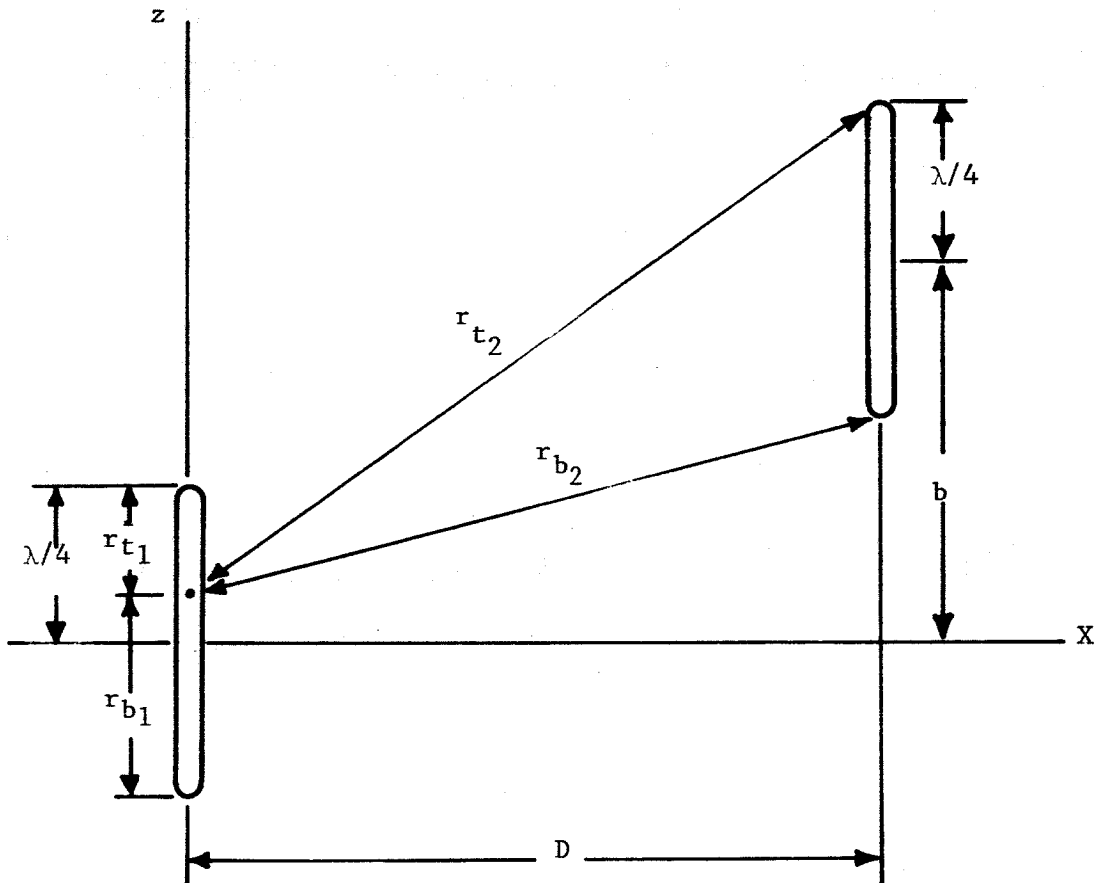
where  $H_z(z)$  is due to the voltage along each slot antenna and is given by

$$H_z(z) = -j \frac{V_T}{2\pi\eta} \left[ \frac{e^{-jkr_{t1}}}{r_{t1}} + \frac{e^{-jkr_{b1}}}{r_{b1}} + \frac{e^{-jkr_{t2}}}{r_{t2}} + \frac{e^{-jkr_{b2}}}{r_{b2}} \right]. \quad (104)$$

The quantities  $r_{t1}$ ,  $r_{t2}$ ,  $r_{b1}$ , and  $r_{b2}$  are shown in Figure 44. Inserting (104) into (103) gives

$$Y_s = \frac{1}{2\pi\eta} \int_{-\lambda/4}^{\lambda/4} \left[ \frac{e^{-jkr_{t2}}}{r_{t1}} + \frac{e^{-jkr_{b1}}}{r_{b1}} \right] \cos(kz) dz \quad (105)$$

$$+ \frac{j}{2\pi\eta} \int_{-\lambda/4}^{\lambda/4} \left[ \frac{e^{-jkr_{t2}}}{r_{t2}} + \frac{e^{-jkr_{b2}}}{r_{b2}} \right] \cos(kz) dz$$



$$r_{t1} = \lambda/4 - z$$

$$r_{b1} = \lambda/4 + z$$

$$r_{t2} = \sqrt{d^2 + (b + \lambda/4 - z)^2}$$

$$r_{b2} = \sqrt{d^2 + (b - \lambda/4 - z)^2}$$

Fig. 44--The geometry for two parallel slots that are  $\lambda/2$  in length.

The first integral is identical with the expression for the terminal admittance of a single isolated slot in equations (99) and (100)

where  $Y_T = Y_{11}$  so the second integral must represent  $Y_{12}$ . Therefore,

$$Y_{12} = \frac{j}{2\pi\eta} \int_{-\lambda/4}^{\lambda/4} \left[ \frac{e^{-jkr_{t2}}}{r_{t2}} + \frac{e^{-jkr_{b2}}}{r_{t2}} \right] \cos(kz) dz \quad (106)$$

The form of  $Y_{12}$  for slots is identical to the form obtained for  $Z_{12}$  for dipoles. Thus, the results of this slot array pattern analysis will apply equally well to a dipole array. By use of Euler's identity  $e^{-jA} = \cos A - j\sin A$  and Simpson's 1/3 rule of integration,  $Y_{12}$  can be used to evaluate the mutual admittance of any two slots in the array and substituted in the admittance matrix represented by expression (79). When there is no mutual coupling, the input admittance would obviously be that of an isolated element and is

$$Y_{11} = \left[ 1.029 + j0.599 \right] \text{ millimhos} \quad (107)$$

or

$$Y_{11} = 1.19 \angle 30.2^\circ \text{ millimhos} \quad (108)$$

## 4. Crossed-Slot Element Description

For the particular case of a dipole of length  $\lambda/2$ , use of the vector potential lends to the following expression for the magnetic field in the far zone:

$$H_{\phi} = \frac{j (I_0) \cos\left(\frac{\pi}{2} \cos\theta\right)}{2\pi r \sin\theta} \quad (109)$$

This expression is based on the geometry in Figure 43. If two dipoles are considered oriented as in Figure 45, the appropriate coordinate transformations lead to the following normalized expressions:

$$H_{\theta_x} = \frac{\sin\phi \cos\left(\frac{\pi}{2} \sin\theta \cos\phi\right)}{1 - \sin^2\theta \cos^2\phi} \quad (110)$$

and

$$H_{\phi_x} = \frac{\cos\theta \cos\phi \cos\left(\frac{\pi}{2} \sin\theta \cos\phi\right)}{1 - \sin^2\theta \cos^2\phi}$$

when the dipole is aligned along the x-axis and,

$$H_{\theta_x} = \frac{\cos\phi \cos\left(\frac{\pi}{2} \sin\theta \sin\phi\right)}{1 - \sin^2\theta \sin^2\phi} \quad (111)$$

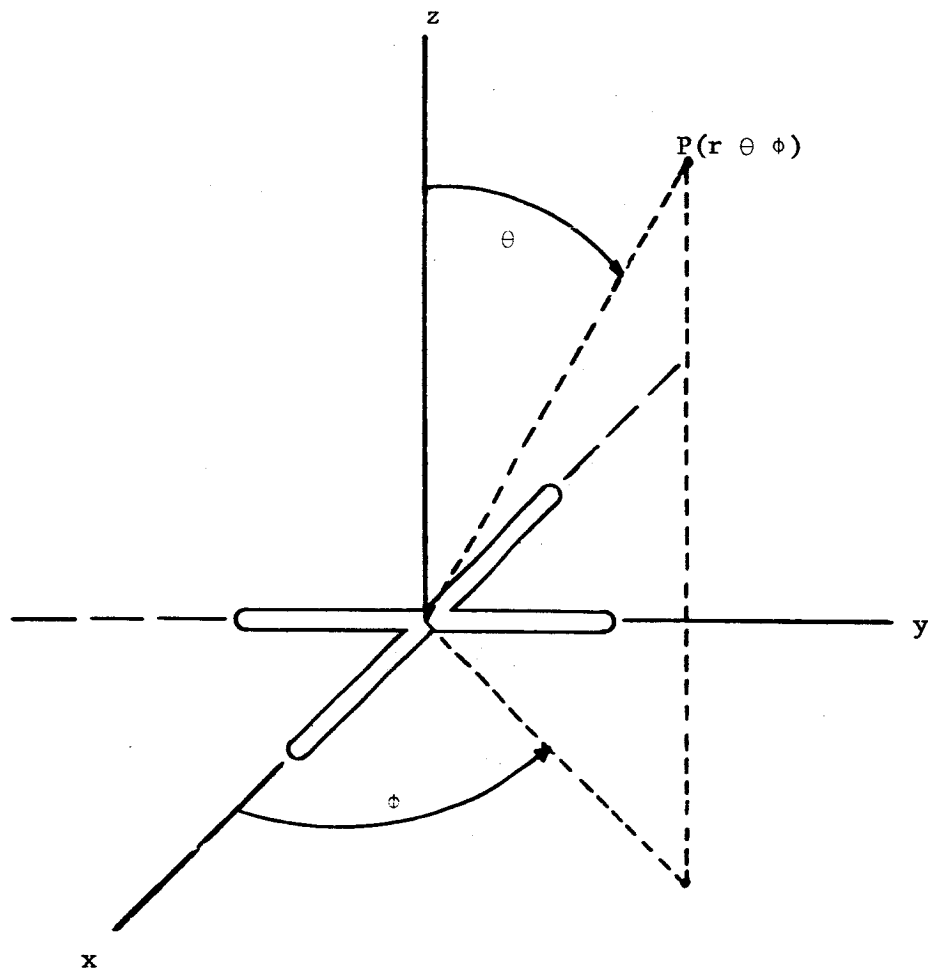


Fig. 45--Crossed-slot geometry



and

$$H_{\phi y} = \frac{\cos\theta \sin\phi \cos\left(\frac{\pi}{2} \sin\theta \sin\phi\right)}{1 - \sin^2\theta \sin^2\phi}$$

for alignment of the dipole along the y-axis.

The electric field of a crossed slot antenna in an infinite ground plane is obtained by application of the duality principle. The normalized electric field components in the radiation field are:

$$E_{\theta x} = \frac{\sin\phi \cos\left(\frac{\pi}{2} \sin\theta \cos\phi\right)}{1 - \sin^2\theta \cos^2\phi}$$

and

(112)

$$E_{\phi x} = \frac{\cos\theta \cos\phi \cos\left(\frac{\pi}{2} \sin\theta \cos\phi\right)}{1 - \sin^2\theta \cos^2\phi}$$

for the slot along the x-axis, and

$$E_{\theta y} = \frac{\cos\phi \cos\left(\frac{\pi}{2} \sin\theta \sin\phi\right)}{1 - \sin^2\theta \sin^2\phi}$$

and

(113)

$$E_{\phi y} = \frac{\cos\theta \sin\phi \cos\left(\frac{\pi}{2} \sin\theta \sin\phi\right)}{1 - \sin^2\theta \sin^2\phi}$$

for a slot along the y-axis. The total electric field for the crossed slot antenna will be the vector sum of (112) and (113). If the excitation in the x-axis slot is chosen as the reference phase and the excitation in the y-axis lags by some phase angle  $\delta$  then

$$E_{\theta} = E_{\theta_x} \cos\omega t + E_{\theta_y} \cos(\omega t - \delta)$$

and

(114)

$$E_{\phi} = E_{\phi_x} \cos\omega t + E_{\phi_y} \cos(\omega t - \delta)$$

or

$$E_{\theta} = (E_{\theta_x} + E_{\theta_y} \cos\delta) \cos\omega t + E_{\theta_y} \sin\delta \sin\omega t$$

and

(115)

$$E_{\phi} = (E_{\phi_x} + E_{\phi_y} \cos\delta) \cos\omega t + E_{\phi_y} \sin\delta \sin\omega t$$

In order to achieve circular polarization it is necessary to have  $\delta = 90^\circ$  and equal amplitudes. Since equations (113) and (114) are both normalized, equal amplitudes are implied, therefore,

$$E_{\theta} = E_{\theta_x} \cos\omega t + E_{\theta_y} \sin\omega t \quad (116)$$

and

$$E_{\phi} = E_{\phi_x} \cos \omega t + E_{\theta} \sin \omega t \quad (116)$$

or

$$E_{\theta} = E_{\theta_x} - jE_{\theta_y}$$

and

$$E_{\phi} = E_{\phi_x} - jE_{\phi_y} \quad (117)$$

The pattern factors for the circularly polarized crossed-slot antenna are then

$$E_{\theta} = \frac{\sin \phi \cos(\frac{\pi}{2} \sin \theta \cos \phi)}{1 - \sin^2 \theta \cos^2 \phi} + j \frac{\cos \phi \cos(\frac{\pi}{2} \sin \theta \sin \phi)}{1 - \sin^2 \theta \sin^2 \phi} \quad (118)$$

and

$$E_{\phi} = \frac{\cos \theta \cos \phi \cos(\frac{\pi}{2} \sin \theta \cos \phi)}{1 - \sin^2 \theta \cos^2 \phi} - j \frac{\cos \theta \sin \phi (\cos \frac{\pi}{2} \sin \theta \sin \phi)}{1 - \sin^2 \theta \sin^2 \phi} \quad (119)$$

The  $\theta$  component is present throughout the hemisphere and has a variation of only 1 db from the maximum value for an infinite ground plane. The  $\phi$  component has approximately a  $\cos\theta$  variation over the hemisphere. A single crossed-slot antenna constructed to the same specifications as an element in the full-size receiving array, was tested. The measured field patterns of this antenna are shown in Figure 46 and 47. The only significant departure from the theoretical patterns described by equations (10) and (11) occurs near  $\theta = 90^\circ$ . This is to be expected since the duality principle was used to obtain the theoretical results. The duality principle requires an infinite ground plane whereas a 4 x 4 foot ground plane was actually used to obtain the measured patterns. A larger ground plane will increase the magnitude of the  $E_\theta$  component and decrease the magnitude of the  $E_\phi$  component. The same criterion, of course, applies to the full size array since the element pattern is multiplied by the array factor to yield the final pattern. Since the crossed-slot antenna was designed for use in an array that is to be phase scanned over a full hemisphere, it was necessary for the element spacing to be less than  $\lambda/2$  in order to prevent the formation of grating lobes. It was necessary to design the cavities with a dielectric fill since conventional air-filled cavities with a square cross section and a length 1.5 times the square dimension may be spaced no closer than about  $0.6\lambda$ . This permits a reduction of the required dimensions inversely proportional to the square root of the relative dielectric constant. Rexolite

1422 was chosen due to its desirable low loss and machineability characteristics. It has a relative dielectric constant of approximately 2.5. This permits a 37% reduction in the physical dimensions of the cavity.

The measured dielectric constant for the cavities used in the antenna array is lower than the manufacturer's specifications because the cavity is not completely filled by the Rexolite. For the receiving array the measured dielectric constant was 2.47 as compared with a specified value of 2.53. A plot of the measured resonant frequency of the 36 element receiving array is shown in Figure 48.

Each loop to a single cavity is fed from a coaxial (TNC) receptacle and terminates thru an adjustable capacitor to ground potential. This is clearly seen in the photograph of a single element in Figure 51. There is an adjustable screw in the center of the cavity that serves to vary the cross coupling between the two loops. This alters the magnetic field configuration (and thereby the impedance) in the vicinity of the loops. Figure 49 shows a plot of the resonant frequency shift versus the depth of penetration of the tuning screw. The optimum position for the screw occurs approximately at  $L/4$ .

A cavity with a loaded Q of 74 has a bandwidth of about 30 MHz at a resonant frequency of 2.214 GHz. For a closed cavity of the dimensions used in the design of the crossed-slot antenna, a theoretical unloaded Q of 1378 is possible. This would imply a lower limit on the bandwidth of about 1.6 MHz. Pattern measurements shown in

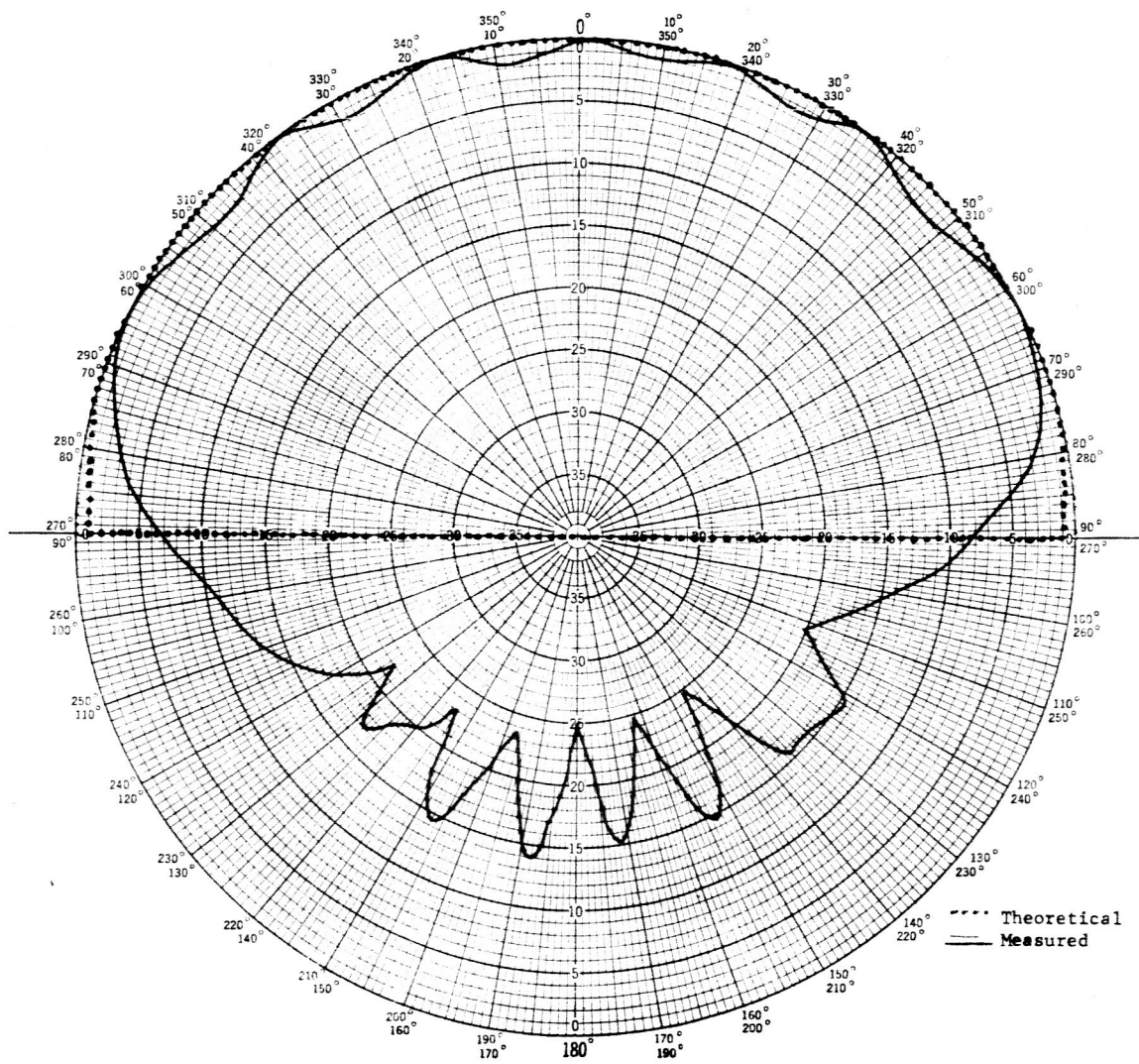


Fig. 46--Variation of the  $E_{\theta}$  component in the  $\phi = 0^{\circ}$  plane for a single, isolated, crossed-slot antenna.

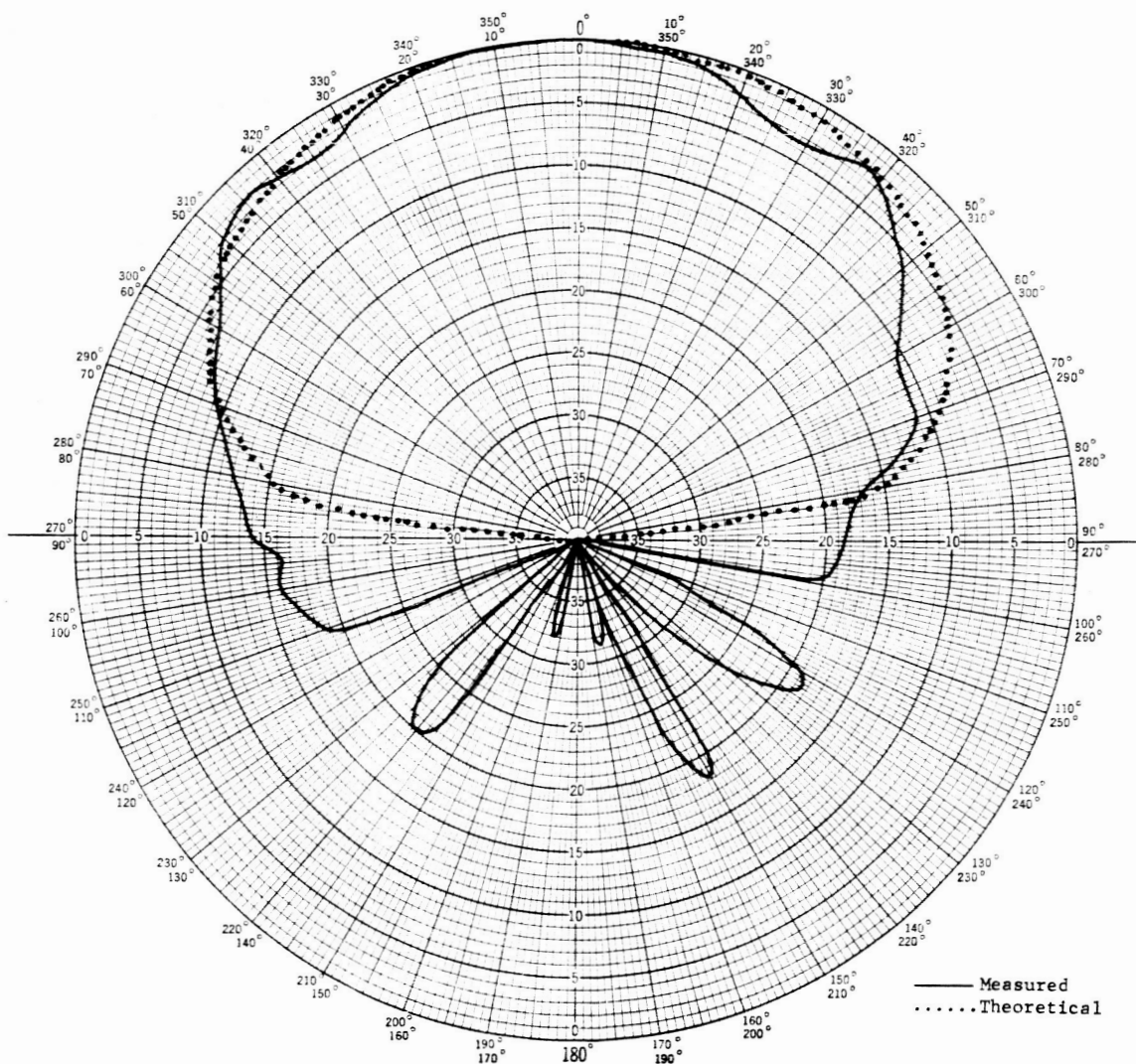
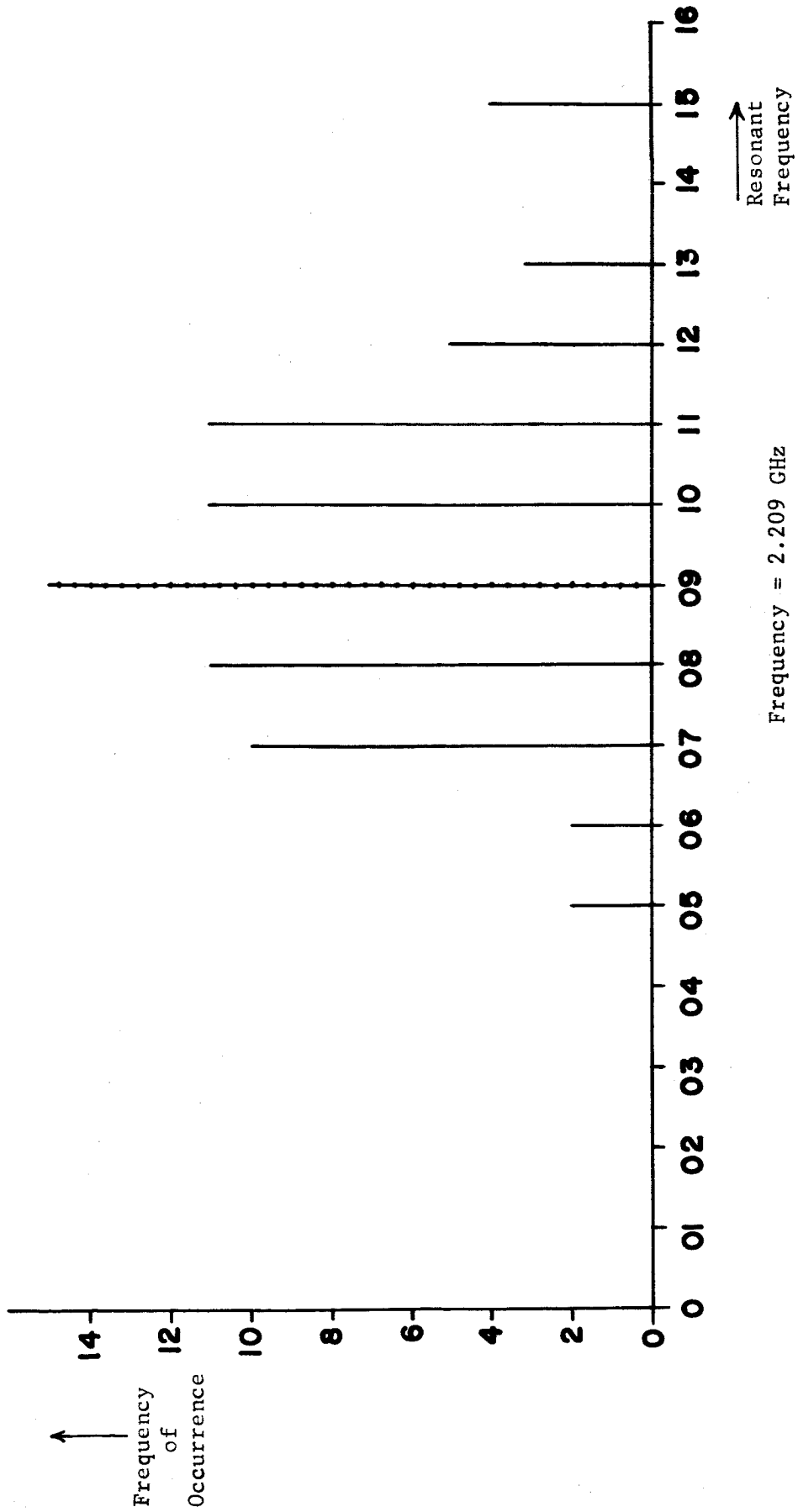


Fig. 47--Variation of the  $E_{\theta}$  component in the  $\phi = 0^{\circ}$  plane for a single, isolated, crossed-slot antenna.

Polar Chart No. 127D  
 SCIENTIFIC-ATLANTA, INC.  
 ATLANTA, GEORGIA



Frequency = 2.209 GHz

Fig. 48--A plot of the measured resonant frequency of the cavities in the 36 element, crossed-slot receiving array versus the frequency of occurrence.



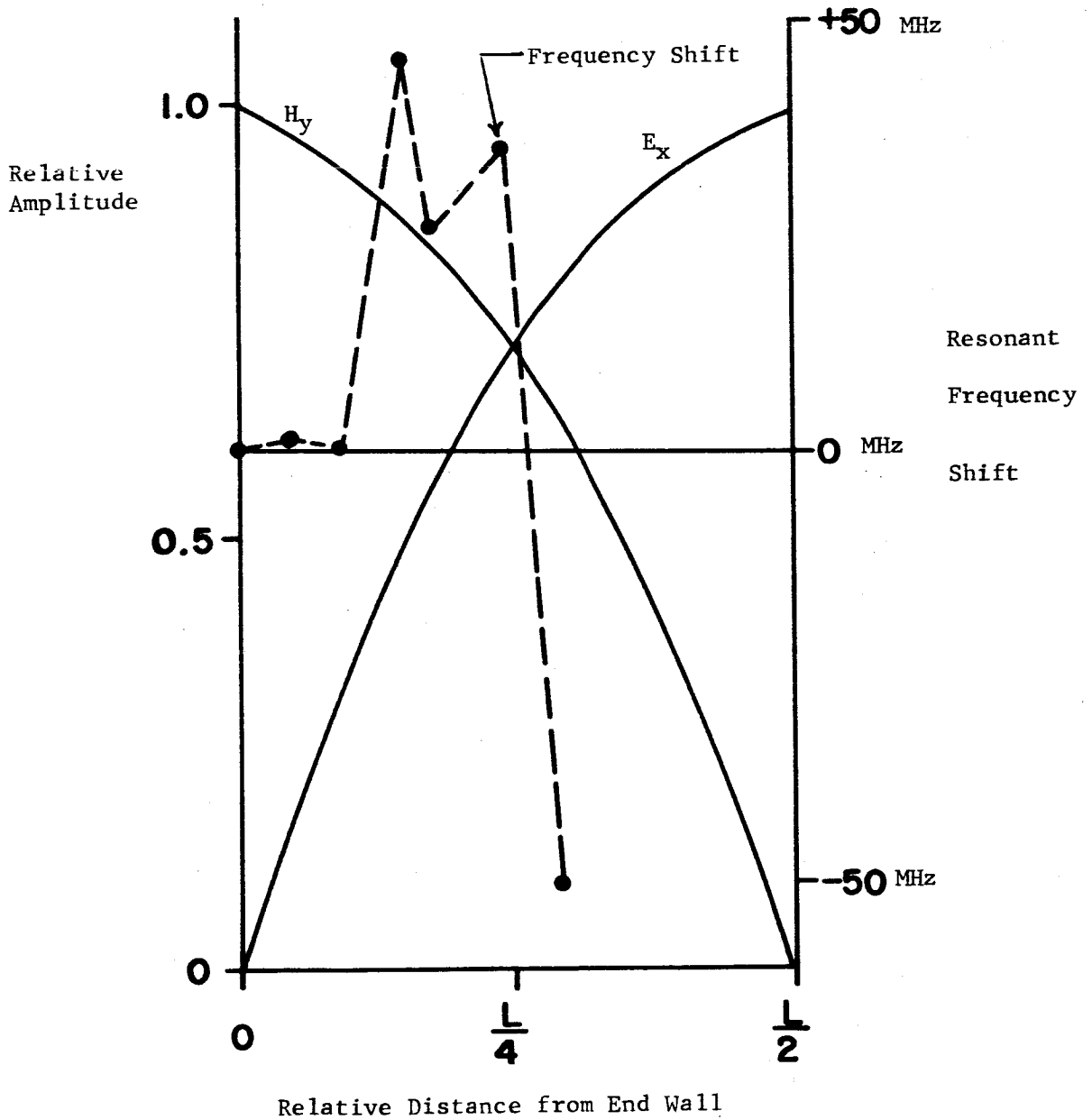


Fig. 49--A plot of the shift in frequency resonance of a single closed cavity as a function of the depth of penetration of the tuning screw.

Figure 50 indicate that the element actually has a bandwidth a little greater than 30MHz. The element shown in Figure 51 operates at a center frequency of 2.200 GHz. The gain drops sharply at the out-of-band frequency of 2.177 GHz. Figure 52 is a photograph of a four element crossed-slot array. This array was used to test the proposed method for constructing the full size 36 element array.

The original method of achieving circular polarization utilized the excitation of two loops. One loop excited a  $TE_{101}$  mode and the other loop excited a  $TE_{011}$  mode (which is identical to the  $TE_{101}$  mode except that all of the components of the  $TE_{011}$  mode are perpendicular to those of  $TE_{101}$  mode). One of the loops was excited at a reference time phase of  $0^\circ$  while the other loop was excited at a time phase of  $90^\circ$ . The crossed slots are aligned on the  $45^\circ$  diagonal with respect to the square walls of the cavity as well as to the  $TE_{101}$  and  $TE_{011}$  modes. However, the time phase is such that the resultant is that required for a circularly polarized wave, i.e. two equal amplitude waves  $90^\circ$  in time phase and in space quadrature.

Figure 53 shows the theoretical polarization patterns that are obtained for time phase lags of  $0^\circ$ ,  $45^\circ$  and  $90^\circ$  for comparison purposes. Figure 54 shows the theoretical polarization patterns for these same values of  $\delta$ , but with one component one half the amplitude of the other component. It is interesting to note from these two figures that the null in a polarization pattern will not shift unless

an amplitude imbalance exists in the system. Test of a single crossed-slot antenna fed thru two loops were made for values of  $\delta$  between  $0^\circ$  and  $360^\circ$ . The resulting polarization patterns indicated the presence of an amplitude mismatch. Furthermore, the degree of mismatch seemed to be a function of  $\delta$  since both a null shift and gain variation were present.

The method that resulted in the nearest circular polarization pattern utilizes a single coaxial input to only one of the loops with the other loop terminated in a matched load. The feed system for this method is greatly simplified since only one cable per antenna element is required rather than a pair of phase critical cables and a two way power divider per antenna element. A further benefit is that the required circular polarization pattern is retained over a wider bandwidth. However, the gain at the maximum, using the singly fed loop, is about 3 db lower than with the method wherein two loops are fed. A shorted termination was also tried in an attempt to improve the gain of the singly fed loop. A 4 db improvement in gain was measured as well as a high degree of circularity. However, the shorted termination was quite narrow banded so the matched termination method was used in the full size array. The success of this feed technique in the 36 element crossed slot receiving array may be seen from the measured polarization pattern in Figure 55.

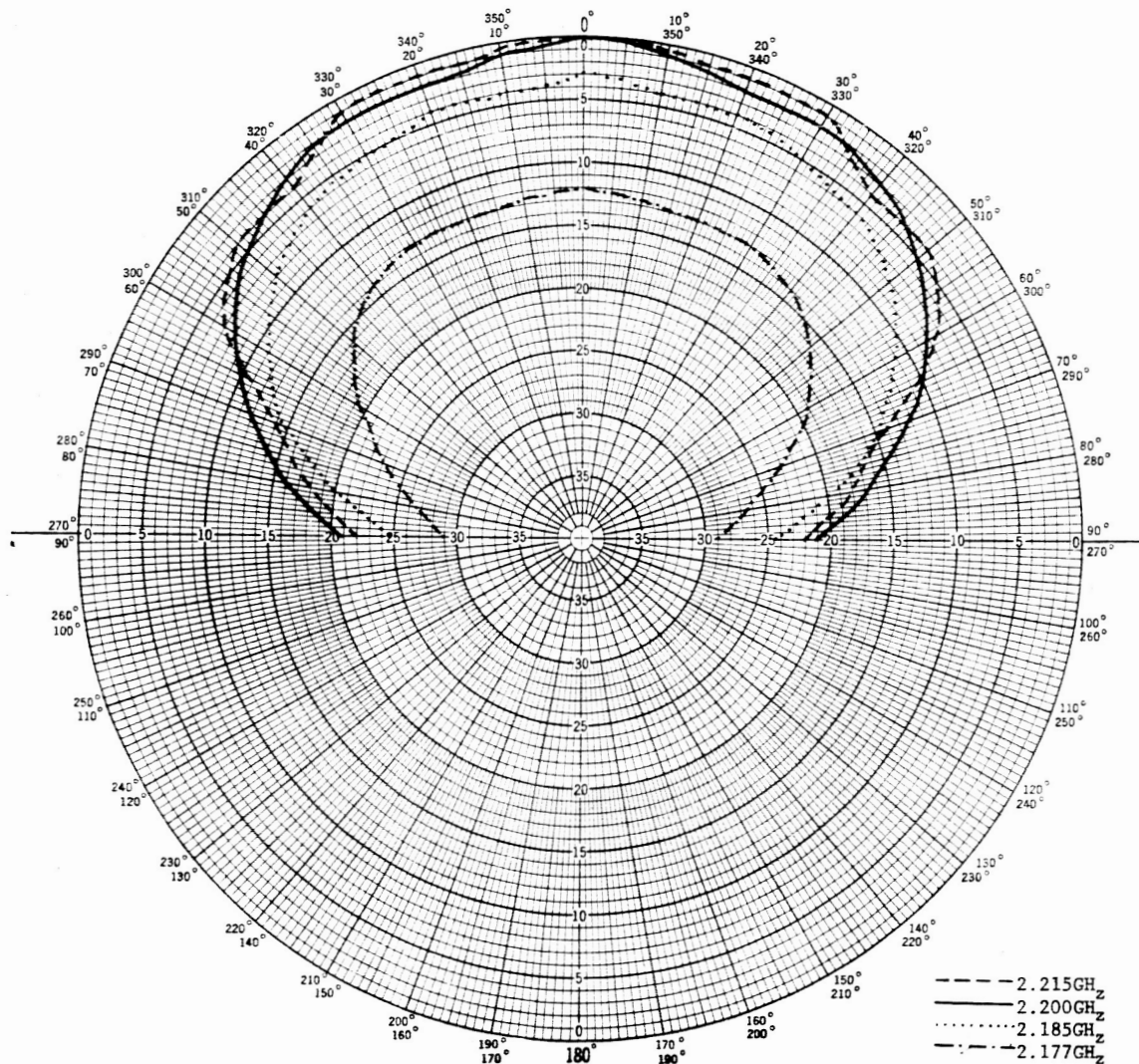


Fig. 50--The average value of  $E_{\phi}$  (averaged overall values of  $\phi$ ) versus  $\theta$  for a single, isolated crossed-slot antenna.

Polar Chart No. 127D  
 SCIENTIFIC-ATLANTA, INC.  
 ATLANTA, GEORGIA

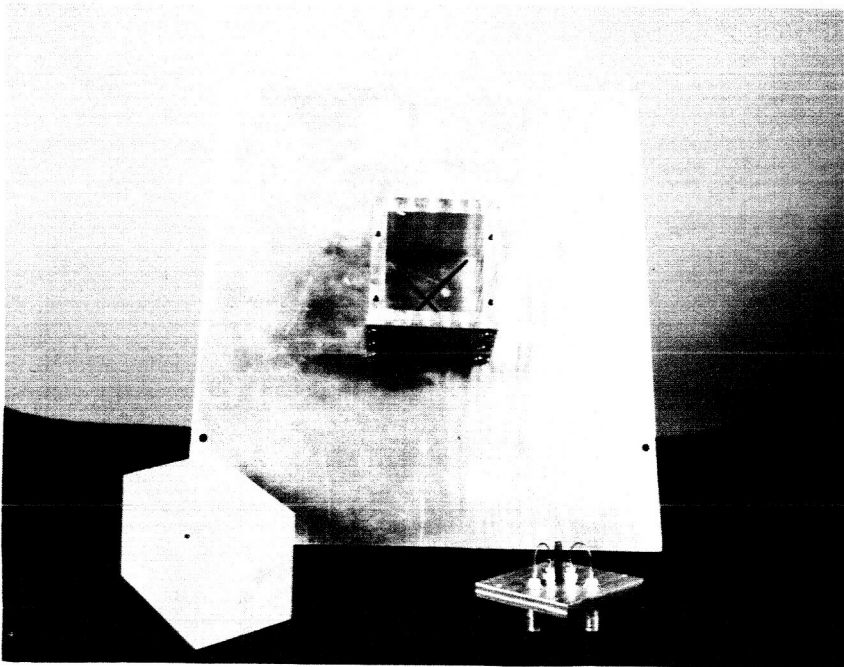


Fig. 51--A back view of the interior of a single, isolated, crossed-slot antenna.

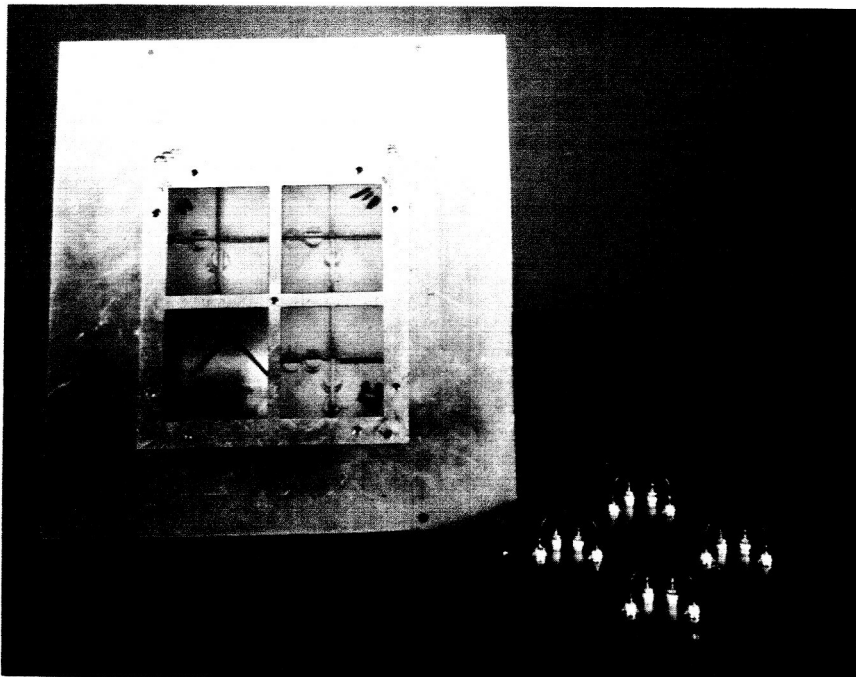


Fig. 52--A back view of the interior of the four element, crossed-slot array.

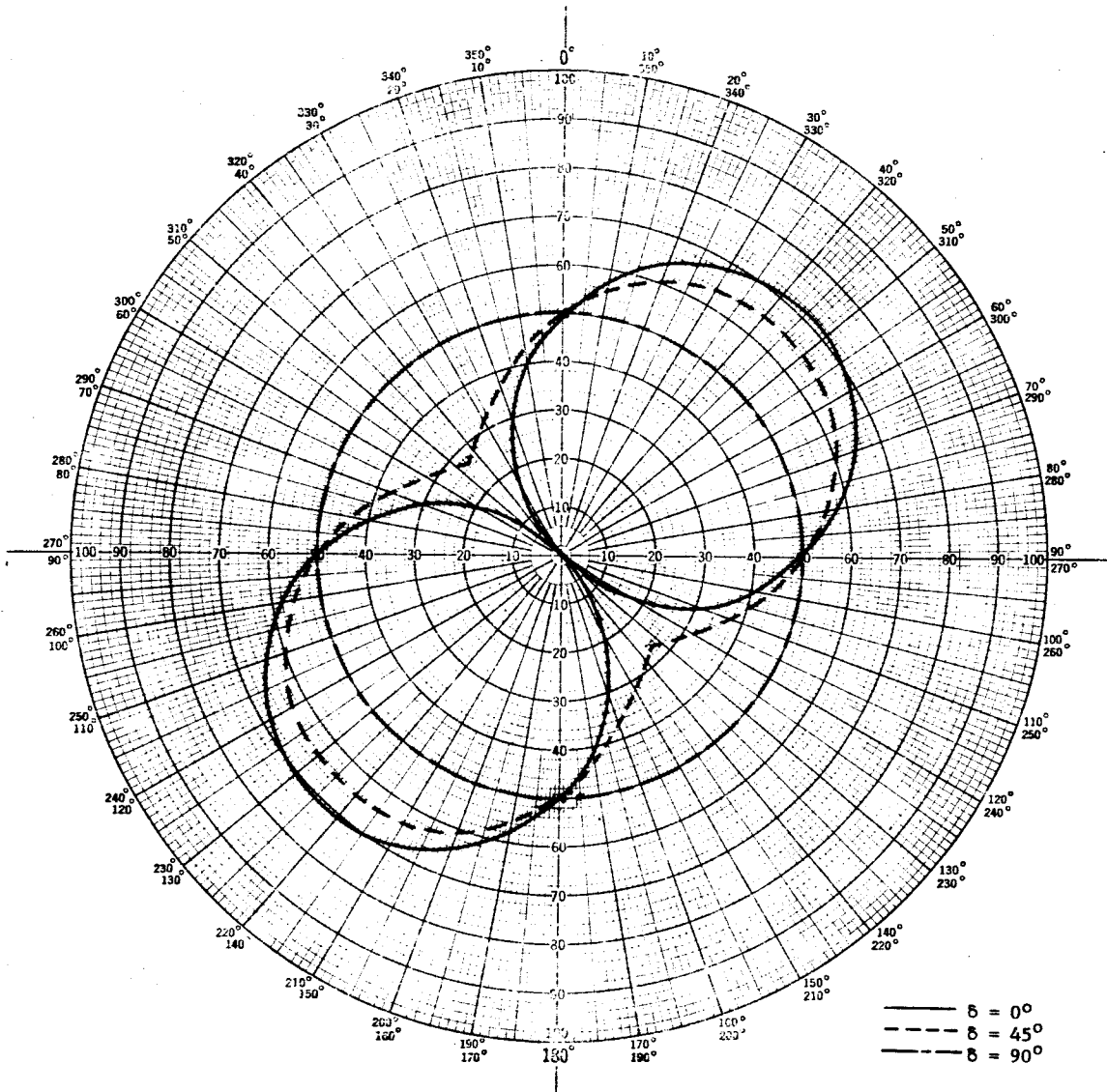


Fig. 53--The combined polarization pattern of two linearly polarized, equal amplitude, sources that are in space quadrature for various values of phase lag.

Polar Chart No. 127  
 SCIENTIFIC-ATLANTA, INC.  
 ATLANTA, GEORGIA

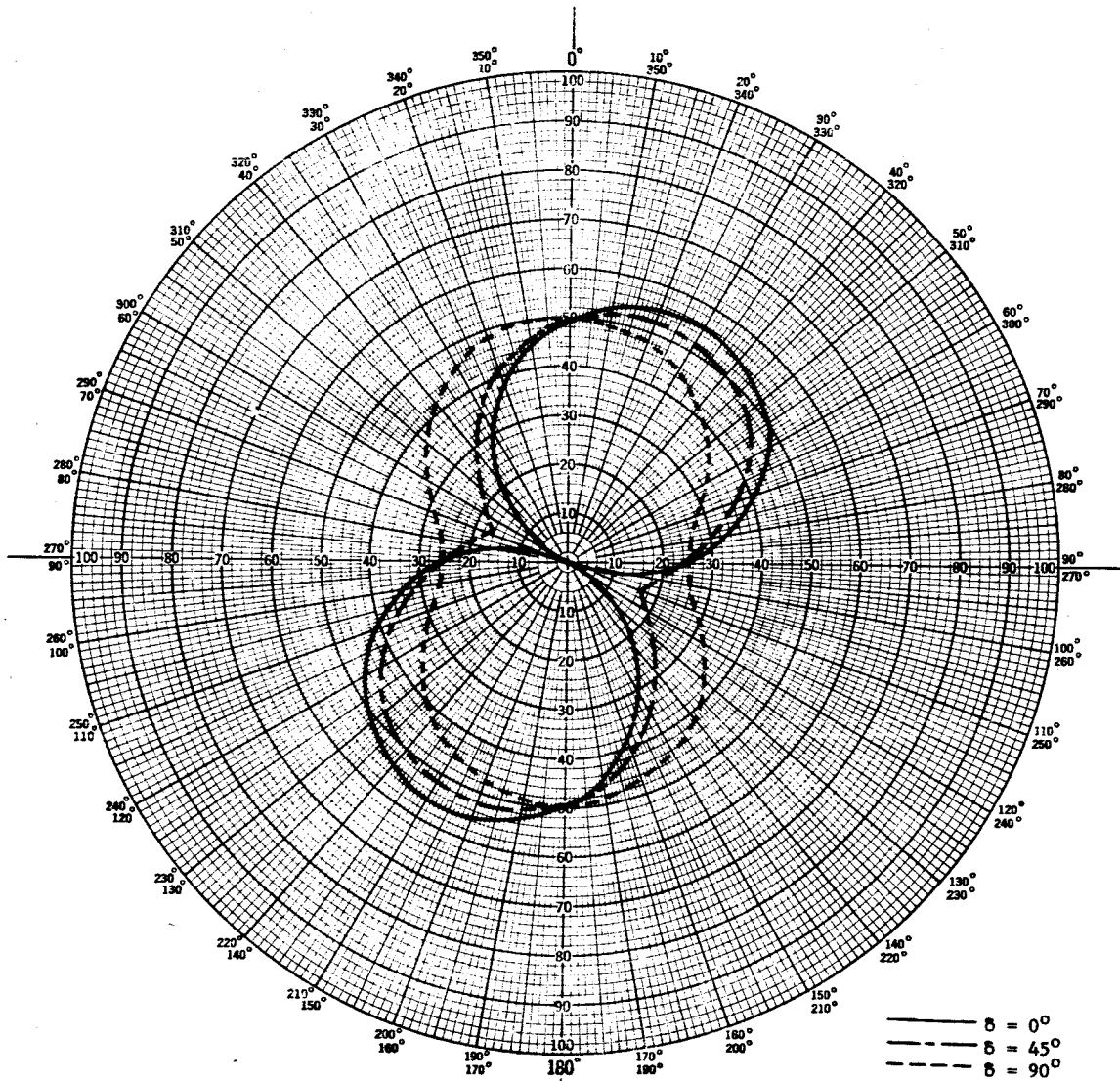


Fig. 54--The combined polarization pattern of two linearly polarized sources (for a 3db amplitude mismatch) that are in space quadrature for various values of phase lag.

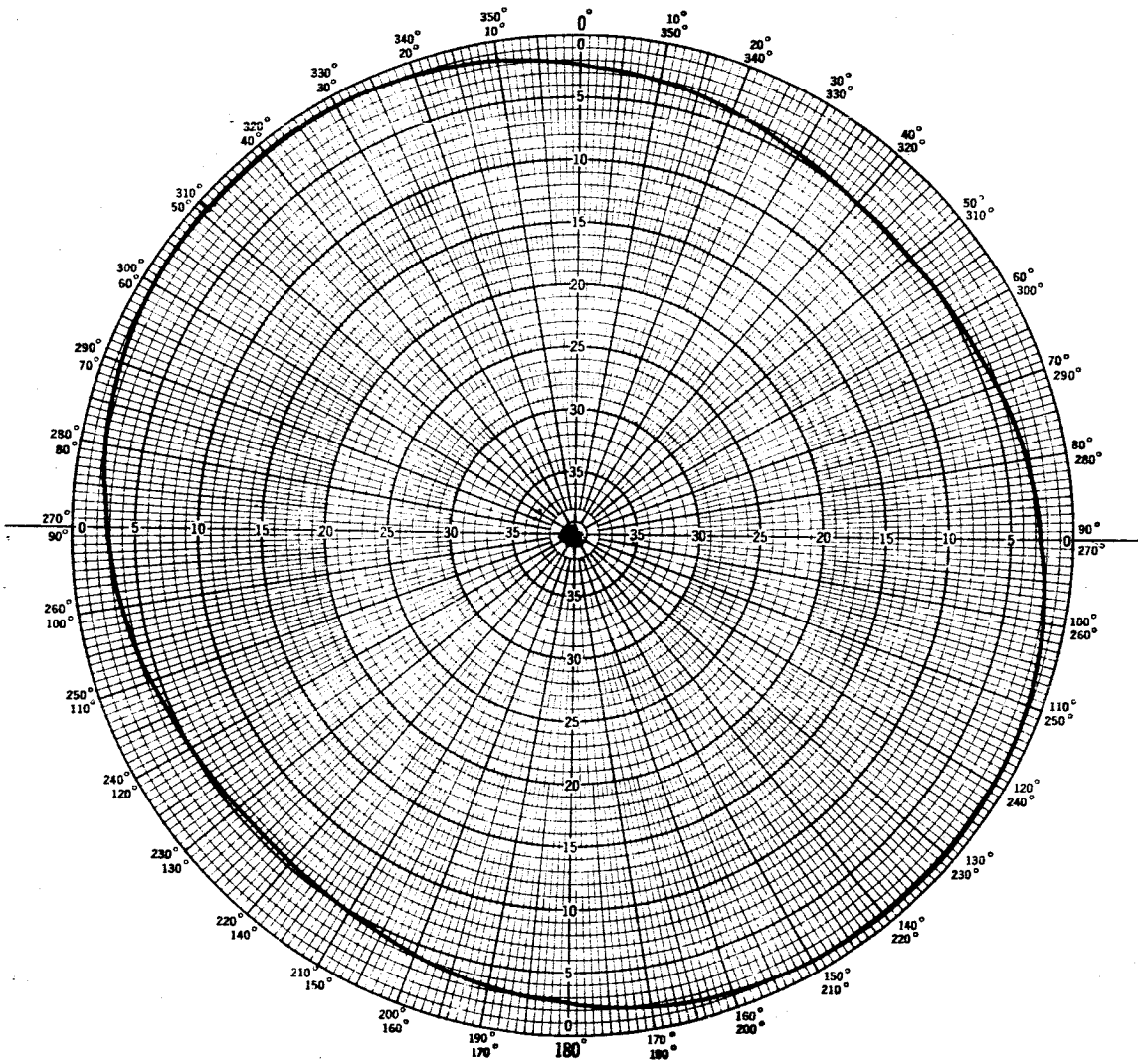


Fig. 55--Polarization pattern of the 36 element cross-slot receiving array for the  $L = 0$ ,  $M = 0$  beam pointing.

Polar Chart No. 127D  
 SCIENTIFIC-ATLANTA, INC.  
 ATLANTA, GEORGIA



### 5. A Stripline Power Divider

A 36-way power divider is required for excitation of the 36 element array. A means of attaining a 36-way power division employing seven 6-way power dividers is shown in the block diagram of Figure 56. For the configuration of Figure 56, one ideally desires the following properties for each of the 6-way power dividers operating under matched input and output conditions:

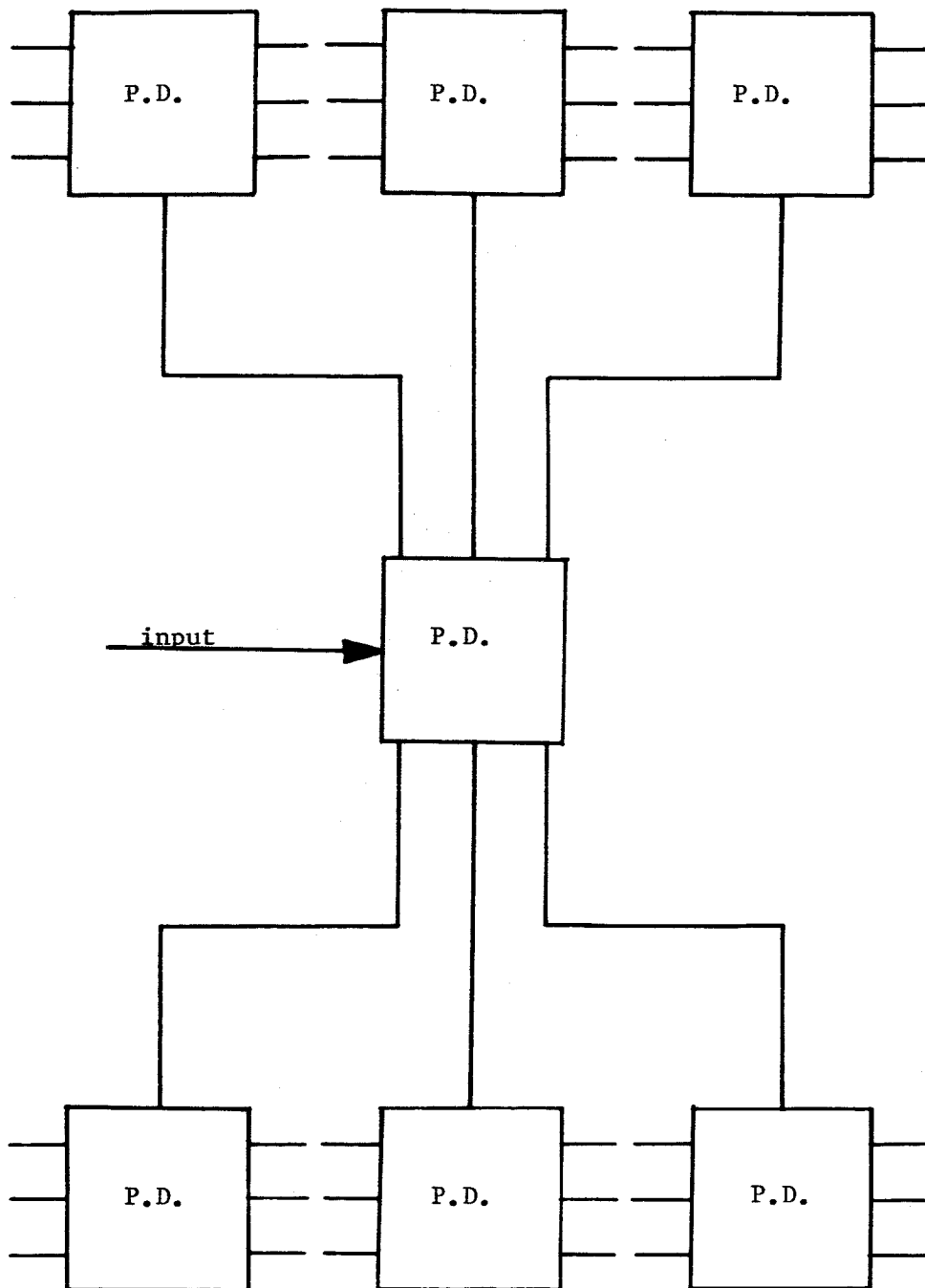
- i) Equal power division into each of the six outputs;
- ii) Equal phase at each output with respect to the input phase;
- iii) A standing-wave-ratio equal to 1;
- iv) An insertion loss equal to zero.

Consider the hybrid-ring configuration of Figure 57 as a method of achieving the above conditions for a 6-way power divider. Choosing the characteristic impedance,  $Z_0$ , of the hybrid-ring to be equal to that of  $l_1, l_2, l_3, l_4, l_5$  and  $l_6$  requires that  $l_7$  have a characteristic impedance'

$$Z'_0 = 1.5Z_0 . \quad (120)$$

The matching transformer is required to match  $l_8$ , with characteristic impedance  $Z_0$  to  $l_7$ .

A model employing the above principles is shown pictorally in Figure 58. This model is constructed of strip-line transmission line with a quarter-wave transformer functioning as the impedance trans-



Legend: P.D. = 6-way power divider

Fig. 56--A 36-way power divider employing seven 6-way power dividers.

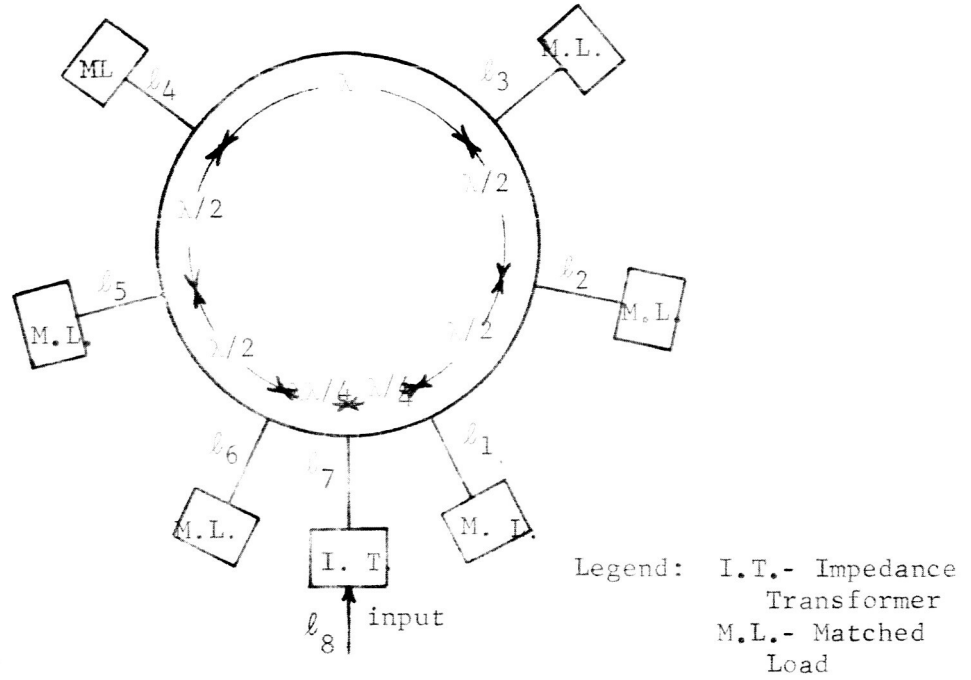


Fig. 57--Hybrid ring configuration for 6-way power divider.

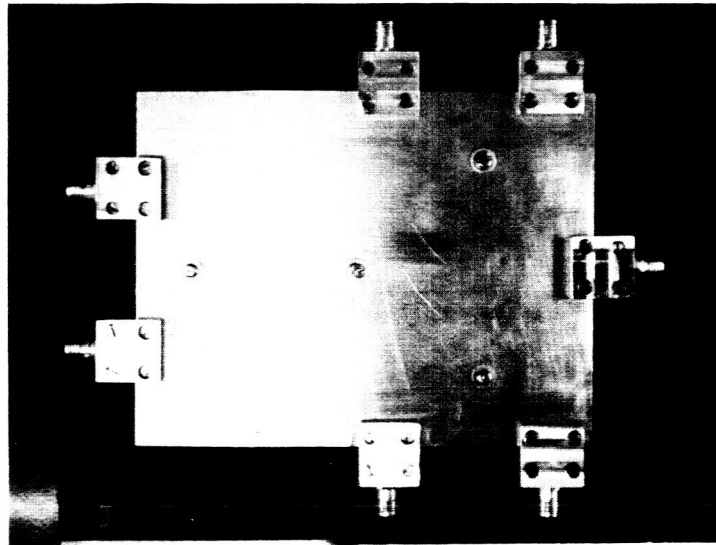


Fig. 58--Photograph of the 6-way power divider constructed.

former of Figure 57. Measurements on this model yielded a V.S.W.R. of 2.2<sup>0</sup> and a maximum power deviation of 0.2 db from any two output part. The connectors used in this model were constructed from TNC bulkhead connectors. The use of TNC to stripline adapters should improve the V.S.W.R. characteristics of these power dividers. The electrical characteristics of these power dividers compare favorably with the present coaxial reactive power dividers that are presently being used.

### III. RESULTS

The results of contract NAS8-11251 at the end of the contract period may be summarized as follows:

(A) Direction Finding System - A prototype of the direction finding system has been constructed and is presently being tested. A computer study of the direction finder antenna has been conducted in order to solve problems connected with the system.

(B) Digital Switching System - A switching system suitable for use with the electronic phase shifters is under construction.

(C) Phase Shifter - An electronic phase shifter employing PIN type diodes has been designed and constructed. The device is economical to manufacture and employs strip line construction. It provides the phase shifts necessary to scan the antenna array in  $22.5^{\circ}$  increments. A solid state device to drive the phase shifters was designed and tested.

(D) Electronically Scanned Antenna Arrays - A prototype of the 6 x 6 scanning array at the receiving frequency of 2.214 GHz was constructed and tested. The results of these test show the radiation patterns correspond closely with the theoretical predictions.

This summarizes the work completed at the close of the contract. Any preliminary work not mentioned here may be found in the introduction.

#### IV. CONCLUSIONS AND RECOMMENDATIONS

(A) The direction finding system chosen fulfills the requirements set forth in this report. The antenna array is composed of halfwave dipoles. The mechanical assembly of the antenna is simple and economical. The performance is satisfactory when mounted above a conducting ground plane. The difficulty in obtaining a reference signal and the null occurring overhead are overcome through the use of simple logic circuitry.

It is recommended that future study concern improvements in the antenna system. These would concern a reduction in the number of pre-amplifiers, possible disposal of the limiters by use of an improved antenna element and equipment survey to determine the feasibility of solid-state phase measuring equipment.

(B) The digital switching system under construction should perform the required operations with no difficulties which may be anticipated at this time.

Future work could concern the application of micro logic circuitry to reduce the size of the switching devices.

(C) The electronic phase shifter prototype constructed satisfactorily fulfills the design requirements. The device performs satisfactorily over the bandwidth allowing a deviation of  $\pm 3^\circ$ . This is due to the phase lines employed in the phase shifter. The

switching time is satisfactory and the insertion loss is low, being only 1.2 db with a voltage standing wave ration of about 1.3:1.0.

The use of diode phase shifters at this frequency seems the best choice in terms of economy, switching time and insertion loss. Ferrite phase shifters are lossy, relatively expensive and lack switching speed in this frequency band.

It is recommended that further study be conducted on the phase shifter. Future considerations will be the employment of branch couplers in place of the hybrid ring couplers. This will enable the entire device to have a smaller physical size therefore allowing packaging problems to be reduced as well as a reduction in material cost.

(D) The electronic scanning array produced beam pointings that closely coincide with the calculated values. The device produces elliptical polarization overhead with only one input to the antenna feed cavity. The small number of elements employed in the array and their simple construction lead to an economical scanning array. The entire configuration is quite rigid and could easily serve in severe environments.

It is recommended that further study be conducted on the scanning array. These studies could include the improvement of dielectric loading, improving of axial ratio and simpler packaging configurations. The interface between the phase shifters and the scanning array might benefit by further study. The construction of small radomes to cover the transmitting and receiving arrays should be conducted.

Construction of an all-stripline feed system for the array would improve the packaging. Investigation of various means for suppressing the sidelobes of the array for large scan angles could be a fruitful future study.



#### REFERENCES

1. H. P. Neff, Jr., R. J. Coleman, and E. R. Graf, "A VHF Direction Finding System", Technical Report Number 5, Contract NAS8-11251, Antenna Research Laboratory, Auburn University, 1966, pp. 8-9.
2. Ibid, p. 15.
3. Ibid, p. 24
4. The PIN Diode, Hewlett Packare Associates Application Note Number 4, 1964.
5. M. E. Hines, Fundamental Limitations on R.F. Switching and Phase Shifting Using Semiconductor Diodes., Proc. IEEE, Vol. 52, 1964, pp. 697-708.
6. H. P. Westman (Ed.) Reference Data for Radio Engineers, I.T.T. Corporation Fourth Edition, 1956, p. 563.